SURFACE AND INTERFACE DYNAMICS IN MULTILAYERED SYSTEMS

Ph.D. committee

Chair:

prof. dr. ir. B. Poelsema	University of Twente / TNW MESA+ Institute for Nanotechnology

Secretary:

prof. dr. ir. B. Poelsema	University of Twente / TNW MESA+ Institute for Nanotechnology

Promoter:

prof. dr. F. Bijkerk	University of Twente / TNW MESA+ Institute for Nanotechnology FOM Institute for Plasma Physics Rijnhuizen

Assistant promoter:

dr. ir. R. W. E. van de Kruijs	FOM Institute for Plasma Physics Rijnhuizen

Opposition:

prof. dr. K. J. Boller	University of Twente / TWN MESA+ Institute for Nanotechnology
prof. dr. A. W. Kleyn	University of Leiden FOM Institute for Plasma Physics Rijnhuizen
prof. dr. P. C. Zalm	University of Salford Philips Research
dr. ing. G. Rijnders	University of Twente / TNW MESA+ Institute for Nanotechnology

---

Cover:
The cover shows a cross-section transmission electron microscopy (CS-TEM) and several scanning electron microscopy (SEM) pictures of capped multilayers and B_4C. The angular resolved x-ray photoelectron spectroscopy (ARPES) setup is also shown.

Surface and interface dynamics in multilayered structures
Ph.D. Thesis, University of Twente, Enschede – Illustrated.
With references – With summary in English and Dutch.
Printed by Ridderprint offsetdrukkerij b.v.

SURFACE AND INTERFACE DYNAMICS IN MULTILAYERED SYSTEMS

PROEFSCHRIFT

ter verkrijging van de graad van doctor
aan de Universiteit Twente, op gezag van
de rector magnificus, prof. dr. H. Brinksma,
volgens besluit van het College voor Promoties
in het openbaar te verdedigen op
vrijdag 26 juni om 15:00 uur

door

Tim Tsarfati
geboren op 7 januari 1982
te Utrecht

Dit proefschrift is goedgekeurd door de promotor:

prof. dr. F. Bijkerk

en de assistent-promotor:

dr. ir. R. W. E. van de Kruijs

ISBN 978-90-5335-197-0
© Tim Tsarfati, 2009

This thesis is based on the following publications:

Chapter 3: T. Tsarfati, E. Zoethout, R. W. E. van de Kruijs, F. Bijkerk, "*Growth and oxidation of transition metal nanolayers*", Surf. Sci. 603, 7, 1041 (2009)

Chapter 4: T. Tsarfati, E. Zoethout, R. W. E. van de Kruijs, F. Bijkerk, "*Carbon coverage, oxidation and atomic O and H exposure of d-metal nanolayers*", accepted for publication in Surf. Sci. (2009)

Chapter 5: T. Tsarfati, E. Zoethout, R. W. E. van de Kruijs, F. Bijkerk, "*In-depth agglomeration of d-metals at Si-on-Mo interfaces*", J. of Appl. Phys. 105, 064314 (2009)

Chapter 6: T. Tsarfati, E. Zoethout, R. W. E. van de Kruijs, F. Bijkerk, "*Chemically mediated diffusion of d-metals and B through Si and agglomeration at Si-on-Mo interfaces*", J. of Appl. Phys. 105, 104305 (2009)

Chapter 7: T. Tsarfati, E. Zoethout, R. W. E. van de Kruijs, E. Louis, F. Bijkerk, "*Reflective multilayer optics for 6.7 nm wavelength radiation sources and next generation lithography*", submitted

Chapter 8: T. Tsarfati, R. W. E. van de Kruijs, E. Zoethout, E. Louis, F. Bijkerk, "*Nitridation and contrast of B_4C/La interfaces and multilayers*", submitted
appended with parts of:
T. Tsarfati, E. Zoethout, E. Louis, R. W. E. van de Kruijs, A. Yakshin, S. Müllender, and F. Bijkerk, "*Improved contrast and reflectivity of multilayer reflective optics for wavelengths beyond the Extreme UV*", Proc. SPIE Advanced Lithography 7271, 72713V (2009)

Patents:

T. Tsarfati, E. Zoethout, E. Louis, F. Bijkerk, "*Method to Enhance layer contrast of a multilayer for reflection at the B absorption edge*"/"*Reflektives Optisches Element und Verfahren zu seiner Herstellung*", P16795DE US 61/079307 (US), DE102008040265 (Germany), priority date 16 September 2008

R. W. E. van de Kruijs, S. Bruijn, T. Tsarfati, A.E. Yakshin, F. Bijkerk, E. Louis, "*Reduction of diffusion at Mo/Si interfaces by boride barriers and boron passivation*", P17091PUSPRO, priority date 7 May 2008

Other publications:

E. Louis, E. Zoethout, R. W. E. van de Kruijs, I. Nedelcu, A.E. Yakshin, S. Alonso van der Westen, T. Tsarfati, F. Bijkerk, H. Enkisch, and S. Müllender, "*Multilayer coatings for the EUVL process development tool*", Proc. SPIE Emerging Lithographic Technologies IX, 5751, 1170 (2005)

E. Louis, A.E. Yakshin, E. Zoethout, R. W. E. van de Kruijs, I. Nedelcu, S. Alonso van der Westen, T. Tsarfati, , F. Bijkerk, H. Enkisch, S. Müllender, B. Wolschrijn and B. Mertens, "*Enhanced performance of EUV multilayer coatings*", Proc. SPIE Optics & Photonics 5900, 590002 (2005)

M. Driessen, T. Tsarfati, "*UHV transport van multilaagspiegels*", NEVACblad 45, 1, 9, (2008)

E. Louis, A. R. Khorsand, R. Sobierajski, E. D. van Hattum, T. Tsarfati, M. Jurek, D. Klinger, J. B. Pelka, L. Juha, J. Chalupsky, J. Cihelka, V. Hajkova, U. Jastrow, S. Toleikis, H. Wabnitz, K. I. Tiedtke, J. Gaudin, F. Bijkerk, "*Damage studies of multilayer optics for XUV FELs*", submitted

Conference presentations:

T. Tsarfati, E. Zoethout, R. W. E. van de Kruijs, F. Bijkerk; "*Surface nanolayer chemistry in multilayer mirrors*"; poster presentation at the APCSSE, Hong Kong, China (2006)

T. Tsarfati, V. I. T. A. Lohmann, E. Zoethout, E. Louis and F. Bijkerk, "*EUV multilayer surface chemistry*"; poster presentation at Physics@FOM, The Netherlands (2007)

T. Tsarfati, R. W. E. van de Kruijs, E. Zoethout, A. E. Yakshin, E. Louis, et al., "*EUV multilayer surface chemistry*"; poster presentation at the 19th Symposium Plasmafysica en Stralingstechnologie, The Netherlands (2007)

T. Tsarfati, E. Zoethout, R. W. E. van de Kruijs, F. Bijkerk; "*Multilayers & Surface Protection*"; oral presentation at the 15th VEIT summer school, Bulgaria (2007)

T. Tsarfati, E. Zoethout, R. W. E. van de Kruijs and F. Bijkerk, "*Noble Metal nanolayers for multilayer surface protection*"; poster presentation at Physics@FOM, The Netherlands (2008)

T. Tsarfati, E. Zoethout, R. W. E. van de Kruijs, F. Bijkerk; "*E-beam PVD of various protective d-metal nanolayers on Mo; an AFM and ARXPS study on homogeneity, intermixture, and oxidation*"; oral presentation at the 9th PXRMS, Montana, USA (2008)

T. Tsarfati, E. Zoethout, R. W. E. van de Kruijs, F. Bijkerk; "*E-beam PVD of various protective d-metal nanolayers on Mo; an AFM and ARXPS study on homogeneity, intermixture, and oxidation*"; poster presentation at the 14th ICSFS, Ireland (2008)

T. Tsarfati, R. W. E. van de Kruijs, E. Zoethout, E. Louis, F. Bijkerk; "*Improved contrast and reflectivity of multilayer reflective optics for wavelengths beyond the Extreme UV*"; oral presentation at the 36th ICMCTF, California, USA (2009)

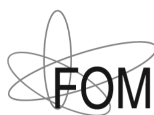

This work is part of the FOM Industrial Partnership Programme I10 ('XMO') which is carried out under contract with Carl Zeiss SMT AG, Oberkochen and the 'Stichting voor Fundamenteel Onderzoek der Materie (FOM)', the latter being financially supported by the 'Nederlandse Organisatie voor Wetenschappelijk Onderzoek (NWO)'.

Contents

1 Introduction ... 9
1.1 Motivation and Valorisation of Lithography ... 9
1.2 Reflective Multilayer Optics ... 10
1.3 Multilayer Research ... 12
1.3.1 Layer and Interface Growth ... 13
1.3.2 Surface chemistry ... 14
1.4 The Contribution of this Thesis ... 14
1.5 References ... 15
2 Experimental ... 19
2.1 Thin Layer Growth ... 19
2.1.1 Magnetron Sputter Deposition ... 20
2.1.2 Physical Vapor Deposition ... 20
2.1.3 Ion Bombardment ... 20
2.2 Characterization ... 21
2.2.1 Quartz Crystal Microbalances ... 21
2.2.2 Mass Spectrometry ... 21
2.2.3 Reflectometry ... 22
2.2.4 Low Energy Ion Scattering ... 23
2.2.5 X-ray Photoelectron Spectroscopy ... 23
2.2.6 Auger Electron Spectroscopy ... 25
2.2.7 Atomic Force Microscopy ... 26
2.2.8 Electron Microscopy and Spectroscopy ... 26
2.3 References ... 27
3 Growth and sacrificial oxidation of transition metal nanolayers ... 29
3.1 Abstract ... 29
3.2 Introduction ... 29
3.3 Experimental details ... 29
3.4 Layer growth kinetics ... 30
3.5 Results and discussion ... 31
3.6 Conclusions ... 38
3.7 Acknowledgements ... 39
3.8 References ... 39
4 Atomic O and H exposure of C-covered and oxidized d-metal surfaces ... 41
4.1 Abstract ... 41
4.2 Introduction ... 41
4.3 Experimental details ... 41
4.4 Results and discussion ... 42
4.5 Conclusions ... 47
4.6 Acknowledgements ... 48
4.7 References ... 48
5 In-depth agglomeration of d-metals at Si-on-Mo interfaces ... 51
5.1 Abstract ... 51
5.2 Introduction ... 51
5.3 Interface kinetics ... 52
5.4 Experimental details ... 53
5.5 Results and discussion ... 53
5.6 Conclusion ... 57
5.7 Acknowledgements ... 58

5.8 References 58

6 Chemically mediated diffusion of d-metals and B through Si and agglomeration at Si-on-Mo interfaces 61

6.1 Abstract 61

6.2 Introduction 61

6.3 Experimental details 62

6.4 Results and discussion 62

6.5 Conclusions 70

6.6 Acknowledgements 70

6.7 References 70

7 Reflective multilayer optics for 6.7 nm wavelength radiation sources and next generation lithography 73

7.1 Abstract 73

7.2 Introduction 73

7.3 Results and discussion 73

7.4 Conclusions 79

7.5 Acknowledgements 79

7.6 References 79

8 Nitridation and contrast of B_4C/La interfaces and multilayers 83

8.1 Abstract 83

8.2 Introduction 83

8.3 Experimental details 83

8.4 Results and discussion 84

8.5 Conclusions 88

8.6 Acknowledgements 88

8.7 References 88

9 Valorisation and Outlook 91

9.1 Photolithography for Society 91

9.2 Improving the Optics Lifetime 91

9.3 Beyond EUVL 93

9.4 References 93

10 Summary 95

11 Samenvatting 97

12 Analytical recommendations 99

13 Acknowledgements 101

14 Curriculum Vitæ 103

1 Introduction

1.1 Motivation and Valorisation of Lithography

This research project is for an important part motivated by required know-how for innovations in photolithography, a technique that uses radiation to imprint patterns and circuits. The collaboration between science and industry provides an atmosphere in which fundamental steps in e.g. material and surface science and photochemistry go hand in hand with commercial application. The continuous R&D on photolithography enables the printing of ever finer features. Following Moore's prediction as formulated in 1965, the number of transistors in a state-of-the-art integrated circuit has roughly doubled every second year to tens of millions nowadays, improving their performance and energy-efficiency while reducing cost per function. The imaging resolution or critical dimension (*CD*) that can be printed in a lithography process is described by the Rayleigh equation

$$CD = k_1 \frac{\lambda}{NA} \quad , \tag{1}$$

where a reduction of process parameter k_1 relates to increasing production efforts and costs. The numerical aperture (*NA*) or optical dimension of the last (objective) lens element can be increased but quadratically decreases the depth of focus, the distance over which a sharp image can be realized. When the depth of focus becomes unacceptably small for practical applications, equation (1) implies that the only practical solution to realize chips with smaller feature dimensions is to use radiation with shorter wavelengths (λ). The depth of focus only decreases linearly with lower λ.

At the start of this research project, ICs were produced by optical projection lithography using deep-ultraviolet (DUV) radiation with wavelengths of 248 and 193 nanometer[1]. Using a wavelength of 248 nm enables line widths of 80 nm, while by using a wavelength of 193 nm it presently appears possible to reach the 45 nm technology node with single patterning[2]. To reduce k_1 below 0.3 for these wavelengths, double patterning techniques that involve a sequence of two separate exposures of the same photoresist layer using two different photomasks have emerged[3]. With the economical crisis in mind, double patterning is currently being explored to extend the resolution capability of currently available state-of-art 193 nm lithography tools[4]. Although it is believed to enable resolutions below 30 nm and postpone the need to address the technical challenges of next-generation lithography technologies[5], double patterning requires recurrence of the costly and time-intensive lithography cycle, resulting in a high Cost of Ownership (CoO) and a limited commercial potential[6].

The lithography and semiconductor industry are in the process of identifying and exploring new lithographic technologies that can carry the miniaturization further. Potential successors, known as "Next Generation Lithographies" (NGL's), include soft x-ray-, ion-beam, and electron-beam projection lithography. Extreme UV lithography (EUVL, $\lambda = 13.5$ nm) is the leading NGL technology[7] and the main innovative project of ASML and Carl Zeiss SMT, as well as the Japanese companies Canon and Nikon. The use of light at a wavelength of only 13.5 nm provides many solutions for IC manufacturing. The EUVL product roadmap of ASML envisions resolutions of 27 nm with $NA = 0.25$ in 2010, 22 to 16 nm with $NA = 0.32$ over 2012 and 2013, and 11 nm with $NA > 0.40$ in 2015[6]. The research described in chapter 7 and 8 brings lithography for

λ = 6.7 nm significantly closer[8,9], enabling even smaller resolutions[10]. EUV lithography may in many respects be viewed as a natural extension of DUV lithography and simultaneously takes optical projection lithography a major step forwards. Some fundamental differences between the two technologies make simple technology transfers from visible light and DUV lithography to EUV lithography a substantial challenge. Most differences occur because the properties of materials in the EUV portion of the electromagnetic spectrum are very different from those in the visible and UV wavelength ranges and strong absorption of EUV light occurs even in ambient air. This means that besides a vacuum lithography tool environment, reflective multilayer optics instead of transmissive lenses make their appearance in lithography.

After several earlier projects in the context of the Sixth Framework program, the European Commission has funded the three year More Moore research program in 2003 with a budget of 23.25 million euro. It was led by ASML and involved tens of academic and research institutes and companies. Aim of the project was to meet the technical challenges of EUVL so the technology could timely be introduced for volume production. During the course of the program, ASML has directly contracted Carl Zeiss SMT AG for the required industrial know-how and actual production of the optical elements. Carl Zeiss SMT AG has outsourced the development of the scientific know-how of the reflective multilayer coatings to the nanolayer Surface & Interface (nSI) department at FOM Rijnhuizen in an industrial partnership program (IPP) named “X-ray Multilayer Optics” (XMO). In the frame of this contract, the research described in this thesis focuses on the multilayer surface region and contributes to several major objectives in making EUVL commercially viable. These include improvement of the EUV throughput and the lifetime of the optics by means of a protective “capping layer”[11,12,13] and a novel in-situ surface cleaning technique[14].

A most eminent example of valorisation of the research in nSI is found in the successful realization of two demonstration projection lithography tools, currently used by end-customers to familiarize and obtain hands-on experience with the EUVL technique[15]. Coating process development in nSI has been advanced to the high level required for industry purposes, and as a result nSI has actually been responsible for coating approximately half the optics used in these demonstration tools. As a result of the successful learning curve achieved using the first generation EUVL demonstration tool, a next generation of pre-production tools has now been ordered. This requires multilayer optics of various dimensions with improved high reflectivity lifetime; an issue that by the research on capping layers is thoroughly addressed in this thesis. Coating technology developed by nSI has now been successfully transferred to partner Carl Zeiss SMT AG, where a deposition setup based on an original nSI design is used for commercial production of multilayer coatings. Further valorization of the research can be found in additional projects that are running or are being set up, including “ACHieVE” (through SenterNovem), the Medea+ project EAGLE, and the Catrene project EXEPT, all involving nSI for fundamental research in multilayer optics and interaction with photons, plasma, and their environment as presented in this thesis.

1.2 Reflective Multilayer Optics

From the visible $380 < \lambda < 750$ nm light towards λ = 13.5 nm Extreme Ultra-Violet (EUV), the refractive indices (n, with a real part $1-\delta$) of materials practically go to unity.

The distinct transparency of e.g. glass for visible light due to photons that cannot excite electrons does not occur for more energetic EUV radiation. The optical contrast with air or vacuum that enables the use of transmissive lenses or single reflective interfaces as optical elements for the visible light diminishes at EUV wavelengths. This limits the reflection (*R*) at normal incidence for any single interface to sub percent levels, while the transmitted radiation would typically be absorbed in the underlying substrate within a depth of hundreds of nanometers to several microns. The transmitted radiation can however again be reflected by subsurface interfaces. Adding more layers will result in a so-called multilayer as shown in Fig. 1. This essentially artificial Bragg crystal is a periodic stack of many thin layers of alternating refractive index where partial reflection occurs at each interface. When the period thickness (*d*) of the multilayer is chosen to fulfill the modified Bragg law

$$n_{\text{int}}\lambda = 2d\sin\theta\left(1-\frac{\delta}{\sin^2\theta}\right) \quad , \tag{2}$$

with n_{int} an integer and θ representing the off-normal angle of incidence, progressive interference of the reflections at all interfaces occurs. Note that the use of the simplified version of Bragg's law is allowed here due to large θ and near-unity refractive indices. A basic multilayer period consists of two relatively transparent and optically contrasting layers of approximately ¼λ thickness. Due to the ½λ phase shift of the reflected wave at a low to higher *n* interface, the reflections at all the interfaces in the multilayer are then in phase[16]. The reflection scales quadratically with the wave amplitude and thus with the number of periods *N*. Absorption (β, the imaginary part of *n*), off-specular scattering and out of phase reflection will in practice result in lower overall reflection. Higher order reflections vanish quickly and can be neglected.

The most important choice to be made in material selection is that of the spacer material. To obtain a maximum multilayer reflectance, this should be a material with an as low as possible absorption at the required wavelength. Absorption of photons by a material is usually caused by electron excitations and is therefore strongly dependant on the electron binding energies of the material, and discontinuities occur around the discrete excitation energies. Depending on the electron shell of interest, the discontinuity is referred to as the K-, L- or M-edge. The degree of absorption is also dependant on the material and electron density; low densities generally result in a lower overall absorption.

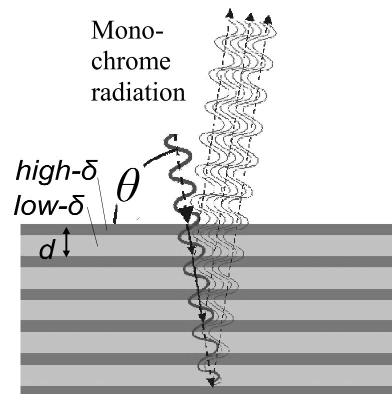

Figure 1: *At each interface, the optical contrast causes the incident ray to refract and partially reflect.*

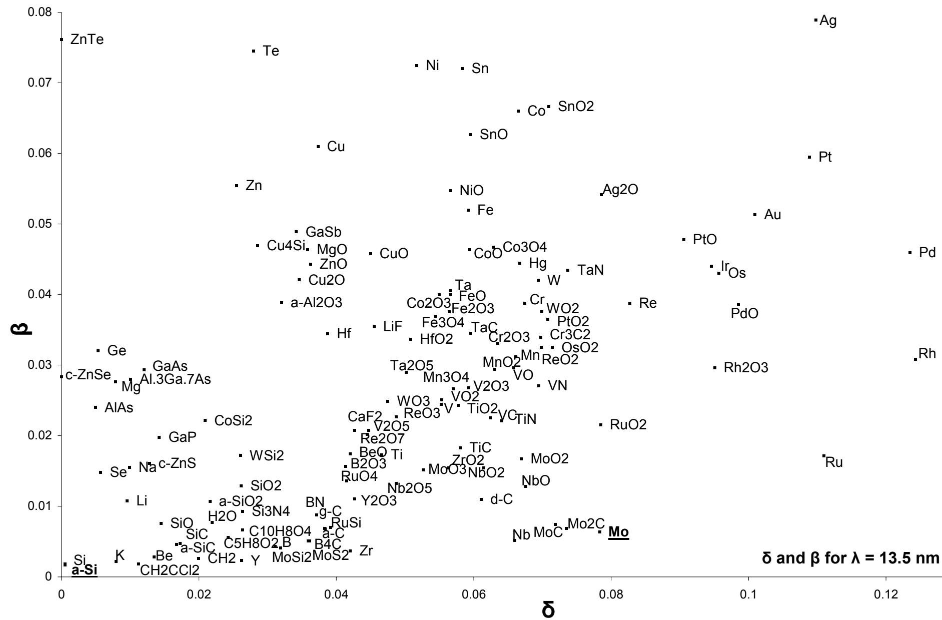

Figure 2: *The δ and β overview for several materials at λ = 13.5 nm, revealing the suitability of amorphous Si (a-Si) and Mo for application in reflective multilayer optics for this wavelength.*

Selection of the second material should be based on a maximum difference in n, specifically in δ. Large differences in β also contribute to reflection at the interface, but higher β values yield lower penetration depths, and this reduces the maximum number of layers (N_{max}) that contribute to overall reflection. The overview of optical properties for EUV in Fig. 2 reveals the particular suitability of amorphous Si in combination with Mo. The comparatively high optical contrast optimizes the reflection per interface and reduces the minimum amount of layers (N_{min}) needed for a target reflection. For a reference 50 period Mo/Si EUV multilayer mirror, record reflections of 69.5% have been achieved in the nSI department at FOM Rijnhuizen[17,18], compared to an absorption limited theoretical maximum of 74%. In the $\lambda = 6.7$ nm region that is considered in this thesis[8,9], the values of δ and β are smaller and N_{max} and N_{min} increase. At least 200 periods of B_4C and La are required to achieve reflectivities over 40%. Limiting the reflectivity and widely discussed in this thesis are the chemical reactivity and diffusion at the interfaces.

1.3 Multilayer Research

Magnetic reflective multilayers, first reported in 1940[19], have led to breakthroughs in magnetoresistance[20,21] and novel applications based on oscillatory interlayer exchange coupling[22]. But more importantly, they have led to a novel understanding of thin film physics, including surface free energy driven (surfactant-mediated) thin layer growth, diffusion and compound formation at interfaces, etc. Non-magnetic multilayers are often used as reflective or transmissive (filtering) optics in EUVL as well as in astronomy and in medical applications. These applications generally share the fundamental requirement that the multilayers have (often atomically) sharp refractive index profiles, and that they

remain inert against surface chemistry and interlayer formation. Development of multilayer optics for these applications therefore generally requires a fundamental understanding and sub-nanometer manipulation of the physics and chemistry that dominate the processes at interfaces and surfaces.

1.3.1 Layer and Interface Growth

When one material is deposited on another material, differences in lattice parameters can result in stress at the interface. In the case of Mo and Si, this so-called growth stress will result in the occurrence of tensile stress for a Mo-fraction (Γ) larger than 0.5, while compressive stress will occur for $\Gamma < 0.5$. Since for optimum reflection a Γ of 0.4 is required, relaxation of the compressive stress will result in substrate deformations at levels unacceptable for EUV applications. In the case of vapor deposition, this can be compensated by several periods with $\Gamma > 0.5$ underneath the actually reflecting multilayer[23,24,25].

Important reasons that the 74% theoretical reflection limit is not reached in practice are the 5-10% lower than bulk densities, the roughness of layer growth and diffuseness at the Mo/Si interfaces. The average diffuseness is of atomic dimensions (~0.3 nm) but nevertheless causes diffuse reflection at the cost of specular reflection. Surface roughness can effectively be smoothened by means of noble gas ion polishing of the deposited layer. The kinetic energy E_k of the ions will add to the mobility of surface atoms that can result in a smoother lateral repositioning. The effect is very much dependant on E_k, the ion to atom mass ratio, and the incidence angle. Besides smoothening surface roughness and increasing the layer density, surface bombardment using noble gas ions also changes the stress and degree of crystallization inside the layers, especially when applied on the polycrystalline Mo layer[26]. As discussed previously, relaxation of the stressed layers yields distortions in the substrate, and ion polishing is therefore in practical application to the Mo/Si multilayers only applied on the surface of the Si layer, optimizing the layer properties.

Since Si has a higher surface energy than Mo, interfaces where Si is deposited on Mo yield less segregation and diffusion than vise versa[27,28,29,30,31]. The difference in crystallinity of the Mo and Si layers further adds to this asymmetry. With reflectometry and x-ray photoelectron spectroscopy (XPS), we observe formation of kinetically favorable silicide interlayers with intermediate optical properties[11,12,32]. The enthalpy of interface formation ($\Delta H^{interface}$) describes the interaction between layers. We observe in chapter 3 that the endothermic $\Delta H^{interface}$ of the Mo substrate layer with the Au and Cu capping layers yields insufficient adhesion and island growth. The growth of a Ru capping layer on a Si substrate layer as investigated in chapter 5 results in a broad interface gradient. It has been proven with a Fourier multilayer reflection theory that interface gradients reduce the reflectivity[33]. Applying a diffusion barrier at the Ru/Si and Mo/Si interface can reduce the intermixing and thereby compensate the effect of reduced interface sharpness. Following the results that are described in chapter 6, MoB was found to be a chemically and optically attrictive compound material and has been patented for this purpose[34]. A more commonly used material that we investigated in chapter 6 and shows interesting features is B_4C[12,35,36]. It is also used as spacer in the B_4C/La optics for λ = 6.7 nm, as described in chapter 7 and 8[8,9,37]. Chapter 8 also reveals the improvement

that can be achieved with nitridation to BN and LaN in these optics, of which the application has also been patented[10].

1.3.2 Surface chemistry

The main focus of the research described in this thesis relates to the multilayers surfaces. Several physical and chemical processes are accelerated by the photo exposure of the multilayer to high EUV fluxes in the oxygen containing lithography tool environment. These processes include e.g. diffusion and oxidation, rendering Mo and Si unsuited for multilayer surface protection. Many capping material candidates have already been tested, among which a passivated Si surface[38,39,40,41]. From a kinetic perspective, the binding energy is however too low to prevent bond breaking by EUV photons. Another possibility is a metal layer that can withstand the EUV radiation. Numerous metals in a range of layer thicknesses have been studied as a part of this thesis, revealing that some actually increase oxidation of the underneath Mo[13]. Selection of a suitable material and layer thickness is essential not to lower initial reflectivity by more than a few percent and simultaneously prevent further deterioration under EUV illumination[42,43,44].

A common problem besides oxidation is the fact that metals often catalyze hydrocarbon dissociation by secondary electron emission - especially during EUV illumination - resulting in a carbon contamination covering the surface. The thickness of the contamination layer will attenuate the standing wave in the multilayer and reflect out of phase, consequently influencing the overall reflection. To balance the effects of surface contamination and oxidation, a higher oxygen partial pressure could be allowed, resulting in “burning away” part of the carbon contamination. This effect is confirmed by Low Energy Ion Scattering (LEIS) measurements performed by Calipso that are presented in this thesis[14]. We have shown that the carbon contamination at the investigated metal caps can be chemically eroded by atomic O exposure, after which the oxidized cap can be fully reduced to metallic state by subsequent atomic H exposure[14].

1.4 The Contribution of this Thesis

One of the most strenuous and ambitious goals in the XMO program is to further increase the multilayer peak reflectance from 63% to 68%, enabling a more than 100% increase of the optics throughput, and to simultaneously improve the effective lifetime from 300 to 30.000 hours. It has become clear that especially the latter improvement calls for a nanometer thin protective capping layer on top of the already highly perfected Mo/Si multilayer optics[45]. The capping layer should protect against oxidation and be non-destructively cleanable from carbonaceous contamination that physisorb and dissociate under the enormous radiation fluxes of the EUV source. The physical and chemical phenomena occurring in the surface region have therefore been an important object of study in this work. Chapters 5 and 6 describe new insight on chemically driven diffusion of capping layer material through Mo[11] or B_4C[12], and in-depth agglomeration of capping material at the subsurface Si-on-Mo interface. On the basis of this research, MoB_x was found to enhance both the chemical stability and the optical contrast of interfaces, and was patented for the application as interface diffusion barrier[46]. Also nitrides can have favorable barrier- and optical properties in multilayer optics for EUVL and beyond, as will be shown in chapter 8.

The growth and oxidation of capping layers on Mo in relation to their thickness is investigated in chapter 3. We observe sacrificial oxidation in the interaction of the capping layers and the Mo substrate layer[13]. The findings could readily be applied in the rapidly growing field of nano-devices to control oxidation that would render electronics useless. Contamination, oxidation, and cleaning of the surface are further studied in chapter 4. The investigations reveal a significantly improved atomic oxygen and subsequent hydrogen surface cleaning technique to remove the problematic carbonaceous contamination and oxidation[14]. This technique is adaptable to a wide range of nano-devices and could even have spin-offs to the more or less reversed process of photo dissociation of water to oxygen and hydrogen to generate clean fuels, as currently studied at Rijnhuizen in the new research theme ‘physics for energy’.

Chapters 7 and 8 describe our research on reflective multilayer optics that include combinations of B or B_4C with metals such as La, Th and U[8]. Our studies on diffusion and surfactant-mediated growth of nitridated B_4C/La interfaces[9] have resulted in a patented invention[10] that enables a major increase of peak reflectance and bandwidth. This makes future application of the optics soft x-ray lithography and free electron lasers for $\lambda < 7.00$ nm realistic. We are currently carrying out further experiments on the optics lifetime at the X-FEL free electron laser in Hamburg, Germany. With the latest results of this research and the patent in the portfolio, a project on multilayer optics for this wavelength region has recently been initiated.

1.5 References

[1] B. Fay, Microelectronic Engineering 61, 11 (2002).
[2] T. Honda, Y. Kishikawa, Y. Iwasaki, A. Ohkubo, M. Kawashima, M. Yoshii, J. Microlith., Microfab., Microsyst. 5, 043004 (2006).
[3] D. Vogler, "Brion powers up to meet DPT challenges at 32nm-22nm Solid State Technology" (2008).
[4] C. Taylor, "Samsung intros 64-Gbit MLC NAND chip," Electronic News, 2007
[5] M. D. Levenson, "SPIE: Tela Innovations lays it all out straight", Microlithograpy World (2008).
[6] www.asml.com/euv
[7] J.E. Bjorkholm, EUV Lithography—The successor to optical lithography, Intel Technology Journal Q3 (1998).
[8] T. Tsarfati, E. Zoethout, R. W. E. van de Kruijs, E. Louis, F. Bijkerk, submitted
[9] T. Tsarfati, R. W. E. van de Kruijs, E. Zoethout, E. Louis, F. Bijkerk, submitted
[10] T. Tsarfati, E. Zoethout, E. Louis, F. Bijkerk, “Method to Enhance layer contrast of a multilayer for reflection at the B absorption edge”, US 61/079307 (US), DE102008040265 (Germany), priority date 16 September 2008
[11] T. Tsarfati, E. Zoethout, R. W. E. van de Kruijs, F. Bijkerk, J. Appl. Phys. 105, 064314 (2009).
[12] T. Tsarfati, E. Zoethout, R. W. E. van de Kruijs, F. Bijkerk, J. Appl. Phys. 105, 104305 (2009).
[13] T. Tsarfati, E. Zoethout, R. W. E. van de Kruijs, F. Bijkerk, Surf. Sci. 603, 7, 1041 (2009).
[14] T. Tsarfati, E. Zoethout, R. W. E. van de Kruijs, F. Bijkerk, Surf. Sci. (2009)

[15] O. Wood et al., “Integration of EUV lithography in the fabrication of 22-nm node devices”, Proc. SPIE Advanced Lithography 7271, 03 (2009).
[16] E. Spiller, Soft X-Ray Optics (1994).
[17] D. Attwood, Soft X-Rays and Extreme Ultraviolet Radiation (2000).
[18] C. Kittel, Introduction to Solid State Physics, John Wiley & Sons, 7 (1996).
[19] J. DuMond, J.P. Youtz, J. Appl. Phys. 11 (5), 357 (1940).
[20] G. Binasch, P. Grünberg, F. Saurenbach, and W. Zinn, "Enhanced Magnetoresistance in Layered Magnetic Structures with Antiferromagnetic Interlayer Exchange," *Phys. Rev. B* 39, No. 7, 4828 (1989).
[21] M. N. Baibich, J. M. Broto, A. Fert, F. Nguyen van Dau, F. Petroff, P. Etienne, G. Creuzet, A. Friederich, and J. Chazelas, "Giant Magnetoresistance of (001)Fe/(001)Cr Magnetic Superlattices," Phys. Rev. Lett. 61, 2472 (1988).
[22] S. S. P. Parkin, N. More, and K. P. Roche, "Oscillations in Exchange Coupling and Magnetoresistance in Metallic Superlattice Structures: Co/Ru, Co/Cr, and Fe/Cr," *Phys. Rev. Lett.* 64, 2304 (1990).
[23] D. Sander, Surface stress: implications and measurements, Solid State and Materials Science 7, 51 (2003).
[24] T.D. Nguyen and T.W. Barbee jr, Stress in Molybdenum/Silicon and di-Molybdenum Carbide/Silicon Multilayer Structures, UCRL-JC-128609 Abs M-000049-01
[25] L.J. Chen, Solid state amorphization in metal/Si systems, Materials Science and Engineering, R29, 115 (2000).
[26] D.E. Savage, J. Kleiner, N. Schimke, Y-H. Phang, T. Jankowski, J. Jacobs, R. Kariotis and M.G. Lagally, Determination of roughness correlations in multilayer films for x-ray mirrors, J. Appl. Phys., 69, 3 (1991).
[27] G. Rossi, I. Abbati, L. Braicovich, I. Lindau, and W. E. Spicer, J. Vac. Sci. Technol. 21, 617 (1982); G. Rossi, I. Abbati, L. Braicovich, I. Lindau, and W. E. Spicer, U. Del Pennino, and S. Nannarone, Physica B+C 117&118B, 795 (1983).
[28] I. Abbati, L. Braicovich, B. De Michelis, A. Fasena, E. Puppin, and A. Rizzi, Solid State Commun. 52, 731 (1984); I. Abbati, L. Braicovich, B. De Michelis, A. Fasena, and A. Rizzi, Surf. Sci. 177, L901 (1986).
[29] T. T. A. Nguyen and R. C. Cinti, J. Phys. (Paris) Colloq. 45, C5-435 (1984).
[30] H. Balaska, R. C. Cinti, T. T. A. Nguyen and J. Derrien, Surf. Sci. 168, 225 (1986).
[31] H. L. Meyerheim, U. Döbler, A. Puschmann and K. Baberschke, Phys. Rev. B 41, 5871 (1990).
[32] I. Nedelcu, R. W. E. van de Kruijs, A. E. Yakshin, F. D. Tichelaar, E. Zoethout, E. Louis, H. Enkisch, S. Müllender, F. Bijkerk, “Interface roughness in Mo/Si multilayers”, Thin Solid Films 5151, 2, 434 (2006)
[33] M. J. H. Kessels, dissertation (2005).
[34] R. W. E. van de Kruijs, S. Bruijn, T. Tsarfati, A.E. Yakshin, F. Bijkerk, E. Louis, “Reduction of diffusion at Mo/Si interfaces by boride barriers and boron passivation”, P17091PUSPRO, priority date 7 May 2008
[35] I. Nedelcu, R. W. E. van de Kruijs, A. E. Yakshin, F. Bijkerk, “Microstructure of Mo/Si multilayers with B_4C diffusion barrier layers”, Appl. Opt. 48, 2, 155, 2009
[36] H. Maury, P. Jonnard, J.-M. André, J. Gautier, F. Bridou, F. Delmotte, M.-F. Ravet, “Interface characteristics of Mo/Si and B_4C/Mo/Si multilayers using non-destructive X-ray techniques”, Surf. Sci. 601, 11, 2315 (2007)

[37] C. Michaelsen, J. Wiesmann, R. Bormann, C. Nowak, C. Dieker, S. Hollensteiner, and W. Jäger, Multilayer mirror for x rays below 190 eV, Optics. Lett. 26, 11 (2001)
[38] G. Agostinelli, P. Vitanov, Z. Alexieva, A. Harizanova, H. F.W. Dekkers, S. de Wolf, G. Beaucarne; Surface Passivation of Silicon by Means of Negative Charge Dielectrics, 19th EU-PVSEC, 132 (2004).
[39] M. Malinowski, C. Steinhaus, M. Clift, L. E. Klebanoff, S. Mrowka, R. Soufli, "Controlling Contamination in Mo/Si Multilayer Mirrors by Si Surface-capping Modifications", Proc. SPIE 4688, 442 (2002).
[40] M.M. de Lima jr., F.L. Freire jr., and F.C. Marques, "Boron Doping of Hydrogenated Amorphous Silicon Prepared by rf-co-Sputtering", Braz. J. Phys. 32, 2A, 379 (2002).
[41] Y. -F. Chen, Role of Bonded Interstitial Hydrogen in Hydrogenated Amorphous Silicon: A New Perspective, Chinese Journal of Physics, 31, 3 (1993).
[42] M. Singh, J.J.M. Braat, Capping layers for extreme-ultraviolet multilayer interference coatings, Opt. Lett. 26, 5, 259 (2001).
[43] M. Malinowski, L. Klebanoff, M. Clift, P. Grunow, C. Steinhaus; Carbon Deposition and Removal on Mo/Si Mirrors (2000).
[44] R.W.E. van de Kruijs, P. Suter, E. Zoethout, A. Yakshin, E. Louis and F. Bijkerk, H. Trenkler, M. Weiss, S. Müllender and M. Wedowski, R. Klein, J. Tümmler and F. Scholze, B. Mertens, Optimization of a protective capping layer for Mo/Si based EUV Optics, Abstract for Physics of X-Ray Multilayer Structures PXRMS, Japan (2004).
[45] S. Bajt, H.N. Chapman, N. Nuygen, J. Alameda, J. C. Robinson, M. Malinowski, E. Gullikson, A. Aquila, C. Tarrio, S. Grantham, Design and Performance of Capping Layers for EUV Multilayer Mirrors, Appl. Opt. 42, 28, 5750 (2003).
[46] R. W. E. van de Kruijs, S. Bruijn, T. Tsarfati, A.E. Yakshin, F. Bijkerk, E. Louis, "Reduction of diffusion at Mo/Si interfaces by boride barriers and boron passivation", P17091PUSPRO, priority date 7 May 2008

2 Experimental

2.1 Thin Layer Growth

The multilayers that have been investigated in this thesis were deposited in a UHV thin film deposition facility. At FOM Rijnhuizen, two deposition facilities are currently in use; the Multilayer Coating facility (MUCO) and the Advanced Deposition Coating facility (ADC). Both systems are based on the same principles, with the ADC having slightly different in-situ deposition and additional in-vacuo analysis facilities. In both coating facilities, the deposition takes place in ultra high vacuum environment, with the MUCO facility schematically shown in Fig. 3. Deposition sources are used to evaporate or sputter from a deposition target onto a substrate holder which rotates to average over deposition flux instabilities. The film growth can be monitored by an in-situ x-ray reflectometer and an array of quartz mass balances. An ion source can be used to supply a large area, low energy, ion beam for thin film surface treatment. The various components used in the deposition process are described in more detail in the next sections.

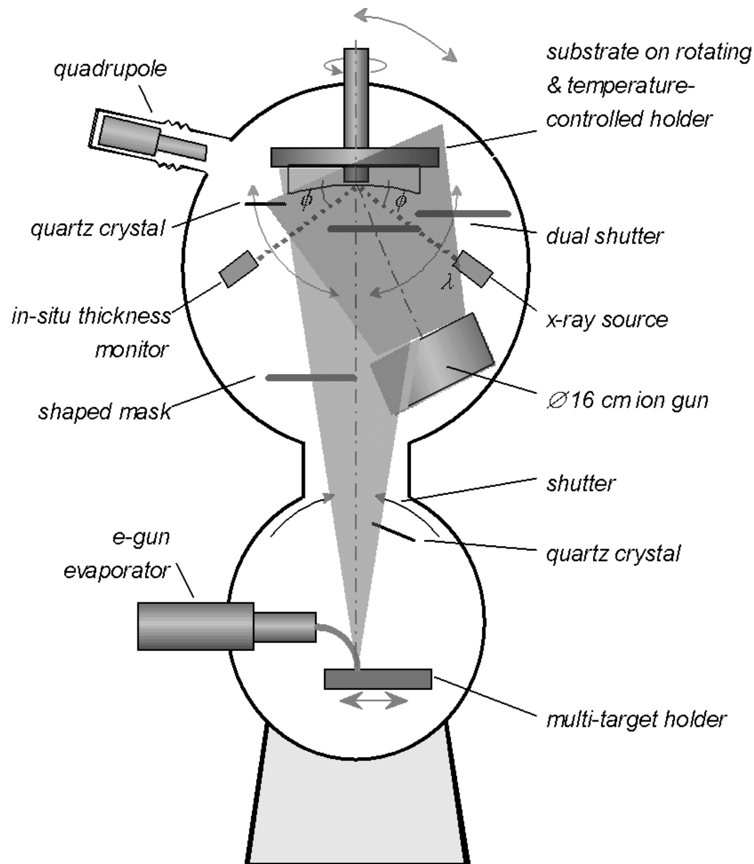

Figure 3: *Schematic overview of the MUCO deposition facility.*

2.1.1 Magnetron Sputter Deposition

To achieve deposition of composite materials, magnetron sputter deposition is commonly used. In a magnetron tube, a cathode emits electrons that migrate towards a circular anode that surrounds the cathode. A magnetic field perpendicular to the moving electrons causes the electrons to assume a circular motion, lengthening their path in a confined area. The gas led into the tube is then ionized by electron impact to create a plasma. The ions produced in the magnetron tube accelerate towards the negatively biased target surface. When accelerated ions collide with target atoms, their kinetic energy can break bonds and sputter target atoms. The ions impinging on the target will also cause emission of secondary electrons, which in turn are accelerated away from the target by the electric field, ionizing more gas atoms upon collision and sustaining the discharge. The deposition rate can be up to a few nm/s for some materials, with an adatom energy of typically tens of eV or more, but these values are dependant on e.g. the choice of gas and plasma power. The ADC employs magnetrons with DC power supplies that can be pulsed up to 100 kHz for materials with insufficient conductivity. Non-conducting materials can be sputtered by magnetrons with RF power supply.

2.1.2 Physical Vapor Deposition

Another common way to deposit an atomically thin layer of material on a substrate is to create a vapor. Vaporization can be achieved by an electron gun. The impact point of the electron beam on the target is swept over the target surface area to assure a homogeneous melt and evaporation.. The deposition rate of the electron beam evaporation process can fluctuate since the vapor pressure is highly dependent on small changes in temperature and morphology of the target that occur over time. The substrate is shielded from the target by a shutter, which is opened when a stable flux is achieved. The shutter is again closed when the required layer thickness is achieved. For conventional thermal evaporation, the adatom kinetic energy generally is below 0.5 eV, determined by the vapor pressure and surface temperature of the material and not adjustable. The low energy minimizes crystallization and damage to the previously deposited film. A drawback is the lower mobility for lateral distribution, resulting in rougher, stochastic growth and a lower layer density. Several compounds dissociate before evaporation and can therefore result in off-stochiometric growth conditions. Depending on required layer growth conditions, vapor or magnetron deposition is chosen for layer growth.

2.1.3 Ion Bombardment

Deposited layers can be smoothened by increasing the mobility of the surface atoms via high energy noble ion bombardment. At a given energy, heavier ions such as Kr^+ have a smaller mean free path, thereby limiting distortion of the subsurface interface. Besides smoothening by lateral repositioning, the ion beam can also smoothen the film via physical sputtering due to preferential sputtering of surface adatoms. For chemical passivation of surfaces and interfaces, also non-noble gasses can be ionized, like in the case of B_4C/La nitridation as described in chapter 8. The ions are produced in a Kaufmann discharge chamber that is bound by pole pieces and anodes on the sides and an accelerator system that covers the downstream end of the chamber. Bombardment of electrons supplied by a filament cathode ionizes the gas. The magnetic fields between the pole pieces shield the anodes, forcing the electrons to follow lengthy paths before reaching the anodes and increasing the probability of ionizing collisions with the neutral

gas atoms in the discharge chamber. The ions produced within the discharge chamber move with near equal probability in all directions. The ions that collide with the anode or other discharge chamber surfaces are lost and recombine with free electrons at those surfaces and then reenter the discharge chamber as neutral atoms. Ions reaching the downstream end are accelerated through the apertures in the negative accelerator grid. The accelerated ions form the directed beam of energetic ions. A neutralizer can be used to provide electrons to the positive ion beam, when charging of a target is undesirable. The neutralizing electrons are readily distributed within the beam's conducting plasma to give a near uniform beam potential for most operating conditions. Beam analysis is performed with a Faraday cup or Retarding Field Analyzer.

2.2 Characterization

2.2.1 Quartz Crystal Microbalances

During deposition, the rate and layer thickness are monitored by off-center positioned quartz crystal microbalances (Fig 4). Their working is based on their mass dependant resonant oscillation frequency. Calibrating for mass density, the frequency derivative during layer deposition and etching is an accurate measure of the growth and etch rate. They are also sensitive to heat changes in their environment, including those from magnetron PVD and ion sources, limiting their applicability for absolute thickness measurements with resolutions beyond ~10^{-2} nm.

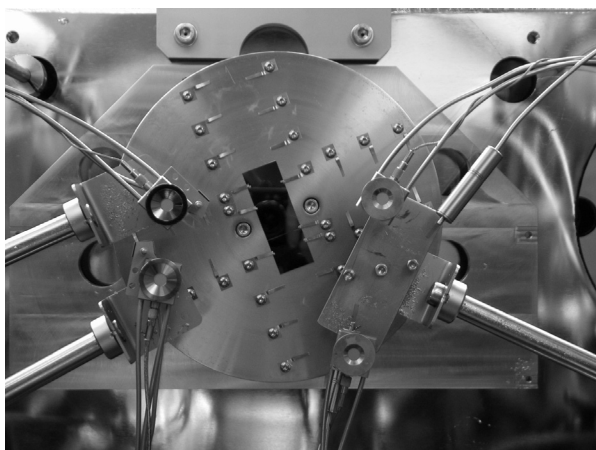

Figure 4: *The rotatable ADC substrate holder with three mounted Si substrate wafers. The four quartz crystal microbalances are visible towards the sides.*

2.2.2 Mass Spectrometry

Mass Spectrometry covers a wide range of techniques with different applications that characterize the mass-to-charge ratio (m/q) of charged particles. It is as such very suited to quantify the vacuum conditions in the deposition setup and the desorption of volatile species from a surface. Particles trapped in the nozzle are ionized and partially dissociated by either electron impact ionization (EI), field ionization (FI), or chemical ionization (CI). Dissociation can help to identify to original molecule. EI occurs by a highly energetic primary electron, usually generated from a tungsten filament. FI removes the electrons from any species by interaction with an intense electrical field. CI forms new ionized species when gaseous molecules interact with ions. Selection by m/q usually occurs in quadrupole or magnetic sector analyzers that use oscillating field selectively stabilizing only certain m/q ions to reach the electron multiplier tube or Faraday cup. Single focusing magnetic sector analyzers focus a circular beam in a path of

180, 90, or 60º. The ions are spatially separated due to their different mass-to-charge ratios. In double focusing analyzers, an electrostatic analyzer is added to separate ions with different kinetic energies. The MUCO, ADC, and atomic H and O exposure chamber as employed in chapter 4 are all equipped with a quadrupole mass spectrometer. In chapter 4 we perform desorption spectroscopy to monitor for e.g. hydrocarbons, H_2O, CO_2, and volatile metal oxides that can desorb from the surface during atomic H and O exposure.

2.2.3 Reflectometry

More extensive optical characterization of the multilayer is possible with ex-situ λ = 0.154 nm Cu-K_α reflectometry. For that purpose, the detector is placed 2θ off axis of the source beam line and the specular reflection is measured for variable θ angles (Fig. 5a) This defines the scattering vector perpendicular to the surface plane and identifying changes in optical density along that vector. Following the modified Bragg law in equation (2), interference peaks at the specific grazing angles reveal the layer thickness, density, and interface diffusiveness. At higher diffraction angles, smaller distances are probed and enable the characterization of the atomic lattice structure of crystalline phases inside the layers.

More extensive optical characterization of the multilayer is possible with ex-situ λ = 0.154 nm Cu-K_α reflectometry. For that purpose, the detector is placed 2θ off axis of the source beam line and the specular reflection is measured for various θ angles, which defines the scattering vector perpendicular to film planes and identifies changes in optical density along that vector (Fig. 5a). Since the beam is partially reflected at each multilayer interface, interference causes a strong angular dependence on the reflection. Following Bragg's law in equation (2), interference peaks at the specific grazing angles reveal the layer thickness, density, and interface diffusiveness, while analysis of the broader spectrum range enables detailed study of crystallites[1]. The technique was mainly used in chapter 7 and 8 to study the layer and interface properties of the novel B_4C/La multilayers. To further study changes in optical density along the surface, e.g. interface diffuseness and surface roughness, the diffuse reflection is measured in a ω-2θ scan. Having the detector at a fixed 2θ, the sample is laterally rotated ("rocked") to measure a range of diffuse scattering angles (Fig 5b).

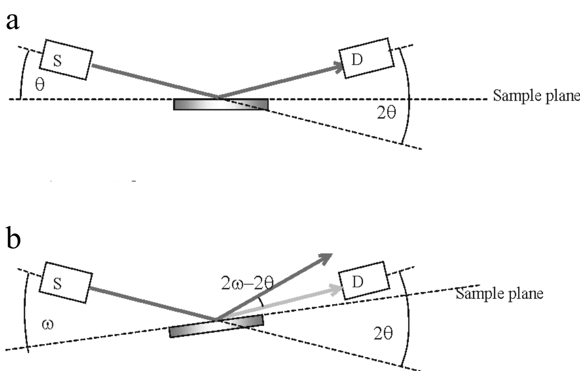

Figure 5: *a) In the θ-2θ scan, specular reflection for various angles is measured during a θ-sweep of source and detector. b) During a ω-2θ scan, source and detector are at fixed position while the multilayer is "rocked", thus measuring diffuse scattering.*

Cu-K_α reflectometry at λ = 0.154 nm is able to provide detailed information on the internal structure, periodicity, and roughness of layered structures. In addition, reflectance measurements performed at 13.5 nm wavelength using synchrotron radiation

sources are used to ultimately link the structural information obtained from other analysis techniques to the device performance at 13.5 nm and normal incidence geometry.

2.2.4 Low Energy Ion Scattering

Low Energy Ion Scattering (LEIS) is based on the energy analysis of probing noble gas ions after elastically scattering from substrate atoms at the surface monolayer (Fig. 6). Depending on their mass ratio (m_r) and the scatter angle (θ), the initial energy (E_0) of typically 0.5 - 20 keV is partially transferred from the incident ion to the target atom. The energy retained (E_1) follows from conservation of momentum and energy in an elastic two-body collision;

$$E_1 = E_0 \left(\frac{m_r \cos\theta + \sqrt{1 - m_r^2 \sin^2\theta}}{1 + m_r} \right)^2 ; \quad m_r = \frac{m_1}{m_2}, \tag{3}$$

and with the mass of the probing ion (m_1) and θ known in an experimental setup with fixed ion source and detector, the mass of the target atom (m_2) is directly obtained. The ions that penetrate the target beyond the surface atomic layer have a high neutralization probability. When they scatter deeper in the bulk and are reionized, they will appear in the LEIS energy spectrum as background with an energy loss that relates to their travel distance. Although particularly suited for elemental analysis of the surface monolayer, LEIS can thus also be used for in-depth studies of e.g. diffusion[2]. The probing depth further increases for medium and high E_0 (MEIS and HEIS), at the cost of surface sensitivity.

For optimum sensitivity and discrimination, the probing ions should be approximately 40% of the target atom mass. For the analysis of carbon contamination in chapter 4, $^3He^+$ is most suited, which can also be used for oxygen and silicon identification with a detection limit in the order of 1%. For higher Z elements, primary $^{20}Ne^+$ can yield a detection limit up to 10 ppm. The elemental sensitivity is determined by mass and nuclear charge of both primary ion and target atom, as well as the energy levels of especially the inner-shell electrons of the target atom. In general, it does not differ more than a factor of 10 for a given primary ion. LEIS has specific sensitivity for the surface monolayer, which is of interest for contamination studies of capped multilayers as presented in chapter 4.

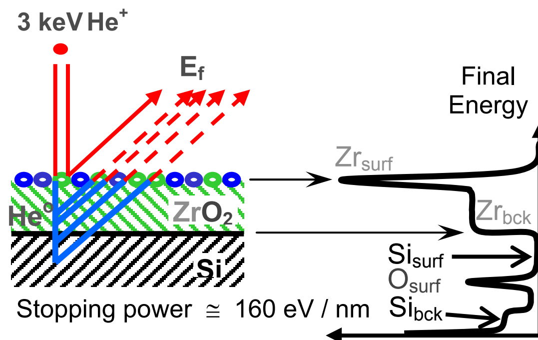

Figure 6: *LEIS, with surface monolayer sensitivity.*

2.2.5 X-ray Photoelectron Spectroscopy

XPS is because of its physical and chemical characterization ability the main technique employed in this thesis. It was developed into an analytical tool in the mid 1960s by Kai Siegbahn et al. who won the Nobel prize for it. The technique is based on the

photoelectric effect discovered by Heinrich Rudolf Hertz in 1887 and further described by Albert Einstein, for which he won the Nobel prize in 1921. By irradiating a sample with monochromatic soft-ray photons of energy $h\nu$, photoelectrons (e^-_p) are generated of which the original binding energy E_b in its atomic orbital can be retrieved via

$$E_b = h\nu - E_k - \Phi_s, \tag{4}$$

with E_k the kinetic energy of the e^-_p and Φ_s the spectrometer work function (Fig. 7a). With $h\nu$ and Φ_s known, E_b follows directly from measurement of E_k and should be regarded as the energy difference between the initial and final states after the photoelectron has left the atom. There are several final states of ions for every element with each a certain photoelectric cross-section (σ), and all but the s orbital become split upon ionization, yielding doublet peaks with a fixed ratio between the peak area. Different elements can have spectral peaks that overlap, e.g. the $Ru3d_{5/2}$ and C1s peak. In our extensive studies of Ru and C, quantification was possible by considering the $Ru3d_{3/2}$ peak area. The area follows from the number of photoelectrons per second of specific E_k, given by

$$I = nf\sigma\varphi y\lambda AT, \tag{5}$$

with f the source flux, φ an angular efficiency factor for the instrumental arrangement based on the angle between e^-_p and the photon path, y the efficiency in the photoelectric process for formation of e^-_p of the normal E_k, λ the e^-_p mean free path in the sample, A the area of the sample from which e^-_p are detected, and T the detection efficiency for e^- emitted from the sample. The combined terms make up for the atomic sensitivity factor (S) from which quantification of the number of atoms per unit area (n) is possible through peak area fitting.

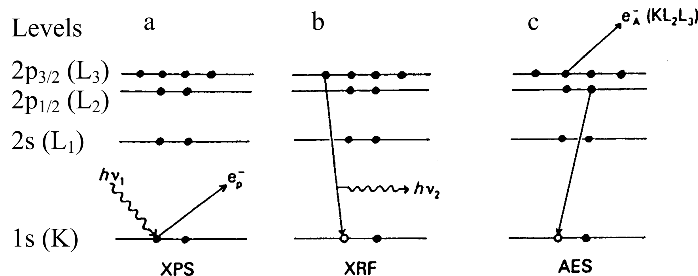

Figure 7: *The basic principle of XPS (a), XRF (b) and AES (c).*

With the atomic orbitals identified, not only the elemental constituency and concentration but also their chemical state can sometimes be determined in the probing depth of typically 5 to 7 nm. The latter feature arises from differences in chemical potential and electronic polarizability of compounds that cause a chemical shift of the photoelectron peaks in the spectrum. We exploited this feature extensively in our research, by monitoring the peak shifts from their elemental value, in relation to the Fermi level. Especially for this analysis, care should be taken to prevent sample charging. The spectrum can also feature Auger, shake-up, energy loss and valence lines and bands as well as multiplet splitting that result from - and can provide information on - variations in the relaxation process. For imperfectly monochromated sources, x-ray satellites and ghost lines can be visible in the spectrum that complicate the analysis. Upon creation of a core level hole, the electron relaxation process can also yield x-ray fluorescence (XRF), as shown in Fig. 7b.

To obtain non-destructive depth resolution within the probing depth range, in chapters 3 and 4 we performed Angular Resolved XPS (ARPES) between 27° and 64° off normal detection. The measurements are modeled to a homogeneous layered system[3] using the factor $e^{\frac{-z}{\lambda \cos\theta}}$ from the depth distribution function that relates the detection angle θ via the attenuation length[4] λ to the sampling depth z. In the case of non-homogeneous layer growth, the set of conditions as described by P. J. Cumpson[3] is not fulfilled and the modeling can result in estimated layer thickness and in-depth distribution errors of up to several nanometers[5].

Further in-depth characterization is possible by repeatedly etching the surface and recording the XPS spectrum. We use low energy (0.5 keV) Ar^+ at 45° incidence to reduce ion beam induced intermixing and forward sputtering to determine the in-depth distribution and compound formation in the multilayers. The penetration and possible ion mixing depths of the used 0.5 keV Ar^+ sputter ions at 45° incidence are ~1.6 nm in Si, ~1.3 nm in B_4C, and ~0.7 nm in d-metals like Mo and Ru[6]. Considering the ~0.7 nm inelastic mean free path of the photoelectrons, the calculated ion mixing components are minor to moderate. Differences in sputter efficiency and electron escape depths for the different materials can result in quantification errors of specific materials. The effect is of negligible influence for the in-depth analysis performed in chapters 5 and 6, considering the focus on the surface composition, and not on the multilayer periodicity. Compensation via the known as-deposited ratio was therefore not carried out. We verified that the observed diffusion was kinetically favored by further reducing the ion energy to 0.25 keV and annealing the sample in specific cases.

The approximate multilayer profile can be reconstructed using the atomic mixing and information depth component from the mixing-roughness-information depth (MRI) model[7]. With a calculated atomic mixing (g_w) of 2 nm and an information depth (g_λ) of 3 nm in linear approximation for a B_4C/La multilayer, we can in chapter 8 e.g. model a 0-100% interface gradient of 1 nm, leaving pure B_4C and La layers of ~0.6 and 0.8 nm thickness respectively.

2.2.6 Auger Electron Spectroscopy

An electron vacancy in the core shell will be filled by a higher shell electron. The usually large energy difference between the two electron orbitals can either be released as an x-ray photon in a process commonly known as fluorescence, or by emission of a so-called Auger electron (Fig. 7c). Their generation yield is higher for irradiation by several keV electrons than by soft x-ray photons. Auger Electrons Spectroscopy (AES) generally employs a monochrome field emission gun (FEG). As an electron beam can readily be focused, this also enables sub-μm resolution Scanning Auger Microscopy (SAM) to elementally map a surface area. The E_k of an Auger electron emitted during non-radiative relaxation can be related to the involved atomic orbitals via

$$E_k = E_b - E_1 - E_2 \quad , \tag{6}$$

with E_b, E_1, and E_2 respectively the core level, first outer shell, and second outer shell electron binding energy. Because the nature of Auger electrons solely lies in relaxation via electron rearrangement, $h\nu$ does not appear in equation (6). The E_k and probing depth are lower than in XPS, which we use in chapter 5 to obtain higher resolution for in-depth

analysis. The Auger peaks appear on a major background of primary and secondary electrons, and element quantification is usually done via derivation of the spectrum and measuring peak-to-valley height with a dependency that resembles equation (5). Their shapes can give insight in the chemical state.

2.2.7 Atomic Force Microscopy

To study the morphology of surfaces, further characterization of capping layer growth is in chapter 3 and 6 performed with atomic force microscopy (AFM). The surface is probed by a tip with a radius of curvature on the order of nanometers at the end of a microscale cantilever. In proximity of a sample surface, forces between the tip and the sample lead to a deflection of the cantilever that can be measured using a laser, optical interferometry, capacitive sensing or piezoresistivity. Depending on the situation, mechanical contact, Van der Waals, capillary, chemical, electrostatic, magnetic, Casimir, and solvation forces can be measured with AFM. In most cases a feedback mechanism is employed to adjust the tip-to-sample distance to maintain a constant force between the tip and the sample, which is generally mounted on a moving piezoelectric tube. AFM is in general operated in contact or tapping mode. Surface roughness well below a nanometer can usually be resolved at a lateral resolution of several to tens of nanometers. AFM has in chapter 3 showed that high roughness and probably island growth occurs in the case of Au and Cu caps on a Mo substrate layer.

2.2.8 Electron Microscopy and Spectroscopy

The diffusion in multilayers is further investigated with cross section transmission electron microscopy (CS-TEM). A focused high energy electron beam (40 to 400 keV) penetrates a thin perpendicular slice of the multilayer. It contains information about the structure of the slice that is magnified by an objective lens system. The spatial variation in this information is viewed by projecting the magnified electron image onto a fluorescent viewing screen coated with a phosphor or scintillator material. The image can be photographically recorded by exposing a photographic film or plate directly to the electron beam, or a high-resolution phosphor may be coupled by means of a lens optical system or a fiber optic light-guide to the sensor of a charge-coupled device (CCD) camera. The resolution that can be achieved is primarily limited by spherical aberration, sample preparation and alignment. Spherical aberrations can be corrected to allow the production of images with sufficient resolution to show carbon atoms in silicon at 0.078 nm at magnifications of 50 million times in high resolution TEM[8]. In our analysis, sample preparation is the critical step, as adhesion of the layers might be lost, and parts of the slice are damaged upon thinning by ions. The multilayer cross section is aligned via the crystalline Si substrate, allowing sub-nm analysis of polycrystallinities and interface diffuseness. Elemental identification can be obtained by spectral analysis of refracted and scattered electrons in electron energy loss spectroscopy (EELS), energy dispersive x-ray analysis (EDX), and elastic recoil detection (ERD).

2.3 References

[1] I. Nedelcu, R. W. E. van de Kruijs, A. E. Yakshin, F. Bijkerk, Phys. Rev. B 76, 245404 (2007)
[2] V. I. T. A. de Rooij-Lohmann, A. W. Kleyn, F. Bijkerk, H. H. Brongersma, A. E. Yakshin, Appl. Phys. Lett. 94, 063107 (2009)
[3] P.J. Cumpson, J. Elec. Spec. Rel. Phen. 73, 25 (1995)
[4] S. Tanuma, C.J. Powell, D.R. Penn, Surf. Interface. Anal. 17, 911 (1991)
[5] P.C. Zalm, Surf. Interface Anal. 26, 352 (1998)
[6] J. F. Ziegler, and J. P. Biersack, Computer code SRIM 2008 program package, http://www.srim.org
[7] S. Hofmann, Surf. Interface Anal. 27, 825 (1999).
[8] P . D. Nellist, M. F. Chisholm, N. Dellby, O. L. Krivanek, M. F. Murfitt, Z. S. Szilagyi, A. R. Lupini, A. Borisevich, W. H. Sides, Jr., S. J. Pennycook, "Direct Sub-Angstrom Imaging of a Crystal Lattice". Science 305**,** 1741 (2004).

3

3 Growth and sacrificial oxidation of transition metal nanolayers

3.1 Abstract

Growth and oxidation of Au, Pt, Pd, Rh, Cu, Ru, Ni and Co layers of 0.3 to 4.3 nm thickness on Mo have been investigated with ARPES and AFM. Co and Ni layers oxidize while the Mo remains metallic. For nobler metals, the on top O and oxidation state of subsurface Mo increase, suggesting sacrificial e^- donation by Mo. Au and Cu, in spite of their significantly lower surface free energy, grow in islands on Mo and actually promote Mo oxidation. Applications of the sacrificial oxidation in nanometer thin layers exist in a range of nanoscopic devices, such as nano-electronics and protection of e.g. multilayer x-ray optics for astronomy, medicine and lithography.

3.2 Introduction

In d-metal on d-metal layer growth, the d-band configuration and surface free energy difference are of important influence. Electrons may be exchanged to achieve an energetically more favorable half filled d-band with only spin up electrons. Segregation or islanding can occur to minimize surface dangling bonds or contact area. We will consider potentially stable systems where Mo, with an approximately half filled d-band and high surface free energy, forms the substrate layer for on top nanolayer growth of d-metals with a range of surface free energies and oxidation enthalpies.

Surface nanolayers that protect the Mo from oxidation can also have applications in Mo/Si multilayer reflective optics for next generation extreme UV lithography (EUVL). The EUV radiation penetrates and reflects from the top 50 Mo/Si periods, the effective maximum. The reflection from each interface contributes to in-phase EUV reflection, adding up to more than 70%. During EUV exposure in a lithography tool vacuum environment, background C_xH_y and H_2O gases can adsorb and dissociate on the mirror surface. Subsequent carbon contamination and oxidation of the multilayer surface reduce mirror reflectance. Although the adsorption of volatile C_xH_y species and subsequent carbon contamination can be controlled by extensive outgassing of the vacuum system and cleaning of the mirror surface [1,2], oxidation is generally considered irreversible. To protect the multilayer mirror against oxidation, a thin protective “capping layer” can be applied at the multilayer surface. The aliphatic hydrocarbons that are observed on the caps can partially shield against oxidation but are not explicitly considered in this work as long as they don’t appear to be of serious influence. Depending on material choice and cap layer thickness, the theoretical reflectance (*R*) of a capped 50 period Mo/Si multilayer can vary by tens of percents. We will relate our observations on layer interaction, oxidation, composition, morphology and diffusion to the application of capping layers on Mo/Si multilayers.

3.3 Experimental details

Si, on top Mo, and capping layers were grown by e-beam physical vapor deposition (PVD) onto natively oxidized super polished Si substrates in a base pressure of $1 \cdot 10^{-6}$ Pa[3]. Growth rates were 0.05 nm/s for Si, 0.04 nm/s for Mo, and 0.01 nm/s for the capping metals. A flux-shaping mask was used to deposit the capping layer with a lateral thickness gradient of 0.3 to 4.3 nm[4], as determined with quartz crystal oscillator

microbalances. The samples were exposed to ambient air for several weeks and subsequently analyzed using angular resolved x-ray photoelectron spectroscopy (ARPES) and scanning Auger microscopy (SAM) in a Thermo Theta Probe with a field emission gun. Simplified, the ARPES measurements between 27° and 64° off normal are modeled to a homogeneous layered system[5] using the factor $e^{\frac{-z}{\lambda \cos\theta}}$ from the depth distribution function that relates the detection angle θ via the attenuation length[6] λ to the sampling depth z. In the case of non-homogeneous layer growth, the set of conditions as described by P.J. Cumpson[5] is not fulfilled and the modeling can result in estimated layer thickness and in-depth distribution errors of up to several nanometers[7]. XPS depth profiling was performed using 0.5 keV Ar^+. An ex-vacuo Schaffer Nanosurf EasyScan 2 high resolution AFM was used to study the lateral material distribution.

3.4 Layer growth kinetics

The morphology of the capping layer grown on the Mo substrate is physically restrained by the low atom mobility for e-beam PVD that limits deviation from Gaussian (stochastic) layer-by-layer growth[8]. Influence on the morphology subsequently occurs chemically via Young's equation $\Delta H^{Total} = \Delta H^{Surface}{}_{cap} + \Delta H^{Interface}{}_{Mo/cap} - \Delta H^{Surface}{}_{Mo}$[9,10]. $\Delta H^{total} \leq 0$ generally results in layer-by-layer (Frank – van der Merwe) growth, while $\Delta H^{total} > 0$ yields island (Volmer – Weber) growth. The relation holds for each individual adlayer, and initial layer-by-layer growth with successive island (Stranski - Krastinov) growth occurs when the substrate-particle affinity is initially strong, but a lattice mismatch between the film and substrate introduces a strain into the growing film[11]. Individual $\Delta H^{surface}$ and $\Delta H^{interface}$ values can result in surface free energy driven intermixing even when $\Delta H^{interface}$ is positive[12]. The segregating material will then agglomerate below the surface to minimize contact area. The Gibbs free energy to form the most stable oxide ($\Delta G^{form}{}_{O}$) gives an indication on the suitability of the metal as a protective cap against oxidation. Table I shows the $\Delta H^{surface}$, $\Delta H^{interface}$, ΔH^{total} and $\Delta G^{form}{}_{O}$ for the materials involved[13].

Cap	$\Delta H^{surface}$	$\Delta H^{interface}$	ΔH^{total}	$\Delta G^{form}{}_{O}$
Mo	188			-167
Co	127	-18	-79	-112
Ni	121	-27	-94	-106
Ru	174	-56	-70	-84
Cu	95	67	-26	-64
Rh	155	-59	-92	-60
Pd	124	-59	-123	-41
Pt	152	-114	-150	
Au	99	14	-75	15

Table I: $\Delta H^{surface}$, *$\Delta H^{interface}$ with Mo, ΔH^{total} with Mo, and $\Delta G^{form}{}_{O}$ at 298 K in kJ/mole of the respective metals.*

For all metals in Table I, $\Delta H^{total} < 0$ when grown onto Mo, favoring layer-by-layer growth. While $\Delta H^{surface}$ of Au and Cu are lowest of all, the positive $\Delta H^{interface}$ partially counters wetting of the Mo and favors minimization of the contact area, i.e. Volmer-Weber (island) growth[14]. Mentioned layer thicknesses hereafter are "as-deposited" and refer to equivalents when layer-by-layer growth would have occurred.

3.5 Results and discussion

As a reference for Mo oxidation and a measure of the protective functionality of a capping layer, a 2.5 nm Mo layer on a 5.0 nm Si layer is deposited without a capping layer. With ARPES we model that approximately 30% of the Mo oxidizes to a MoO_3 film of ~0.6 nm thickness under ambient conditions (Fig. 8). Oxidation accelerates under EUV exposure in lithography tool vacuum due to H_2O dissociation by secondary electrons[1].

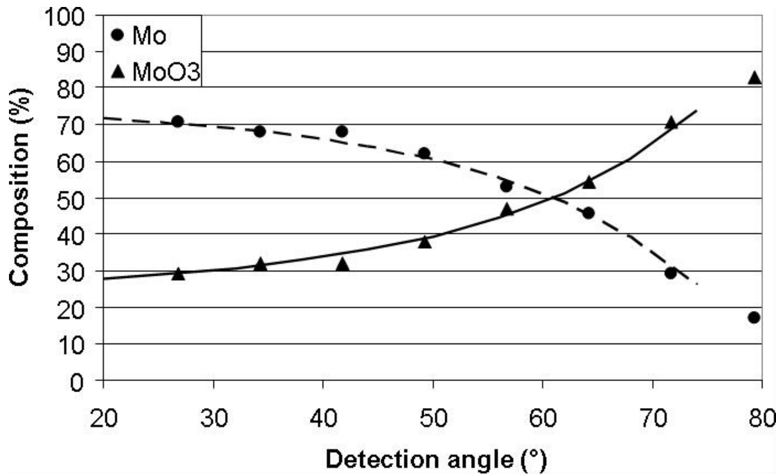

Figure 8: *Modeling of the ARPES results indicates that bare Mo oxidizes to a ~0.6 nm thick MoO_3 layer at the surface in ambient conditions.*

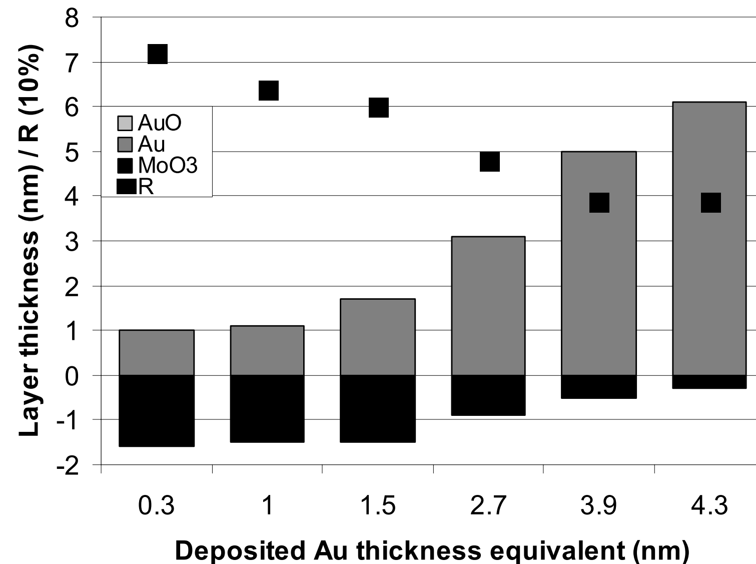

Figure 9: *Modeled ARPES results on the Au cap, with 0 nm defined as the original Au-on-Mo interface. In the positive direction extends the cap adlayer, in the negative direction oxidation of the Mo substrate layer. The calculated reflectance R for a capped 50 period multilayer is also shown.*

The as-deposited oxidation state of uncapped Mo is now compared to the case when a Au capping layer is applied (Fig. 9). As pointed out in the previous section, layer-by-layer and island growth compete while Au intermixture or compound formation with Mo is certainly not expected.

Figure 9 shows that for Au layers up to 1.5 nm thick, a constant 40% of Mo is oxidized to MoO_3, while the Au does not oxidize. Mo oxidation increases to almost 80% after several months in ambient environment[15]. Modeling of ARPES and XPS depth profiling measurements both indicate layer intermixture, showing equivalent amounts of Au and MoO_3 in the top few nm's, and a region of increased MoO_3 to elemental Mo concentration below. It is remarkable that Mo oxidation is actually increased and relatively constant up to 1.5 nm Au. Au islanding or intermixture might expose Mo for oxidation and increase the electron escape depth, causing overestimation in layer thickness modeled with ARPES. With SAM we observe dots of oxygen and a somewhat irregular distribution of Au. Verification of suspected inhomogeneous layer growth is performed with AFM on the 4 nm thick Au capping layer, as shown in Fig. 10.

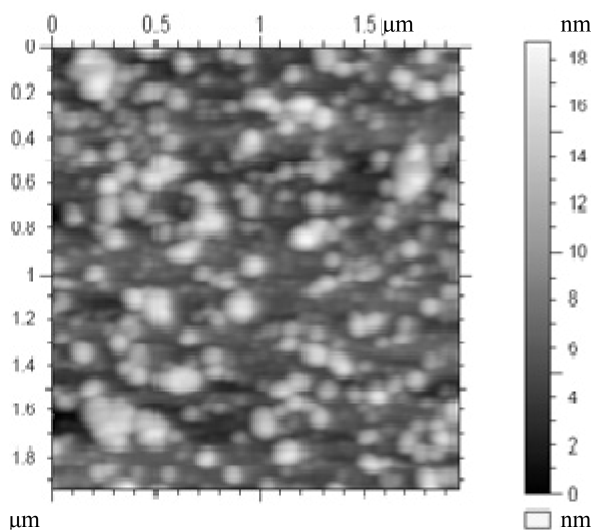

Figure 10: *AFM on a 4 nm thick Au capping layer shows a significant roughness with a lateral structure that suggests Volmer-Weber growth.*

AFM reveals surface roughness of 3.06 nm (RMS) and a peak-to-valley height of 18.7 nm, a value much larger than the as-deposited Au layer thickness. The difference is most probably explained by grain boundaries, in addition to the agglomeration in islands of typically 100 nm in diameter that we observe in Fig. 10, acknowledging island growth. The activation barrier for interface formation of Au with Mo apparently hinders layer-by-layer growth and protective functionally of Au capping layers.

The next noblest metal, Pt, has the most negative $\Delta H^{interface}$ with Mo of all metals investigated, favoring intermixture instead of island growth. A range of Pt capping layer thicknesses was characterized with ARPES (Fig. 11).

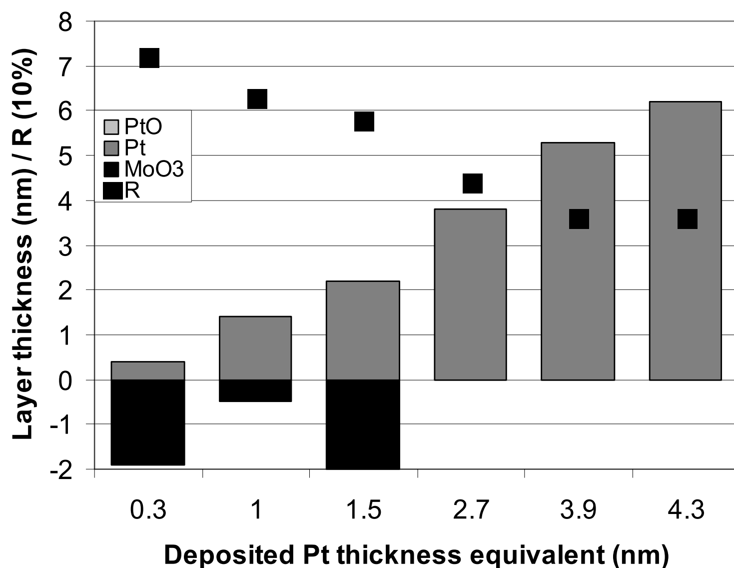

Figure 11: *Modeled ARPES results on the Pt cap, showing subsurface Mo oxidation and layer intermixture.*

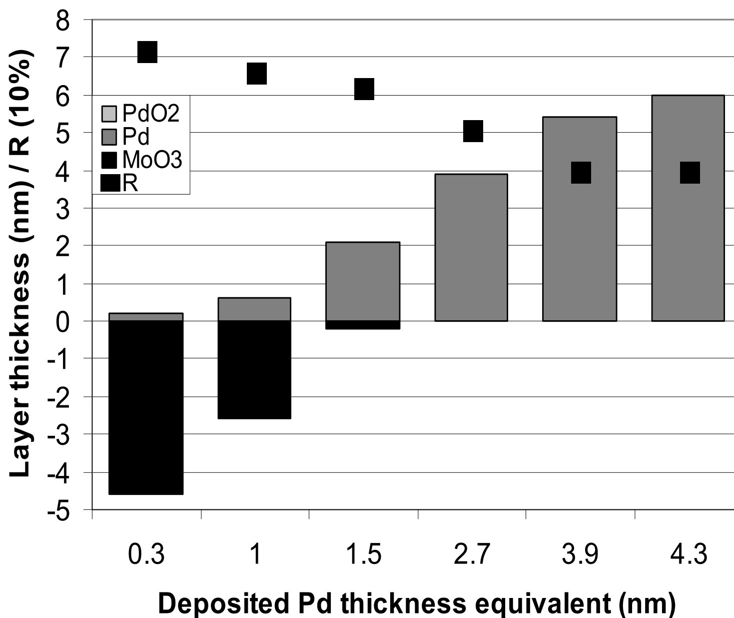

Figure 12: *Modeled ARPES results on the Pd cap, revealing more subsurface Mo oxidation than under Pd.*

For a Pt capping layer of 0.3 nm thickness, approximately 70% of the Mo appears oxidized to MoO_3, even more than in the case of Au. When the Pt capping layers thickness is 1.0 nm, about 25% of the Mo is oxidized to MoO_3, for 1.5 nm Pt this is

reduced to 10%. Modeling of the ARPES measurements suggests significantly thicker Pt layers than were deposited and complete intermixture with abundant MoO_3 for up to 1.5 nm thick Pt layers. The observation by Jeon et al.[16] that Na provides additional oxidation sites in the Ge surface might also apply for the Pt-Mo interlayer. For Pt layers thicker than 1.5 nm, no Mo oxidation and no Mo at grazing detection angles are observed in ARPES, indicating the Pt layer is now closed. XPS depth profiling reveals a Pt/Mo/Si layered structure. The roughness of an as-deposited 4 nm thick Pt capping layer is below the AFM measurement accuracy, suggesting that no islanding indeed occurs.

Pd has a moderately negative $\Delta H^{interface}$ with Mo, and is expected to grow layer-by-layer with less intermixing compared to Pt on Mo. Fig. 12 shows the surface state as determined with ARPES for the different Pd layer thicknesses. When a 0.3 nm thick Pd capping layer is applied on Mo, ~85% of the Mo oxidizes. With a 1.0 nm thick Pd layer, this is approximately 50%, still more than bare Mo. The Pd does not yet appear closed and surface MoO_3 is visible. A 1.5 nm thick Pd capping layer limits Mo oxidation to ~30%. XPS depth profiling reveals that only moderate intermixture occurs. For thicker Pd layers, traces of MoO_3 are visible for all but the most grazing detection angles. The Pd layer appears to form a closed layer at the surface in these cases. Traces of PdO are observed near the surface over the complete range of layer thicknesses. The observation that Pd promotes Mo oxidation even more than Pt is not readily fully attributed to creation of extra oxidation sites in the Pd-Mo interlayer, since it's both theoretically and experimentally established to be thinner. We propose here that e^- donation from Mo to the nobler Pd might occur, similar to the extensively studied Pd-H system[17]. In effect, Mo would function as a sacrificial metal and increase its oxidation state.

Having the same $\Delta H^{interface}$ with Mo as Pd, Rh also is expected to grow layer-by-layer. XPS depth profiling studies have shown that diffusion through the Mo and underlying Si layer and agglomeration at the Si-on-Mo interface prominently occur in the case of Rh[18]. Fig. 13 shows the modeled ARPES results for the characterized Rh layer thicknesses.

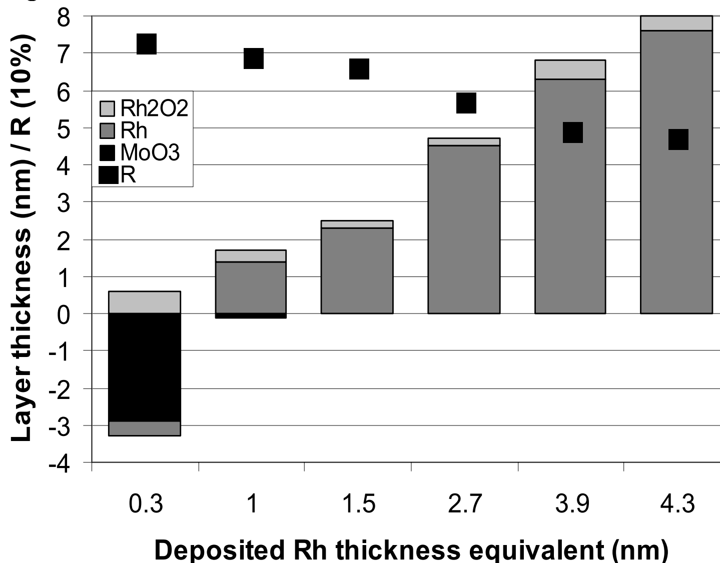

Figure 13: *Modeled ARPES results for the Rh cap, suggesting major layer expansion.*

A 0.3 nm thick Rh layer yields ~70% Mo oxidization to surface MoO_3, again more than for uncapped Mo. A 1.0 nm thick Rh layer limits Mo oxidation to less than 10%, while thicker Rh layers stop it altogether. A ~0.3 nm thick Rh_2O_3 and on top CO film is formed on the Rh caps that appear significantly thicker in ARPES.

Cu deposition on Mo involves similar considerations as discussed for Au on Mo. The highly positive $\Delta H^{interface}$ obstructs layer-by-layer growth more than Au growth on Mo, but this growth mode is still predicted by Young's law, due to the low $\Delta H^{surface}$ of Cu. A range of Cu capping layer thicknesses was characterized with ARPES (Fig. 14).

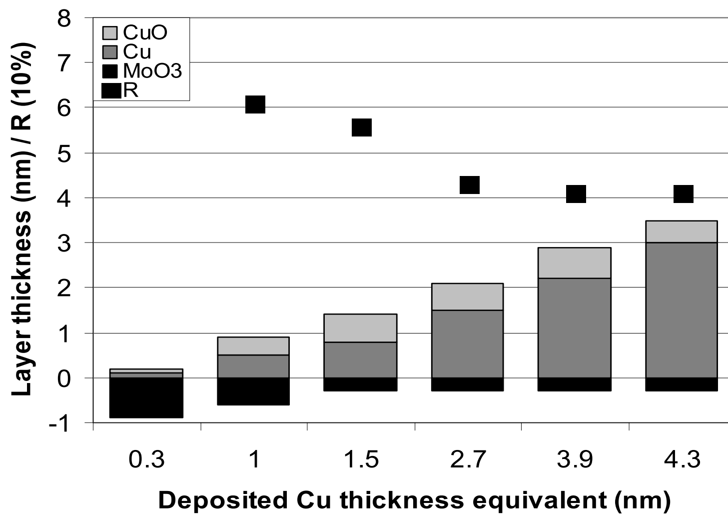

Figure 14: *Modeled ARPES results on the Cu cap, with apparent layer-by-layer growth and oxidation of Cu and Mo.*

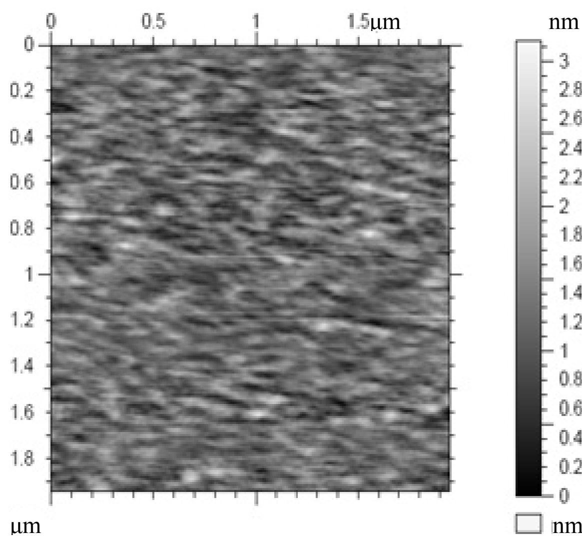

Figure 15: *AFM on a 4 nm thick Cu capping layer shows a moderate roughness compared to Au.*

With a Cu capping layer, we observe Mo oxidation over the complete layer thickness range as in the case of Au, although the Cu layer thickness is of more influence on the degree of Mo oxidation. For 0.3 nm Cu, about 50% of the Mo is oxidized to MoO_3, for 1.0 nm Cu this is ~35%. With thicker Cu layers, some 20% of the Mo is oxidized. We observe significant amounts of CuO near the surface with both ARPES and XPS depth profiling; in the thickest layers, a CuO film up to 0.7 nm is present. The CuO appears to effectively cover the Mo already for the thinnest Cu layers, albeit not protecting it against oxidation. To study the layer homogeneity, AFM is performed on a 4 nm thick Cu layer, as shown in Fig. 15.

AFM shows a surface roughness of 0.35 nm (RMS) and a peak-to-valley height of 3.1 nm for an as-deposited 4 nm thick Cu capping layer. The lateral resolution of SAM is insufficient to reveal whether chemical inhomogeneity is present at the surface. The observations provide no certainty whether island growth occurs. If so, it is less pronounced than for Au on Mo. This is remarkable, since Au is kinetically less likely to grow in islands on Mo than Cu is. Possibly, Cu oxidation lowers the $\Delta H^{interface}$ with Mo, shifting the balance.

Ru is the material that is generally used as capping material for EUV multilayer mirrors[19]. Due to it's moderate optical absorption of EUV, R is considerably higher for multilayers capped with Ru than with any other metal of similar thickness discussed here. Table 1 shows that the $\Delta H^{interface}$ with Mo is similar to that of Pd and Rh. The $\Delta H^{surface}$ is per unit area slightly higher than that of Mo. Ru was also found to diffuse and agglomerate at the Si-on-Mo interface[18]. This might allow for subsequent Mo oxidation, but ARPES reveals that this is not the case, as shown in Fig. 16.

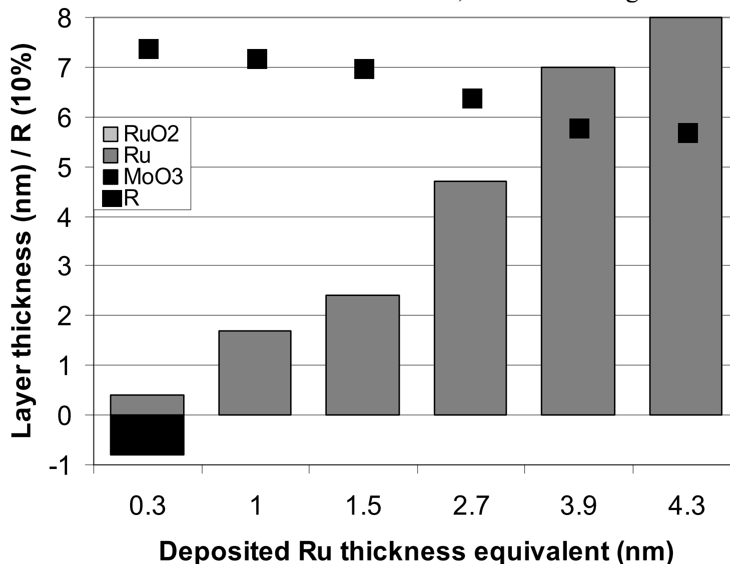

Figure 16: *Modeled ARPES results on the Ru cap, with only the 0.3 nm thick layer showing slightly increased Mo oxidation compared to bare Mo.*

A 0.3 nm thick Ru layer allows Mo to oxidize for about 40% to MoO_3, for 1.0 nm Ru and more, no Mo oxidation occurs under ambient conditions, nor do we identify any Ru oxidation, although the material is less noble than the above mentioned materials. We attribute this to the higher catalytic activity of Ru to dissociate and physisorb C species 1,15. C is difficult to identify on Ru due to peak overlap in XPS, but it can protect against oxidation of the Ru[20,21]. Also the Ru appears significantly thicker in ARPES, which is an artifact caused by low Mo detection, possibly enhanced by the Ru diffusion that will be discussed in chapter 5 and 6.

Kinetics especially favor Ni and Co layer-by-layer growth, given their low $\Delta H^{surface}$ and moderately negative $\Delta H^{interface}$ with Mo, as is shown in Table 1. Ni and Co yield a lower R and are more susceptible to oxidation than earlier discussed metals, but could still protect against Mo oxidation. Fig. 17 shows the ARPES characterization of the Ni caps.

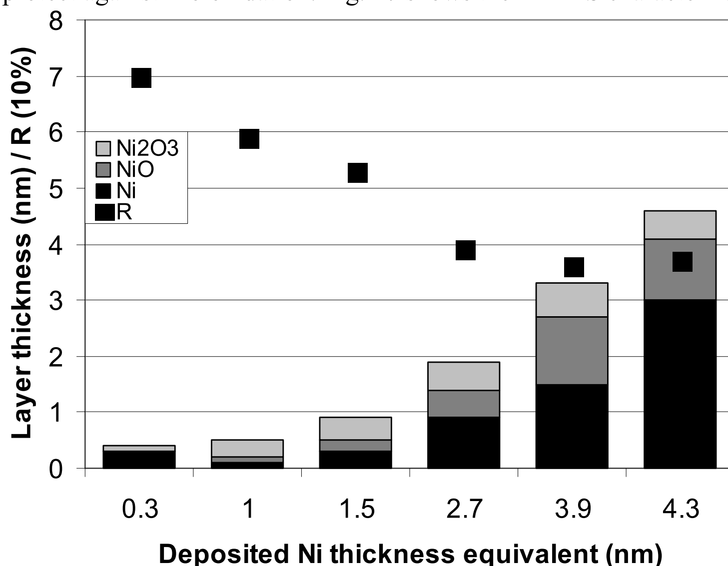

Figure 17: *Modeled ARPES results on the Ni cap, which itself is significantly oxidized but limits oxidation of Mo.*

A Ni capping layer of 0.3 nm thickness already limits Mo oxidation to only ~15%, which is a significant reduction compared to the situations mentioned above. A 1.0 nm thick Ni capping layer further limits Mo oxidation to about 10%. Only trace amounts of MoO_3 are visible when thicker Ni layers are applied. The major part of Ni itself is oxidized up to a 0.6 nm thick Ni_2O_3 film as well as an increasing amount of NiO with deposited layer thickness. Also XPS depth profiling shows a layered Ni_2O_3/NiO/Ni/Mo structure for 1.5 nm Ni that efficiently limits subsequent Mo oxidation.

Figure 18 shows that similar observations with ARPES are made for Co. With a 0.3 nm thick Co cap, approximately 12% of the Mo is oxidized. For 1.0 nm thick Co this is ~7% and for thicker Co layers, virtually no Mo oxidation is observed to occur. ARPES and XPS depth profiling indicate mainly oxide presence at surface, the top monolayer bound to C, subsurface bound to Co. Co presence occurs deeper into the structure, above the Mo. The Co layer is closed and completely oxidized to CoO and on top a CoO_x film, with

x > 3. Though heavy Co and also Ni oxidation occur and R is comparatively low, very thin layers already limit Mo oxidation under ambient conditions considerably[22], possibly by electrochemically acting as a galvanic coating [23,24].

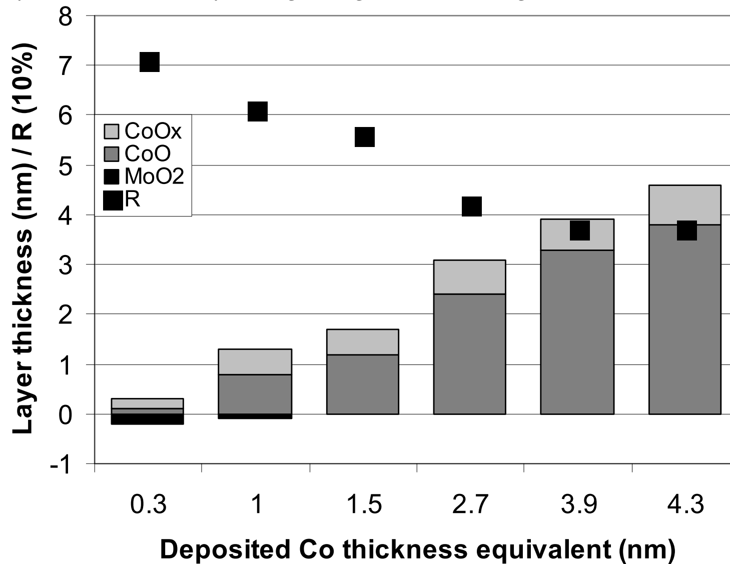

Figure 18: *Modeled ARPES results on the Co cap, completely oxidized but even more limiting Mo oxidation.*

3.6 Conclusions

A range of d-metal nanolayers, deposited on a Mo-on-Si substrate layer, has been studied for growth properties and protective qualities against Mo oxidation under ambient conditions as a function of nanolayer thickness. Nobler d-metal layers do oxidize less, but fail to limit Mo oxidation. These metals actually promote Mo oxidation under ambient conditions, compared to bare Mo. Significant surface roughness occurs for Cu and especially Au capped multilayers, with agglomeration in islands of typically 100 nm in diameter for Au, while Young's law predicts layer-by-layer growth. The positive $\Delta H^{interface}$ of Au with Mo appears too high a barrier for layer-by-layer growth, resulting in oxidation of exposed surface Mo to MoO_3.

Thin Pt, Pd, and Rh layers strongly promote Mo oxidation. We attribute this to creation of additional oxidation sites in the formed interlayer. The metallic Pt, Pd, and Rh generally do cover the oxidized Mo, while no subsurface oxygen is observed. Due to the more negative enthalpy for oxidation compared to the nobler metals, subsurface Mo appears to act as a sacrificial metal in an e^- donation process to support surface oxide, thus increasing its oxidation number. Rh and Ru layers of 1.0 nm and thicker grow in layer-by-layer mode on Mo and no oxidation of either metal occurs under ambient conditions. Oxidation of these catalytic capping metals is limited by on top coverage by a CO monolayer and (hydro)carbon species that absorb from the ambient and occupy absorption sites for H_2O and O_2.

With regards to surface chemistry, special interest goes to Co and Ni capping layers. ARPES modeling suggests layer-by-layer growth, as predicted by Young's law. The layers are completely oxidized and covered with large amounts of non-metallic oxide, while even single monolayers manage to largely prevent Mo oxidation. The nanolayers appear to strongly interact and involve electrochemical functioning as a galvanic coating.

3.7 Acknowledgements

This work is part of the FOM Industrial Partnership Programme I10 ('XMO') which is carried out under contract with Carl Zeiss SMT AG, Oberkochen and the 'Stichting voor Fundamenteel Onderzoek der Materie (FOM)', the latter being financially supported by the 'Nederlandse Organisatie voor Wetenschappelijk Onderzoek (NWO)'. The author wishes to thank Dr. J.G.M. van Berkum of Philips Research for the CS-EELS, HAADF-STEM and EDX analysis.

3.8 References

[1] L. E. Klebanoff, M. E. Malinowski, P. A. Grunow, W. M. Clift, C. Steinhaus, A. H. Leung, S. J. Haney, Proceedings of SPIE 4343, Emerging Lithographic Technologies V, Elizabeth A. Dobisz 342 (2001).
[2] N. Benoit, S. Yulin, T. Feigl, N. Kaiser, Physica B: Condensed Matter 357, 1 (2005).
[3] E. Louis, H.-J. Voorma, N. B. Koster, L. Shmaenok, F. Bijkerk, R. Schlatmann, J. Verhoeven, Yu. Ya. Platonov, G. E. van Dorssen, H. A. Padmore, Microelectron. Eng. 23, 215 (1994).
[4] R. W. E. van de Kruijs, E. Louis, A. E. Yakshin, P. Suter, E. Zoethout, F. Bijkerk, S. Müllender, H. Enkisch, H. Trenkler, M. Wedowski, M. Weiss, B. Mertens, B. Wolschrijn, R. Jansen, A. Duisterwinkel, A. van de Runstraat, R. Klein, S. Plőger, F. Scholze, Poster 122, Proceedings of the 2nd International EUV Lithography Symposium, Antwerp (2003).
[5] P.J. Cumpson, J. Elec. Spec. Rel. Phen. 73, 25 (1995).
[6] S. Tanuma, C.J. Powell, D.R. Penn, Surf. Interface. Anal. 17, 911 (1991).
[7] P.C. Zalm, Surf. Interface Anal. 26, 352 (1998).
[8] J. Camarero, T. Graf, J. J. de Miguel, and R. Miranda, Phys. Rev. Lett. 76 (1996) 23.
[9] T. Young, Philos. Trans. 95, 65 (1805).
[10] H. Roder, R. Schuster, K. Kern, Phys. Rev. Lett. 71, 13 (1993).
[11] M. Ohring, Mat. Sci. Thin Films; Deposition and Structure. San Diego: Academic Press. 2nd ed. (2002).
[12] B. M. Clemens, W. D. Nix, V. Ramaswamy, J. Appl. Phys. 87, 6 (2000).
[13] F. R. de Boer, R. Boom, W. C. M. Mattens, A. R. Miedema, A. K. Niessen, Cohesion in Metals: Transition metal alloys (North-Holland, Amsterdam, 1988).
[14] S. H. Payne, H. J. Kreuzer, A. Pavlovska, E. Bauer, Surf. Sci. Lett. 345 (1996).
[15] T. Tsarfati, E. Zoethout, R. W. E. van de Kruijs, F. Bijkerk, Surf. Sci. (2009).
[16] D. Jeon, T. Sakurai, K. D. Lee, and J. W. Chung, Surf. Sci. 559 (2004).
[17] J. W. Simons, T. B. Flanagan, Canadian J. Chem. 43 (1965).
[18] T. Tsarfati, E. Zoethout, R. W. E. van de Kruijs, F. Bijkerk, J. of Appl. Phys. 105, 064314 (2009).
[19] S. Bâjt, J. Alameda, T. Barbee, M. Clifi, J. A. Folta, B. Kauffman, E. Spiller, Soft X-Ray and Extreme Ultra-Violet Imaging Systems 11, San Diego, California (2001).

[20] A.E. Yakshin, E. Louis, E.L.G. Maas, F. Bijkerk, R. Klein, F. Scholze, P. C. Zalm, F. Stietz, M. Wedowski, S. Muellender, B. Mertens, H. Meiling, ASET/SEMATECH Workshop on EUV Lithography, Matsue (2001).
[21] B.M. Mertens, N. Koster, R. Jansen, A. van de Runstraat, H. Werij, F. Stietz, M. Wedowski, H. Meiling, R. Klein, R. Thornagel, F. Scholze, G. Ulm, R. Kurt, P. Zalm, E. Louis, A. Yakshin, ASET/SEMATECH Workshop on EUV Lithography, Matsue (2001).
[22] N. S. McIntyre, D. Johnston, L. L. Coatsworth, J. R. Brown, Surf. Interface Anal. 9, 4 (2004).
[23] E. Gómez, E. Pellicer, E. Vallés, J. Electro Anal. Chem. 556, 238 (2003).
[24] G. V. Kozlova, T. G. Smirnova, V. P. Molchanova, Z. A. Tubyshkina, Metal Science and Heat Treatment 4, 7 (Springer New York, 2004).

4 Atomic O and H exposure of C-covered and oxidized d-metal surfaces

4.1 Abstract

Carbon coverage, oxidation and reduction of Au, Pt, Pd, Rh, Cu, Ru, Ni and Co layers of 1.5 nm thickness on Mo have been characterized with ARPES and desorption spectroscopy upon exposure to thermal H and O radicals. We observe that only part of the carbon species is chemically eroded by atomic H exposure, yielding hydrocarbon desorption. Exposure to atomic O yields complete carbon erosion and CO_2 and H_2O desorption. A dramatic increase in metallic and non-metallic oxide is observed for especially Ni and Co surfaces, while for Au and Cu, the sub-surface Mo layer is much more oxidized. Although volatile oxides exist for some of the d-metals, there is no indication of d-metal erosion. Subsequent atomic H exposure reduces the clean oxides to a metallic state under desorption of H_2O. Due to its adequacy, we propose the atomic oxygen and subsequent atomic hydrogen sequence as a candidate for contamination removal in practical applications like photolithography at 13.5 nm radiation.

4.2 Introduction

In previous work we presented a study on the growth of thin d-metal surface layers with different oxidation, interface, and surface enthalpies[1] in a range of thicknesses onto Mo[2] and B_4C[3,4]. Both in ambient conditions and during intense illumination in vacuum, background C_xH_y and H_2O has been observed to adsorb and dissociate on the surface[5,6,7,8], resulting in condensed carbonaceous and oxide contaminants at the nanolayer surface[9,10,11]. Atomic hydrogen exposure (AHE)[12,13,14,15] and atomic oxygen exposure (AOE)[16,17] are two viable options to selectively remove these contaminants, respectively via rehydrogenation, or via oxidation to volatile molecules. AHE has been reported to produce both metal and semiconductor surfaces entirely free of contamination[18]. It can chemically erode contaminants such as oxygen on silicon and carbon on GaAs[19,20]. The arsenic and gallium oxides are reduced to volatile species of elemental arsenic, gallium oxide, gallium hydroxide and water, while LEED indicates good preservation of stoichiometry and surface order[21,22]. AOE yields an aggressive oxidation process that can mimic photo oxidation under high illumination fluxes. We use desorption spectroscopy and angular resolved x-ray photoelectron spectroscopy (ARPES) to investigate the potential of AHE and AOE. With the study of subsequent AOE and AHE, we also explore the feasibility of complete and faster contaminant erosion and recovering the surface to a metallic state. AHE and AOE are readily adaptable to in situ use in ultrahigh vacuum. Applications exist in a range of nano-devices and e.g. reflective multilayer optics for astronomy, medicine, and Extreme UV lithography (EUVL).

4.3 Experimental details

All investigated nanolayer surfaces or “caps” have been grown onto a Mo-on-Si layer on natively oxidized super polished Si substrates with ~0.1 nm rms roughness in an UHV electron beam evaporation coater with a base pressure of $1 \cdot 10^{-6}$ Pa[23]. Growth rates in this particular work are 0.05 nm/s for Si, 0.04 nm/s for Mo, and 0.01 nm/s for the other d-metals. The deposited material mass is monitored by quartz crystal oscillator microbalances, which is recalculated to targeted homogeneous cap thickness equivalents of 1.5 nm for all materials. In case of closed layer-by-layer growth, the Mo layer is then

protected from oxidation and the average ARPES intensity is optimal for identification[1,24,25]. Mentioned thicknesses are only an indication for the material quantity or average layer thickness, as several of the investigated d-metals are observed not to grow homogeneously onto Mo.

After deposition, the samples are stored in ambient conditions for saturation with oxide and hydrocarbon species of the multilayer surface. This is also the state in which they will be mounted for application as optical elements. The samples are as such introduced into an exposure chamber with a base pressure of $1\cdot10^{-6}$ Pa for 1 hour 1.0 sccm AHE to hydrogenate the condensed carbonaceous contamination to volatile species that desorb from the surface. Subsequently, 30 minute 0.5 sccm AOE is applied which should oxidize the remaining C contamination to volatile carbon oxides. To reduce the resulting clean metal oxide surface, AHE is repeated. The H_2 and O_2 are catalytically dissociated in a water cooled Oxford Applied Research TC50 thermal cracking source that produces no ions[26,27]. It is directed at the sample surface at ~70 mm distance at a 45° angle. During AHE and AOE, the multilayer surface temperature does not exceed 358 K and 351 K resp. The pressure during treatment is $3.5\cdot10^{-3}$ Pa, the desorbing fragments were monitored with a Prisma QMS 200 mass spectrometer.

In-depth distribution, compound formation, and chemical states before and after subsequent AHE and AOE were characterized with ARPES in a Thermo Theta Probe[1]. The setup is equipped with a field emission gun for secondary electron microscopy (SEM) and scanning Auger electron spectromicroscopy (SAM). SAM was implemented to provide increased lateral resolution in particular cases. Low Energy Ion Scattering (LEIS) measurements have been performed at Calypso in Eindhoven, The Netherlands, to quantify surface monolayer composition and coverage in particular cases[28].

4.4 Results and discussion

As a reference for Mo oxidation, a 2.5 nm Mo layer on a 5.0 nm Si layer is deposited, without any protective capping layer. With ARPES we determined that approximately 30% of the Mo oxidizes to a MoO_3 film of ~0.6 nm thickness under ambient conditions for several weeks[1]. The oxide is however not self-terminating and oxidation continues until only MoO_3 is visible by ARPES. This process also occurs under EUV exposure in lithography tool vacuum due to physisorbed H_2O dissociation by secondary electrons[12]. The MoO_3 is reduced to Mo at the surface to within ~0.5 nm depth and to MoO_2 at the subsurface below upon AHE. The observation of surface Mo and subsurface MoO_2 suggests a two step process, where only direct interaction of H radicals with MoO_3 completely reduces it to Mo. This could then induce oxide segregation and $Mo + 2MoO_3 \rightarrow 3MoO_2$, leaving subsurface MoO_2 unreachable for direct interaction with H radials. The Mo is again completely oxidized to MoO_3 by AOE, but it can be recovered to the pre-AOE state by repeating the AHE. Since the oxidation of Mo yields layer degradation due to swelling, and cannot be fully recovered by AHE, the Mo surface should be capped by a separate capping layer with more appropriate process stability.

With a deposited equivalent of a 1.5 nm thick Au capping layer, selected as a first candidate capping material, the major fraction of the Mo is oxidized to MoO_3, with a $Mo3d_{5/2}$ peak appearing at 232.7 eV binding energy (BE) with a full width half maximum (FWHM) of 1.2 eV (Fig. 19). The O1s peak appears at 530.7 eV BE with 1.5 eV FWHM.

The largely promoted oxidation, compared to bare Mo, can be attributed to earlier observed Au island growth on Mo due to an endothermic $\Delta H^{interface}$, resulting in high surface roughness and sacrificial functionality of the Mo[1,29]. The shape and position of the single Au4f doublet line of $Au4f_{7/5}$ at 83.9 eV BE and with 0.9 eV bandwidth at FWHM indicates that Au is not oxidized. Modeling of a C1s peak at 284.4 eV BE which dominates at grazing detection angles, indicates that the surface is covered by averagely 0.7 nm thick layer of C with mainly sp^2 hybridization, assuming bulk density. It is chemically viable that C preferentially resides at Au instead of MoO_3. AHE reduces all MoO_3 to MoO_2 and Mo in a 3:5 ratio, while the C content is some 55% lower. Observed CH_4 and H_2O desorption during AHE confirm hydrogenation of C and reduction of MoO_3. During subsequent AOE, CO_2 desorption is observed, indicating oxidation and erosion of remaining carbonaceous contamination. ARPES reveals no C and no elemental Mo beside the MoO_3, while the Au remains entirely metallic. AHE reduces all MoO_3 to MoO_2 and Mo.

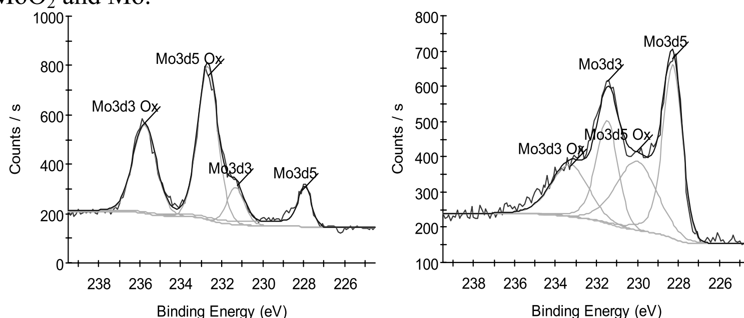

Figure 19: *Au cap: The Mo3d peaks before (left) and after (right) treatment sequence. All MoO_3 after AOE is reduced to MoO_2 and Mo by AHE.*

With a 1.5 nm thick Pt cap layer, selected next, 10% of the Mo is oxidized to MoO_3, which appears to be intermixed with the Pt. The surface is covered by a 0.8 nm thick C layer. AHE erodes half of the C and most of the O content. Subsequent AOE erodes all C and dramatically increases the O content, although only some 20% of the Mo is oxidized to MoO_3. A second Pt4f doublet is detected for grazing angles with $Pt4f_{7/2}$ at 73.4 eV BE and ~1.5 eV bandwidth, suggesting 10% of the Pt is oxidized to PtO or Pt_3O_4 (Fig. 20). We observe no fragments that would suggest erosion by formation of volatile PtO_2. With AHE, the surface is reduced to pre-AOE state.

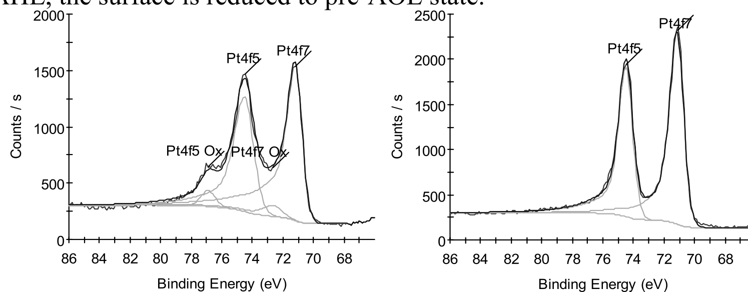

Figure 20: *Pt cap: The Pt4f peaks after AOE (left) and after subsequent AHE (right). The Pt is quite resistant to atomic O and can be fully reduced to its elemental state by AHE.*

A 1.5 nm thick Pd capping layer allows for 60% of the Mo to oxidize to MoO_3, a ~0.3 nm thick PdO_2, a ~0.8 nm thick C overlayer and a CO monolayer. AHE reduces all PdO_2 and MoO_3 to it's elemental state and erodes all CO, but leaves some carbonaceous contamination. AOE erodes this and oxidizes about 70% of the Pd to only PdO, with no visible PdO_2 (Fig. 21). Mo oxidizes for 20% to MoO_3, mainly located at the surface. No oxide remains after AHE.

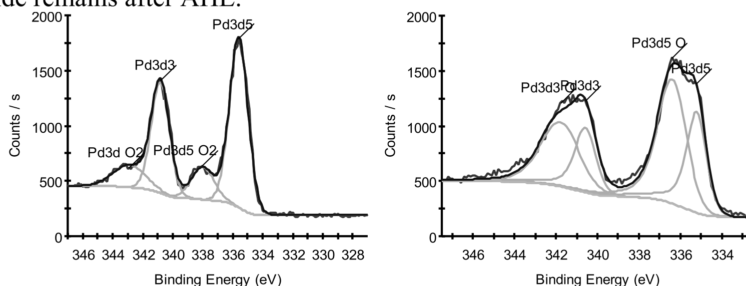

Figure 21: *Pd cap: The Pd3d peaks before first AHE (left) and after AOE (right), which yields about 70% PdO but no PdO_2. All oxide is reduced by AHE.*

A 1.5 nm thick Rh capping layer oxidizes for 20% to Rh_2O_3 with a ~0.8 nm thick C overlayer. Within the XPS detection range, no Mo but only MoO_3 is visible (Fig. 22). Both RhO and RhO_2 are volatile and would thus not occur in XPS. As these oxides have a positive formation enthalpy[29], formation is unlikely under ambient conditions, but possible in more aggressive environments. AHE results in reduction to MoO_2 (Fig. 22) and Rh, while most C remains. During AOE, we observe no fragments that could indicate Rh erosion via RhO or RhO_2 formation. The AOE does erode the remaining C, it oxidizes 55% of the Rh to Rh_2O_3 and all Mo to MoO_3. Upon subsequent AHE, the Rh_2O_3 and MoO_3 are fully reduced to their elemental state by AHE.

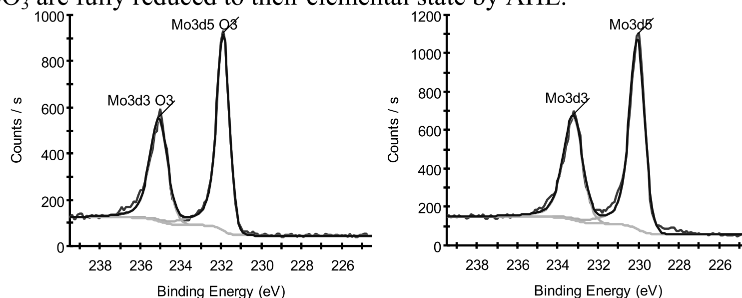

Figure 22: *Rh cap: The Mo3d peaks before (left) and after (right) treatment sequence. All MoO_3 after AOE is reduced to Mo by the afterward AHE.*

A 1.5 nm thick Ru layer, the material that is widely reported as a standard reference material[7], is covered by an equivalent of a 0.8 nm thick C layer, assuming bulk density. With ellipsometry, we have observed that the layer is actually ~2.0 nm thick, with 40% of the bulk graphite density. We cannot identify any Ru or Mo in oxidized state with ARPES before AHE. We do observe O with predominantly O1s at 531.0 eV binding energy, suggesting Ru or Mo oxidation. AHE erodes all O and some 35% of the C. Subsequent AOE erodes the remaining C and yields about 60% Ru oxidation, with significant O1s peaks at 529.5 and 530.7 eV, the latter predominantly at grazing detection

angles, i.e. more towards the surface. The O1s peak at 530.7 eV persists upon AHE, although Ru is fully reduced and the O1s peak at 529.5 eV is nearly gone.

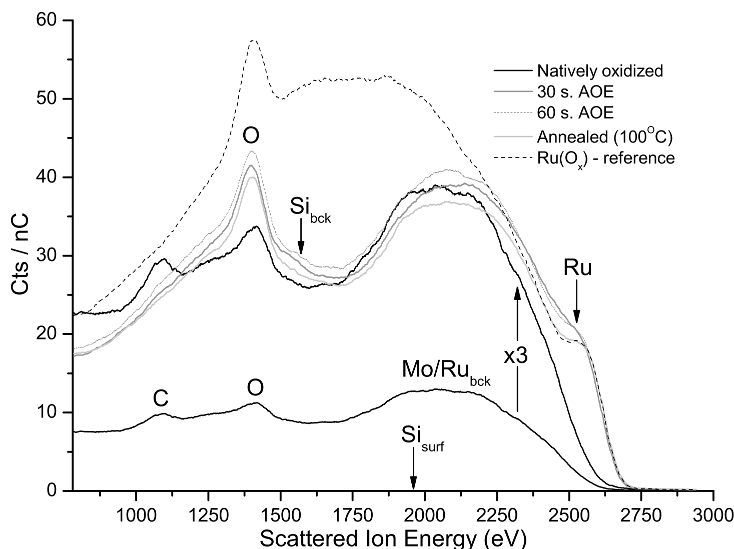

Figure 23: *The LEIS spectrum of a Ru surface before and after exposure to O-plasma and annealing at 100° C.*

Because of its reference status, we performed additional Low Energy Ion Scattering (LEIS) analysis on a separate Ru surface, showing that it is initially completely covered by C and O in an approximately 1:1 ratio, with likely additional H (Fig. 23). Exposure to atomic oxygen for only 30 s. erodes all C and largely saturates the surface with O. Additional 30 s. AOE and moderately increases the total surface O content. Annealing for 30 min. at 100° C removes part of the O, after which the Ru surface composition appears similar to that of a reference 7 nm thick Ru cap on a multilayer, denoted Ru(O_x).

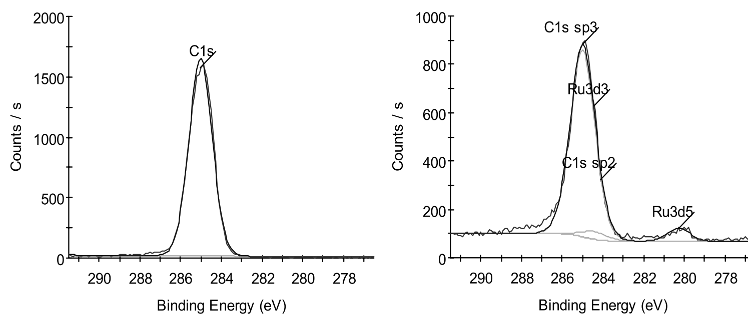

Figure 24: *The C1s peak of a diamond film (left) and on a Ru capped multilayer surface exposed to EUV radiation (right) suggest similar C hybridization.*

We exposed another Ru capped sample to EUV radiation. This results in a significant C1s peak at 285.0 eV (Fig. 24). A reference untreated diamond film shows a single C1s peak at 285.0 eV as well, which would imply that C contamination grown during EUV illumination is mainly sp^3 hybridized. Comparison to literature suggests more sp^2

hybridized C contamination, generally mentioning sp^3 C1s at 285.5 eV, and sp^2 C1s at 284.6 eV.

A 1.5 nm thick Cu capping layer shows oxidation to a 0.6 nm thick CuO layer and 30% of the Mo is oxidized to MoO_3. Also the Cu has earlier been observed with AFM to grow on the Mo in islands, albeit smaller than the Au islands and not generating the same roughness. The surface is covered by a 0.9 nm thick C layer, of which some 60% is eroded by AHE. CuO and MoO_3 are no longer detected. AOE erodes the remaining C. Practically all Mo and Cu is oxidized to MoO_3 and CuO respectively. We identify O contents that are too high to attribute to metal oxides only and could be physisorbed as O_2 or H_2O. This is eroded by AHE, reducing all MoO_3 to MoO_2 and CuO to Cu (Fig 25).

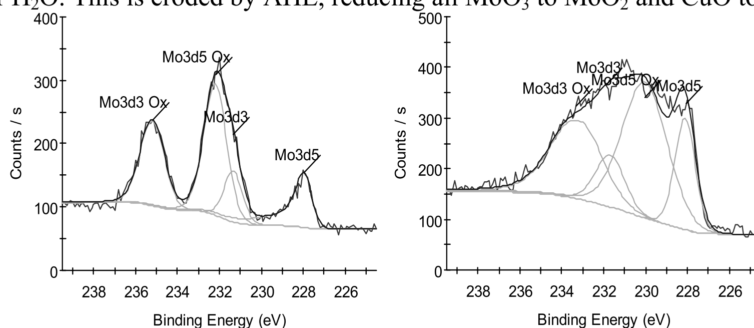

Figure 25: *Cu cap: The Mo3ds peak after atomic O (left) and subsequent H (right) treatment. All MoO_3 after AOE is reduced by AHE, mainly to MoO_2.*

A 1.5 nm thick Ni capping layer is oxidized to 0.2 nm NiO and on top 0.4 nm Ni_2O_3, covered by a 0.8 nm thick C layer. A smaller C1s peak at 288.5 eV and a substantial O1s peak at 531.5 eV binding energy possibly hint at carboxyl or carbonate groups. A less prominent O1s peak that occurs at 530.0 eV and indicates NiO, disappears upon AHE, while the O1s peak for Ni_2O_3 at 531.5 eV persists, now mainly at grazing detection angles. All Ni oxide is reduced, while 75% of the C persists (Fig. 26).

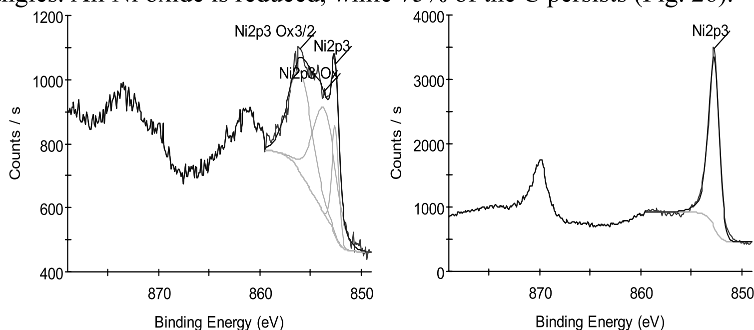

Figure 26: *Ni cap: The Ni2p peaks before (left) and after (right) AHE. All Ni_2O_3 and NiO is reduced to Ni.*

The C is fully eroded by AOE. Of the Ni, 50% is oxidized to NiO and another 25% is oxidized to Ni_2O_3, while a fraction of the Mo is oxidized to MoO_3. A dramatic increase occurs for the O1s peaks at 530.0 and more towards the surface at 531.5 eV. It only

marginally decreases upon AHE and the NiO persists, while all Ni_2O_3 and MoO_3 is reduced.

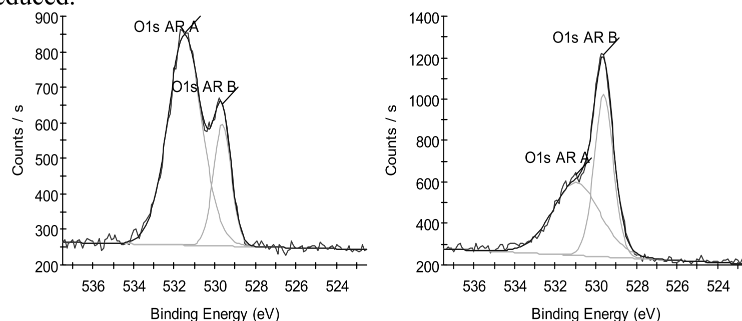

Figure 27: *Co cap: The O1s peak before first AHE (left) and after atomic O treatment (right), revealing that CO is eroded by H and Co is oxidized by AOE.*

A 1.5 nm thick Co capping layer completely oxidizes under ambient conditions over time. The elemental $Co2p_{3/2}$ peak at 778.3 eV BE is not separately identifiable from a peak around 780.7 eV BE which is quite high for CoO_x and points more in the direction of $Co(OH)_2$. O1s peaks occur at 529.6 (CoO_x) and mainly 531.6 eV, either $Co(OH)_2$ or CO. The surface is covered by a 1.0 nm C film with C1s at 284.8 eV, while a C1s peak at 288.6 eV can also be observed. Upon AHE, only metallic Co remains, compared to some 65% O and 80% C erosion. Only traces of C remain upon AOE. The $Co2p_{3/2}$ peak now occurs at 780.0 eV BE. The O1s peak at 531.6 eV is lower than before initial AHE, while a strong increase occurs for the O1s peak at 529.6 eV (Fig. 27). These observations indicate that CoO_x such as CoO, Co_2O_3, and Co_3O_4 are now formed. Also these oxides are completely reduced after AHE, yielding a metallic Co on Mo layered system.

4.5 Conclusions

Atomic hydrogen exposure (AHE) and atomic oxygen exposure (AOE) of eight d-metal nanolayer surfaces, deposited on a Mo-on-Si substrate layer, have been studied with ARPES and desorption spectroscopy. All surfaces are covered by directly absorbed CO and an averagely 0.7 to 1.0 nm thick carbonaceous layer, semi dependant on the catalytic activity of the d-metal but also on the surface morphology. We observe no or only very mild oxidation of Au, Pt, and Pd, due to insufficient formation enthalpy of their oxides. Also Cu, Rh, and Ru show little oxidation, which could additionally be explained by protective functionality of carbonaceous absorbents. With the higher formation enthalpy, Ni and Co are almost completely oxidized. In all investigated cases, the carbonaceous layer can be partially eroded by AHE under hydrocarbon desorption. The CO and remaining carbonaceous absorbents can be eroded by AOE, with CO_2 as the main desorbing molecule. For all but the Au cap, the oxide content dramatically increases upon AOE. All investigated capping layers, including Ni and Co, can be fully reduced to metallic state by subsequent AHE, with desorption of H_2O.

We observe significant differences in initial Mo oxidation under each of the eight capping layers investigated. Mo oxidation is not limited or even promoted in the case of Au and Cu capping layers, which grow rough and in islands due to endothermic $\Delta H^{interface}$. The heavily oxidized Ni and Co capping layers, covered with large amounts of

catalytically absorbed non-metallic oxide, (sacrificially) prevent oxidation of Mo. The other investigated metals take an intermediate position in affecting Mo oxidation. The initial and post AOE observations have been shortly summarized in Table II. For AHE, we can generally state that it reduces all the capping materials to their metallic state. Reduction of MoO_3 appears to be a two step process, where only direct interaction of H radicals with MoO_3 completely reduces it to Mo, inducing oxide migration and $Mo + 2MoO_3 \rightarrow 3MoO_2$, leaving subsurface MoO_2 unreachable for direct interaction with H radials and apparently to stable to be reduced indirectly via Mo.

Cap	Initial and post AOE observations
Au	Au islands, extra Mo oxidation
Pt	Pt/Mo intermixed, more O than oxidation
Pd	Much MoO_3, some PdO, PdO_2 upon AOE
Rh	Much MoO_3, some Rh_2O_3
Ru	Ru oxidation only upon AOE
Cu	CuO and MoO_3
Ni	Much NiO and Ni_2O_3, almost no MoO_3
Co	Much CoO_x, almost no MoO_3

Table II. *Summarized initial and post AOE observations per cap.*

Based on the above, we have identified an AOE and subsequent AHE sequence to obtain clean, oxide free metal surfaces. Due to its adequacy, this procedure can be considered a candidate for usage in practical applications like photolithography at 13.5 nm radiation. In addition, we identified Ni and Co as potentially suitable capping material candidates to prevent Mo oxidation for this application.

4.6 Acknowledgements

This work is part of the FOM Industrial Partnership Programme I10 ('XMO') which is carried out under contract with Carl Zeiss SMT AG, Oberkochen and the 'Stichting voor Fundamenteel Onderzoek der Materie (FOM)', the latter being financially supported by the 'Nederlandse Organisatie voor Wetenschappelijk Onderzoek (NWO)'.

4.7 References

[1] T. Tsarfati, E. Zoethout, R. W. E. van de Kruijs, F. Bijkerk, Surf. Sci. 603, 7, 1041 (2009)
[2] T. Tsarfati, E. Zoethout, R. W. E. van de Kruijs, F. Bijkerk, J. Appl. Phys. 105, 064314 (2009)
[3] T. Tsarfati, E. Zoethout, R. W. E. van de Kruijs, F. Bijkerk, J. Appl. Phys. 105, 104305 (2009)
[4] T. Tsarfati, E. Zoethout, R. W. E. van de Kruijs, F. Bijkerk, submitted
[5] B. Mertens, M. Weiss, H. Meiling, R. Klein, E. Louis, R. Kurt, M. Wedowski, H. Trenkler, B. Wolschrijn, R. Jansen, A. van de Runstraat, R. Moors, K. Spee, S. Plöger, R. van de Kruijs, Microelectronic Engineering 73–74 (2004)

[6] H. Oizumi, A. Izumi, K. Motai, I. Nishiyama, A. Namiki, Jpn. J. of Appl. Phys. 46, 25 (2007)
[7] S. Bajt, H. N. Chapman, N. Nguyen, J. Alameda, J. C. Robinson, M. Malinowski, E. Gullikson, A. Aquila, C. Tarrio, S. Grantham, Appl. Opt. 42, 28, 5750 (2003)
[8] J. Chen, C. J. Lee, E. Louis, F. Bijkerk, R. Kunze, H. Schmidt, D. Schneider, R. Moors, Diamond & Related Materials (2008), doi:10.1016/j.diamond.2008.11.030
[9] S. Graham, C. E. Steinhaus, M. Clift, L. E. Klebanoff, and S. Bajt, “Atomic hydrogen cleaning of EUV multilayer optics,” in Emerging Lithographic Technologies VII, R. L. Engelstad, ed., Proc. SPIE 5037, 460–469 (2003)
[10] H. Oizumi, H. Yamanashi, I. Nishiyama, K. Hashimoto, S. Ohsono, A. Masuda, A. Izumi, H. Matsumura, Emerging Lithographic Technologies IX. Edited by Mackay, R. Scott, Proc. SPIE 5751, 1147 (2005)
[11] M. E. Malinowski, P. Grunow, C. Steinhaus, W. M. Clift, L. E. Klebanoff, Proc. SPIE 4343, 347 (2001)
[12] L. E. Klebanoff, M. E. Malinowski, P. A. Grunow, W. M. Clift, C. Steinhaus, A. H. Leung, S. J. Haney, Proc. SPIE 4343 Emerging Lithographic Technologies V 342 (2001)
[13] M. E. Malinowski, C. Steinhaus, W. M. Clift, L. E. Klebanoff, S. Mrowka, R. Soufli. Proc. SPIE 4688 (2002)
[14] L. E. Klebanoff, W. M. Clift, M. E. Malinowski, C. Steinhaus, P. Grunow and S. Bajt. J. Vac. Sci. Technol. B 20 (2002)
[15] T. E. Madey, N. S. Faradzhev, B. V. Yakshinskiy, N. V. Edwards, Appl. Surf. Sci. 253, 4, 1691 (2006)
[16] R. E. Robinson, R. L. Sandberg, D. D. Allred, A. L. Jackson, J. E. Johnson, W. Evans, T. Doughty, A. E. Baker, K. Adamson, A. Jacquier, Proc. Annual Technical Conference 47, 368 (2004)
[17] C. Gwyn, SPIE magazine, 22-24 (2002)
[18] Y. Luo, D. A. Slater, R. M. Osgood, Appl. Phys. Lett. **67**, 55 (1995)
[19] Z. Yu et al., Appl. Phys. Lett. **69**, 82 (1996)
[20] T. Maruyama, D.-A. Luh, A. Brachmann, J. E. Clendenin, E. L. Garwin, S. Harvey, R. E. Kirby, and C. Y. Prescott, Appl. Phys. Lett. 82, 23 (2003)
[21] M. Yamada, Jpn. J. Appl. Phys. Lett. 35, L651 (1996)
[22] M. Yamada, Y. Ide, Jpn. J. Appl. Phys. Lett. 33, L671 (1994)
[23] E. Louis, H. -J. Voorma, N. B. Koster, F. Bijkerk, Yu. Ya. Platomov, S. Yu. Zuev, S. S. Andreev, E. A. Shamov, N. N. Salashchenko, “Multilayer coated reflective optics for Extreme UV lithography”, Microelectronic Engineering 27 (1-4), 235-238 (1995)
[24] P. J. Cumpson, J. Elec. Spec. Rel. Phen. 73, 25-52 (1995).
[25] P.C. Zalm, Surf. Interface Anal. 26, 352-358 (1998).
[26] T. D. Veal, I. Mahboob, C. F. McConville, T. M. Burke, T. Ashley, Appl. Phys. Lett. 83, 1776 (2003)
[27] L. F. J. Piper, T. D. Veal, I. Mahboob, C. F. McConville, H. Lu, W. J. Schaff, Phys. Rev. B 70, 115333 (2004)
[28] V. I. T. A. de Rooij-Lohmann, A. W. Kleyn, F. Bijkerk, H. H. Brongersma, A. E. Yakshin, Appl. Phys. Lett. 94, 063107 (2009)
[29] F. R. de Boer, R. Boom, W. C. M. Mattens, A. R. Miedema, A. K. Niessen, Cohesion in Metals: Transition metal alloys (North-Holland, Amsterdam, 1988)

5 In-depth agglomeration of d-metals at Si-on-Mo interfaces

5.1 Abstract

Reflective Si/Mo multilayer mirrors with protective d-metal surfaces onto a range of upper Mo and Si layer thicknesses have been grown with PVD and investigated on diffusion and in-depth compound formation. Laterally inhomogeneous upward Si and downward d-metal diffusion occurs through Mo layers up to 2 nm thickness. Especially Ru and Rh agglomerate and form silicides such as Ru_2Si_3 and Rh_2Si not in the midst of the Si layer but at the Si/Mo interface. This appears to be mediated by $MoSi_2$ presence at the Si/Mo interface that acts as precursor via better lattice compatibility and lowering of formation energy.

5

5.2 Introduction

Multilayer mirror optics, acting as artificial Bragg crystals, find their application in e.g. Extreme UV (EUV) lithography, soft x-ray spectroscopy, fluorescence analysis and imaging. For the EUV lithography case, silicon is particularly suited as a transparent "spacer" material for photon-energies just below its L absorption edge at 100 eV. A high contrast Mo/Si layer combination with individual layer thicknesses of ~3.5 nm is generally used for normal incidence EUV reflective optics. Layer periodicity and interface width tolerances throughout the multilayer are typically in the Ångstrom regime.

During EUV exposure in a vacuum system, surface adsorption and molecular dissociation of background C_xH_y and H_2O yield carbon contamination as well as oxidation of the multilayer surface. Although the adsorption of volatile C_xH_y and subsequent carbon contamination can be controlled by extensive outgassing of the vacuum system and cleaning of the mirror surface[1], oxidation is generally considered irreversible. To protect the multilayer mirror against oxidation, a thin protective "capping layer" can be applied at the multilayer surface. Given its oxidation resistance, known from e.g. catalysis research, Ru is generally proposed as a reference capping material in the EUV optics community[2]. It has been widely used by way of standard for optics lifetime studies in several development programs and will therefore be the object of study here. In view of the interface contrast and the generated standing wave, a Ru/Si/(Mo/Si) multilayer with sharp interfaces is required for high near normal reflectance. Literature on heteroepitaxial growth of platinum-group metals on Si and interface formation in UHV is quite limited. As will be discussed hereafter, these interfaces are generally much broader than the Mo/Si interface, of which the exact sharpness, reactivity, and growth mode are still a matter of debate[3,4,5,6,7]. To omit the Ru/Si interface and Ru diffusion into the Si, a Mo layer can be applied between the Ru and Si layer[2]. The thus acquired Ru/Mo/Si/(Mo/Si) is non-ideal from a perspective of optical contrast, transparency and EUV reflectivity and will be considered here solely for its chemical and diffusion properties.

We will start this paper by providing thermodynamic arguments on some of the observations/viewpoints for Ru/Si and Mo/Si interfaces. We then continue by addressing our observations on in-depth distribution and compound formation of a Ru capping layer when applied on the upper Si or Mo layer, to determine the diffusion and distribution of the Ru.

5.3 Interface kinetics

During the growth process, atoms arrive at the substrate with a certain kinetic energy. For e-beam physical vapor deposition (PVD), the kinetic energy is thermal (~0.1 eV) and the mobility of the deposited atoms or molecules is very low compared to deposition by, for example, magnetron or ion beam sputtering (~1 - 10 eV). In this work we focus on low ad-atom energy deposition via evaporation to exclude direct implantation. Interlayer formation at the interfaces should then be limited to diffusion.

For solid-state reactions involving substitutional diffusion as in the case of Ru, Mo, and Si, the presence of vacancies is essential. The thermal equilibrium concentration of monovacancies c_{vac} is directly related to their Gibbs free energy of formation $\Delta G^{for}{}_{vac}$

$$c_{vac} = e^{\frac{-\Delta G^{for}{}_{vac}}{RT}} = e^{\frac{\Delta S^{for}{}_{vac}}{R}} \cdot e^{\frac{-\Delta H^{for}{}_{vac}}{RT}}, \tag{7}$$

with $\Delta S^{for}{}_{vac} \approx 0.6\,R$ as quoted by Seeger[8]. $\Delta H^{for}{}_{vac}$ in Si is only 60 kJ/mole, compared to 185 kJ/mole in Ru and 200 kJ/mole in Mo[9]. Consequently, c_{vac} in Mo and Ru are negligible compared to c_{vac} in Si, and substitutional diffusion is expected to preferentially occur into Si. Interface formation of Si with d-metals, i.e. overlap of Si p-type and metal with mainly d-type electron wave functions, depends on d-band filling but is always exothermic, with $\Delta H^{interface}{}_{Ru\ in\ Si}$ = -133 kJ/mole and $\Delta H^{interface}{}_{Mo\ in\ Si}$ = -126 kJ/mole. Closed interlayer growth is therefore energetically preferred over either island growth or layer-by-layer growth. The additional enthalpy of surface compared to bulk Si, $\Delta H^{surface}{}_{Si}$, is with 74 kJ/mole considerably lower than both $\Delta H^{surface}{}_{Ru}$ (174 kJ/mole) and $\Delta H^{surface}{}_{Mo}$ (188 kJ/mole). A surface monolayer coverage with Si is therefore energetically favored over a surface monolayer coverage with either Ru or Mo atoms.

Based on the above, Ru and Mo adlayers will segregate into the Si substrate layer. Silicide formation will occur with such orientation that Si occupies the surface monolayer. $\Delta H^{surface}$ is always positive since bulk symmetry is broken, which results in dangling bonds, i.e. electron orbitals without overlap. Ru or Mo should thus be considered the diffusing species during segregation. Direct segregation to the subsurface during initial growth and the difference in c_{vac} would account for our observation in CS-TEM that the Mo/Si interface results in a broader interlayer than the Si/Mo interface, where no segregation occurs since $\Delta H^{surface}{}_{Si}$ is lowest. Petford-Long et al.[10], Holloway et al.[11], and Slaughter et al.[12] also observed this difference between the Mo/Si and Si/Mo interface.

There is a general trend that noble metals interdiffuse more with Si than mid d-block metals, supposedly caused by the physical effect of size, implying that the metal is the main diffusing species. Considering the relatively prominent interdiffusion and more negative $\Delta H^{interface}$ of left-hand d-metals compared to mid d-block metals[13,14], electron exchange between the d-metal and Si to lower the energy in a more half-filled d-band configuration might also contribute to diffusion. The relative stability of the Mo/Si interface compared to Ru/Si should reduce overall diffusion when Ru is deposited on Mo. In this paper, the Ru distribution and chemical state in Ru/Si/(Mo/Si) and Ru/Mo/Si/(Mo/Si) multilayers is studied using a range of upper Mo layer thicknesses. When Ru is deposited onto Mo, the combined Ru/Mo layer can be regarded as EUV absorbing and should be of limited thickness. Depending on the exact Mo layer thickness

that is deposited on Si, the substrate for Ru layer growth is expected to comprise of some Mo-Si compound that affects subsequent on top Ru growth.

5.4 Experimental details

The Ru/Si/(Mo/Si) and Ru/Mo/Si/(Mo/Si) multilayers have been grown in an UHV e-beam evaporation coater with a base pressure of $1 \cdot 10^{-6}$ Pa[15]. Growth rates in this particular work are 0.05 nm/s for Si, 0.04 nm/s for Mo, and 0.01 nm/s for Ru. Quartz crystal oscillator microbalances and in situ x-ray reflection measurements are used for layer thickness control. A flux-shaping mask is used to deposit the Mo layer with a lateral thickness gradient, before depositing the Ru capping layer[16]. The Mo layer thickness is varied over a range from 0 (Ru directly on Si) to 4 nm to determine the effects on layer chemistry.

X-ray photoelectron spectroscopy (XPS) and AES depth profiling with 0.5 keV Ar^+ at 45° incidence are used to determine the in-depth distribution and silicide formation in the multilayers. The Ar^+ ions have a penetration depth of ~1.6 nm in Si and ~0.7 nm in d-metals like Mo and Ru[17]. AES offers better surface sensitivity and depth resolution, with lower chemical resolution. Quantification is done with the derivative method, while similar results are obtained when the peak area is fitted. AES mainly probes the distorted area where Ar^+ induced intermixing and silicide formation artifacts might occur. The depth scale in the graphs shown in this study is ascribed based on the known deposited bilayer thicknesses and periodicity in the multilayer. Differences in sputter efficiency and electron escape depths for the different materials result in under-estimation of the Si content in the multilayer. The effect is of negligible influence in this work, considering the focus on the surface composition, and not on the multilayer periodicity. Compensation via the known as-deposited ratio is therefore not carried out.

High-angle annular dark field scanning transmission electron microscopy (HAADF-STEM) and energy dispersive X-ray (EDX) analysis were performed with a FEI Tecnai F30ST, operated at 300 kV. The samples were prepared by focused ion beam (FIB) using a FIB2000. This procedure damages the upper ~20 nm of the sample. The sample is first analyzed “as-FIBbed”, i.e. with sample thickness ~100 nm and ion beam damage on both sides. Further thinning to <80 nm is achieved with low-energy ions.

5.5 Results and discussion

Figure 28 shows the atomic percentage of Ru as a function of depth from the surface, when deposited onto a range of thicknesses of the upper Mo layer (left) or Si layer (right).

Observed from the surface into the multilayer, the Ru content in the upper Mo and Si layer shows an exponential decay that is readily related to normal diffusion behavior and additional ion beam mixing. Towards the first Si/Mo interface, the Ru content rises above the exponential function. It agglomerates at this interface for all but the 4 nm thick Mo layer directly underneath the Ru, which is apparently of sufficient thickness to block the Ru diffusion. To exclude forward sputtering effects and investigate on possible diffusion along grains in the Mo microstructure[18], a focused ion beam prepared cross section of the

multilayer with a 2 nm thick Mo directly under the Ru is analyzed with cross section HAADF-STEM (Fig. 29).

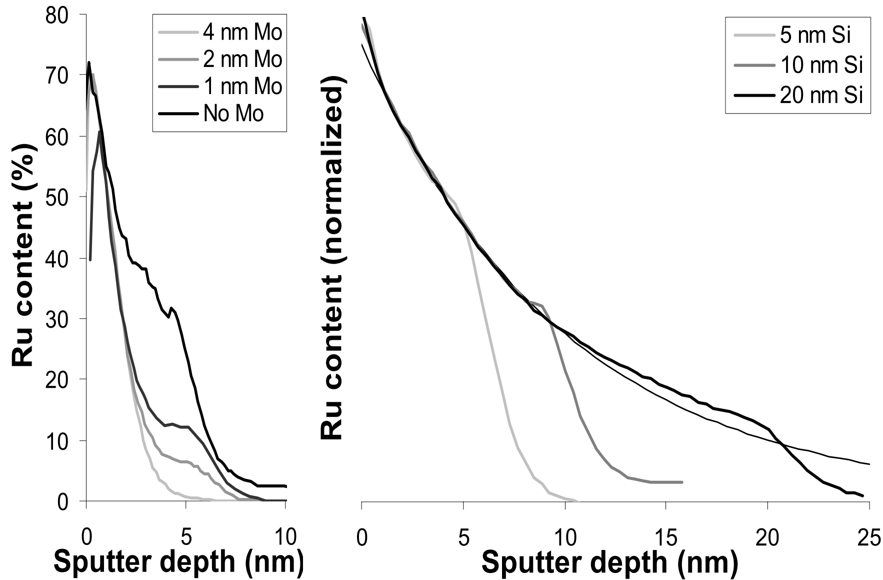

Figure 28: *XPS analysis of the Ru content as a function of depth in Ru/Mo/Si/(Mo/Si) (left) and Ru/Si/(Mo/Si) (right) multilayers. A range of thicknesses for the layer directly under the Ru is explored.*

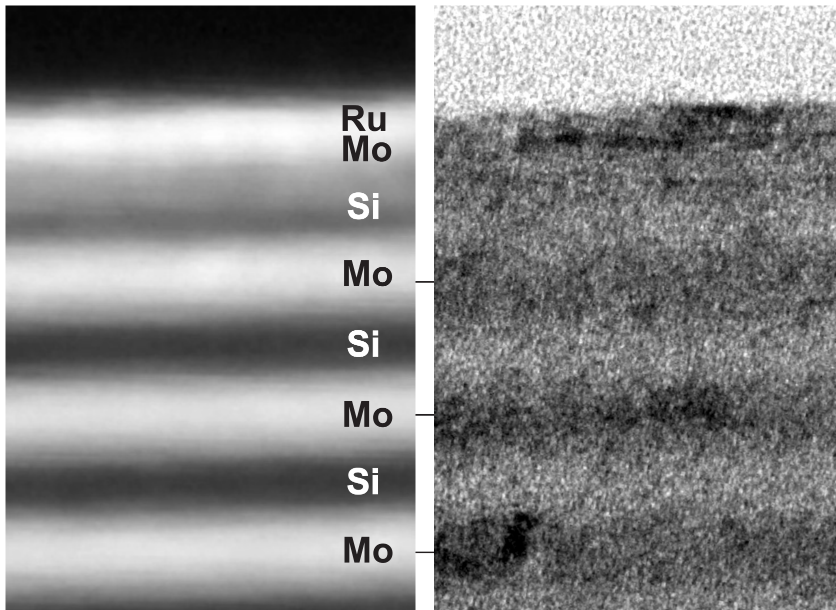

Figure 29: *Cross section HAADF-STEM image with <1 (left) and <0.3 nm (right) footprint of the multilayer with a 2 nm thick Mo layer directly underneath the Ru. The Si appears dark in EDX and bright in HAADF-STEM.*

Fig. 29 shows a broad interface gradient of medium brightness under the Ru and upper Mo layer that shows some lateral inhomogeneousness. This broad interface is absent under the other Mo layers and corresponds to the Ru diffusion as observed in Fig. 28. The cross section suggests that the Mo layer underneath the Ru is not completely closed and that Si diffuses upwards to the Ru layer. A darker region is visible between the Ru and Mo layer in HAADF-STEM, suggesting Si presence. The Ru layer itself appears rather homogeneous, in contrast to Au and Cu capping layers that form a rough surface with island growth on the Mo[19]. The inhomogeneous Mo layer structure seems responsible for the Ru diffusion as observed in Fig. 28. We make similar observations when a layer of B_4C is applied between the Ru and Si layer[20]. B_4C is not known to form polycrystallinities and grain boundaries, while significant upward Si segregation does occur. Si presence in the diffusion barrier layer would thus appear of main influence on Ru diffusion. To confirm the Ru and Si diffusion through the Mo layer, Fig. 30 shows the in-depth EDX quantification of Si, Mo and Ru for the multilayer displayed in Fig. 29.

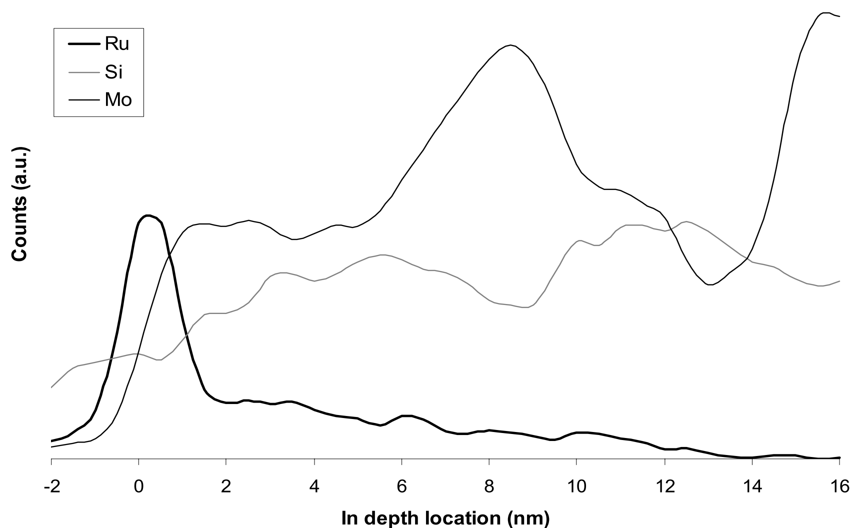

Figure 30: *EDX intensities for Si, Mo and Ru, with a correction for Mo K_β and Ru K_α peak overlap.*

The EDX profile offers insufficient resolution for detailed conclusions on possible in depth Mo and Si distributions. We do observe indications of Si segregation and a pure Ru layer with a residue below the Mo diffusion barrier layer, similar to results obtained with XPS. For the sample thickness, the volume of X-ray generation is estimated to be approximately 3 nm in diameter. This value can be decreased by analyzing thinner sample regions, but only at the cost of counting statistics, already marginal in this case. We investigated several d-metal capping layers on Mo and Si with AES depth profiling for improved depth resolution. All these structures show upward Si and downward capping metal diffusion and agglomeration, which appear similarly or even more pronounced at lower sputter energies to further reduce forward sputtering. Thermal behavior was also investigated with in-depth AES analysis, as shown in Fig. 31 for Ru and Rh capped multilayers before and after 48 hour anneal at 300° C.

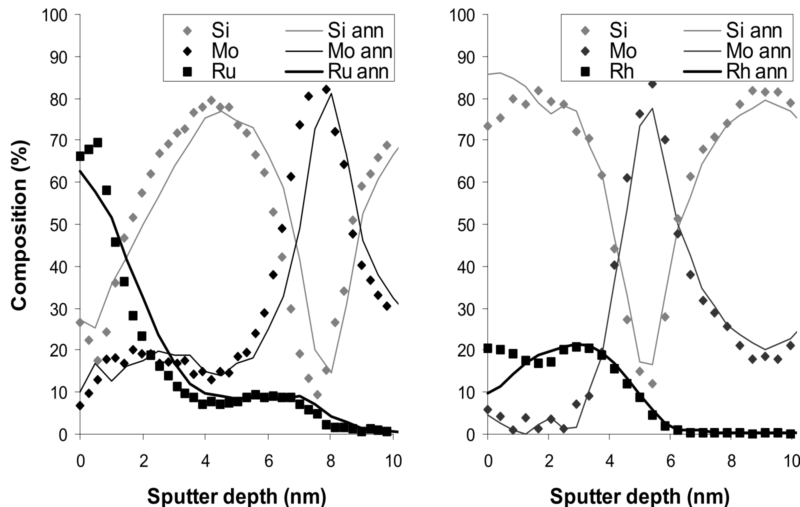

Figure 31: *In-depth AES analysis of Ru (left) and Rh (right) capped multilayers, with a 1.0 nm and no Mo barrier respectively, before and after 48 hour anneal at 300° C.*

The diffusion and agglomeration of Ru and Rh at the Si/Mo interface in Fig. 31 was also observed for Nb and Ir capping metals. This feature is further enhanced by thermal anneal, confirming the agglomeration as a thermally preferred configuration. Instead of Mo, we also applied surfactant metals such as Y or Sb between the Ru and Si to limit Ru diffusion into Si via surfactant mediated growth[21,22,23]. These surfactants are observed to diffuse to the surface, unable to prevent again considerable Ru agglomeration at the Si/Mo interface[24].

The Si/Mo interface is increasingly Mo-rich with lower c_{vac} in depth, and would therefore be expected to support lower instead of enriched capping metal concentrations. The observed agglomeration at the interface might be explained by a diffusion mechanism via channels through the upper Mo and Si layer. This could hinder migration back into the Si upon arrival at the Si/Mo interface, although this should not be expected to yield amounts higher but only equivalent to in the midst of the Si layer. The Si, Mo and capping metal distribution diffuse upon annealing due to increased atom mobility, but agglomeration at the Si/Mo interface front is persistent. The observed agglomeration implies that these d-metals preferentially reside at the Si/Mo interface front; a feature that cannot be explained by vacancy mediated substitutional diffusion.

To identify the process responsible for the observed Ru distribution and agglomeration at the Si/Mo interface front, the in-depth chemical state analysis of Ru, i.e. the $Ru3d_{5/2}$ electron binding energy (BE) is analyzed with XPS. RuO_x and Ru_2Si_3 appear as up- and downward $Ru3d_{5/2}$ peak shifts respectively, which are plotted as a function of depth in Fig. 32.

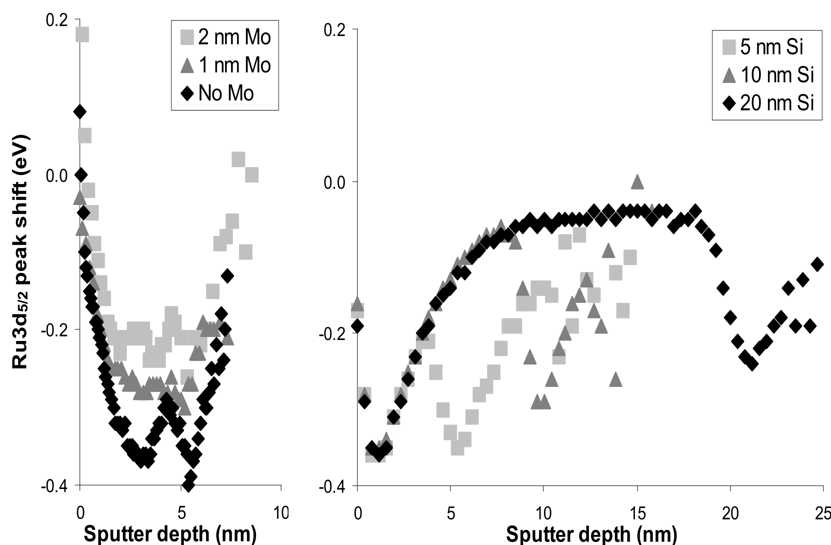

Figure 32: *The $Ru3d_{5/2}$ peak shift from its elemental value of 280.0 eV BE as a function of depth in the Ru/Mo/Si/(Mo/Si) (right) and Ru/Si/(Mo/Si) (left) multilayers with a range of thicknesses for the layer directly under the Ru.*

Figure 32 shows a remarkable in-depth modulation of the Ru peak shift and thus its chemical state. Especially when Ru is directly deposited onto Si, Ru_2Si_3 formation is observed at the Ru/Si and Si/Mo interface, while Ru remains in elemental state in the midst of the Si layer. When Ru is deposited onto a 1 or 2 nm thick Mo layer, Ru_2Si_3 presence is also visible between the Ru and Mo layer, where upward diffused Si yields a Si/Mo interface (Fig. 29). Analysis of the $Mo3d_{5/2}$ and Si2p BE indicates $MoSi_2$ presence at the Si/Mo interfaces that apparently enhances Ru_2Si_3 formation. Formation of $MoSi_2$ ($E_{act} \approx 130$ kJ/mole) can be an intermediate or precursor for Ru_2Si_3 ($E_{act} \approx 174$ kJ/mole). In turn, Ru_2Si_3 formation induced by $MoSi_2$ presence can sustain Ru diffusion and agglomeration at the Si/Mo interface, and explain the thermodynamic stability upon annealing. Ronay and Schad[25] observed a somewhat similar precursor functionality of Cu_3Si, which lowers the formation temperature of $ReSi_2$, generalizing the observations described.

5.6 Conclusion

The in-depth distribution and compound formation of a thin Ru layer when applied on the upper Si or Mo layer have been characterized with XPS. Ru segregation and diffusion are reduced when Ru is deposited onto increasingly thick Mo layers.

The Mo layer underneath the Ru shows an inhomogeneous structure with Si presence in and on top of it. We observe a continuous decrease in Ru diffusion with increasing upper Mo layer thickness, without significant additional Ru diffusion through grain boundaries in thicker polycrystalline Mo layers. Ru_2Si_3 formation is more prominent for thinner Mo layers and mainly occurs at the Si/Mo interfaces, which we attribute to $MoSi_2$ precursor functionality. When used as a surface capping layer, several other d-metals, amongst

which Rh most prominently, show similar in-depth distributions with in-depth agglomeration and silicide formation at the Si/Mo interface.
Si and $MoSi_2$ presence, yielding vacancy mediated diffusion and Ru_2Si_3 formation, appear of more influence on Ru diffusion through the Mo layer than the effect of Mo crystallization. Formation of Ru_2Si_3 via a $MoSi_2$ precursor induces Ru migration and agglomeration at the Si/Mo interface already at room temperature and thermodynamically stabilizes it.

5.7 Acknowledgements

This work is part of the FOM Industrial Partnership Programme I10 ('XMO') which is carried out under contract with Carl Zeiss SMT AG, Oberkochen and the 'Stichting voor Fundamenteel Onderzoek der Materie (FOM)', the latter being financially supported by the 'Nederlandse Organisatie voor Wetenschappelijk Onderzoek (NWO)'. The author wishes to thank Dr. J.G.M. van Berkum of Philips Research for the CS-TEM, HAADF-STEM and EDX measurements.

5.8 References

[1] L. E. Klebanoff, M. E. Malinowski, P. A. Grunow, W. M. Clift, C. Steinhaus, A. H. Leung, and S. J. Haney, Proceedings of SPIE 4343, Emerging Lithographic Technologies V, Elizabeth A. Dobisz, 342 (2001).
[2] S. Bâjt, J. Alameda, T. Barbee, M. Clifi, J.A. Folta, B. Kauffman, E. Spiller, submitted to Soft X-Ray and Extreme Ultra-Violet Imaging Systems 11, San Diego, California (2001).
[3] G. Rossi, I. Abbati, L. Braicovich, I. Lindau, and W. E. Spicer, J. Vac. Sci. Technol. **21**, 617 (1982); G. Rossi, I. Abbati, L. Braicovich, I. Lindau, and W. E. Spicer, U. Del Pennino, and S. Nannarone, Physica B+C 117&118B, 795 (1983).
[4] I. Abbati, L. Braicovich, B. De Michelis, A. Fasena, E. Puppin, and A. Rizzi, Solid State Commun. 52, 731 (1984); I. Abbati, L. Braicovich, B. De Michelis, A. Fasena, and A. Rizzi, Surf. Sci. 1**77**, L901 (1986).
[5] T. T. A. Nguyen and R. C. Cinti, J. Phys. (Paris) Colloq. 45, C5-435 (1984).
[6] H. Balaska, R. C. Cinti, T. T. A. Nguyen and J. Derrien, Surf. Sci. 168, 225 (1986).
[7] H. L. Meyerheim, U. Döbler, A. Puschmann and K. Baberschke, Phys. Rev. B 41, 5871 (1990).
[8] A. Seeger, Crystal Lattice Defects 4, 221 (1973).
[9] F. R. de Boer, R. Boom, W. C. M. Mattens, A. R. Miedema, and A. K. Niessen, Cohesion in Metals: Transition metal alloys (North-Holland, Amsterdam, 1988)
[10] A. Petford-Long, M. B. Stearns, C. H. Chang, D. G. Stearns, N. M. Ceglio and A. M. Hawryluk, J. Appl. Phys. 61, 1422 (1987).
[11] K. Holloway, K. Ba Do, and R. Sinclair, J. Appl. Phys. 65, 474 (1989).
[12] J. M. Slaughter, Patrick A. Kearney, Dean W. Schulze and Charles M. Falco, Proc. SPIE 1343, 73 (1991).
[13] K. M. Unruh, W. J. Meng, and W. L. Johnson, Materials Research Society Symposium Procedings, edited by J. M. Gibson and L. R. Dawson (Materials Research Society, Pittsburgh, 1985), 37, 551.
[14] P. Guilman, P. Guyot, and G. Marchal, Phys. Lett. A 109, 174 (1985).

[15] E. Louis, H.-J. Voorma, N.B. Koster, L. Shmaenok, F. Bijkerk, R. Schlatmann, J. Verhoeven, Yu. Ya. Platonov, G.E. van Dorssen and H.A. Padmore, Microelectron. Eng. **23,** p. 215 (1994).
[16] R. W. E. van de Kruijs, E. Louis, A. E. Yakshin, P. Suter, E. Zoethout, F. Bijkerk, S. Müllender, H. Enkisch, H. Trenkler, M. Wedowski, M. Weiss, B. Mertens, B. Wolschrijn, R. Jansen, A. Duisterwinkel, A. van de Runstraat, R. Klein, S. Plőger and F. Scholze, "Optimization of protective capping layers for EUVL optics", Poster 122, Proceedings of the 2nd International EUV Lithography Symposium, Antwerp (2003).
[17] J. F. Ziegler, and J. P. Biersack, Computer code SRIM 2008 program package, http://www.srim.org
[18] S. Bâjt, D. G. Stearns, and P. A. Kearney, J. Appl. Phys. 90, 1017 (2001).
[19] T. Tsarfati, E. Zoethout, R. W. E. van de Kruijs, F. Bijkerk, Surf. Sci. 603, 7, 1041 (2009)
[20] T. Tsarfati, E. Zoethout, R. W. E. van de Kruijs, F. Bijkerk, J. Appl. Phys. 105, 104305 (2009)
[21] T. Tsarfati, E. Zoethout, R. W. E. van de Kruijs, F. Bijkerk, in preparation
[22] A-L. Barabási, Phys. Rev. Lett. 70, 26 (1993).
[23] B. M. Clemens, W. D. Nix, and V. Ramaswamy, J. Appl. Phys. 87, 6 (2000).
[24] T. Tsarfati, E. Zoethout, R. W. E. van de Kruijs, F. Bijkerk, unpublished results
[25] M. Ronay, R. G. Schad, Phys. Rev. Lett. 64, 2043 (1990).

6 Chemically mediated diffusion of d-metals and B through Si and agglomeration at Si-on-Mo interfaces

6.1 Abstract

Chemical diffusion and interlayer formation in thin layers and at interfaces is of increasing influence in nanoscopic devices, such as nano-electronics and reflective multilayer optics. Chemical diffusion and agglomeration at interfaces of thin Ru, Mo, Si and B_4C layers have been studied with XPS, CS-EELS, HAADF-STEM and EDX in relation to observations in Ru-on-B_4C capped Mo/Si multilayers. Rather than in the midst of the Si layer, silicides and borides are formed at the Si-on-Mo interface front, notably $RuSi_x$ and MoB_x. The interface apparently acts as a precursor for further chemical diffusion and agglomeration of B, Ru, and also other investigated d-metals. Reversed "substrate-on-adlayer" interfaces can yield entirely suppressed reactivity and diffusion, stressing the influence of surface free energy and the supply of atoms to the interface via segregation during thin layer growth.

6

6.2 Introduction

The morphology of layer growth on a dissimilar substrate layer is affected by the lattice mismatch, the chemical reactivity, and the surface free energy difference[1,2]. In this paper we characterize the influence of these factors by considering nanometer thin Ru, Mo, Si and B_4C substrate and adsorbate layers to cover a wide range of interface characteristics. Ru does not readily react with Mo and the two transition metals have comparable lattice spacings and surface free energies that are very different from Si and B_4C. Mo forms a relatively stable silicide interface with Si[3], while Ru and some other d-metals diffuse into a Si substrate layer without significant reactivity[4]. B_4C dissociates upon deposition and readily forms borides with Mo and Ru, while carbides are only kinetically favored with Mo and Si. All materials involved are considered both as ad- and substrate layer to study the effect of dissociative B_4C deposition as observed by I. Nedelcu et al.[3], and the surface free energy driven intermixture (segregation) on the adsorbate/substrate dependency for compound formation. Layer and interface growth and compound formation can be optically studied in multilayer coatings that act as artificial Bragg crystals. Reflective multilayer x-ray optics are also of increasing importance for applications in astronomy, medicine and next generation lithography.

For extreme UV lithography (EUVL, $\lambda = 13.5$ nm), high contrast Mo/Si multilayers with individual layer thicknesses of 3 to 4 nm are applied as condenser, illuminator and projection optics. To protect the reflecting mirror surface against photo induced oxidation and the resulting decrease in reflectivity, a capping layer is applied on top of the multilayer[5], with Ru as a common reference material[6,7]. Cap thickness and intermixture with the layers beneath strongly influence the overall reflection and the protection that the cap offers. We relate our characterization of the interlayers between B_4C, Ru, Mo, and Si to the application of a B_4C diffusion barrier layer between the Ru and subsurface Si. This could reduce the overall intermixing and limit subsequent reflection loss, as proposed by Bâjt et al.[7].

6.3 Experimental details

The layers have been grown onto natively oxidized super polished Si (100) substrates that are pre-coated with Si in an electron-beam physical vapor deposition (PVD) setup with a base pressure of $1{\cdot}10^{-6}$ Pa[8]. This deposition technique was used for Si, B_4C, Mo, and Ru to limit direct implantation of high energy atoms that might occur using higher adatom energy deposition techniques such as magnetron sputtering. Quartz crystal oscillator mass balances and in situ C-K_α x-ray reflectometry are used for layer thickness control. A flux-shaping mask is used to deposit the B_4C diffusion barrier with a lateral layer thickness gradient from 0.4 to 5.0 nm[9,10], before depositing the Ru capping layer.

A Thermo Theta Probe monochromated Al-K_α x-ray photoelectron spectroscopy (XPS) setup with ion gun was used for sputtering and immediate subsequent on spot analysis of the in-depth material distribution and compound formation. The penetration and possible ion mixing depths of the used 0.5 keV Ar^+ sputter ions at 45° incidence are ~1.6 nm in Si, ~1.3 nm in B_4C, and ~0.7 nm in d-metals like Mo and Ru[11]. Considering the ~0.7 nm inelastic mean free path of the photoelectrons[12], the calculated ion mixing components are minor to moderate.

Differences in sputter efficiency and electron escape depths for the different materials result in underestimation of the Si content in the multilayer. This can result in early detection of subsurface elements during depth profiling, i.e. an apparent layer front shift to the surface. Thin layer systems thus appear more smeared out than they are. Considering that the XPS probing depth is considerably larger than the range of ion-beam induced chemistry, the in-depth modulation of electron binding energies, i.e. XPS peak shifts, can give a good indication of in depth chemical states.

The depth scale in the graphs shown in this study is determined from the deposited layer thicknesses and periodicity in the multilayer as established by quartz microbalances and in-situ reflection measurements. Differences in sputter efficiency and electron escape depths for the different materials that result in under-estimation of the Si content in the multilayer are not of influence in the presented results, considering our focus on the surface composition and not on multilayer periodicity.

Cross section electron energy loss spectroscopy (CS-EELS), high-angle annular dark field scanning transmission electron microscopy (HAADF-STEM) and energy dispersive X-ray (EDX) analysis were performed with a FEI Tecnai F30ST, operated at 300 kV. The samples were prepared by focused ion beam (FIB) using a FIB2000. This procedure damages the upper ~20 nm of the sample. The sample is first analyzed with a sample thickness of ~100 nm and ion beam damage on both sides. Further thinning to <80 nm was achieved with low-energy ions.

6.4 Results and discussion

Figure 33 shows the sputter depth profiles of three $Ru/B_4C/Si/(Mo/Si)$ multilayers with B_4C layer thicknesses of 5.0 nm (solid line), 1.7 nm (dashed line) and 0.4 nm (dotted line). The Ru and Si layers are kept at constant 1.5 and 2.5 nm thicknesses respectively[4]. The profiles are matched to the multilayer periods, with the top Si-on-Mo interface defined at 0.0 nm sputter depth.

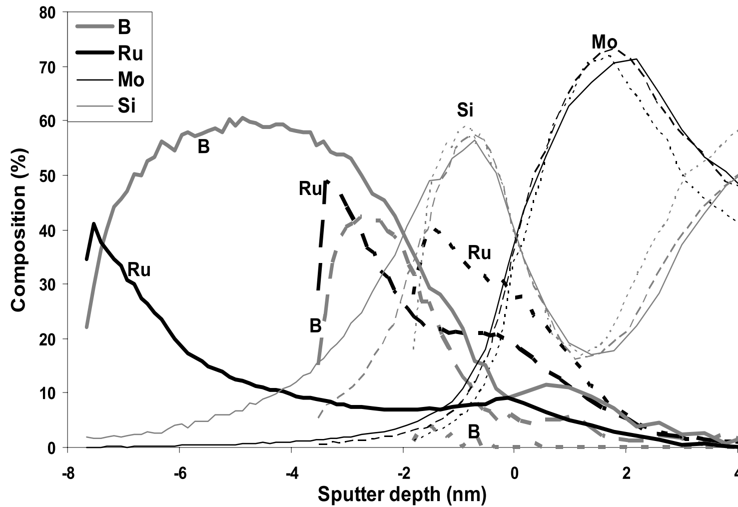

Figure 33: *XPS sputter depth profiles of three Ru/B_4C/Si/(Mo/Si) multilayers with 5.0 nm (solid line), 1.7 nm (dashed line), and 0.4 nm (dotted line) thick B_4C diffusion barriers.*

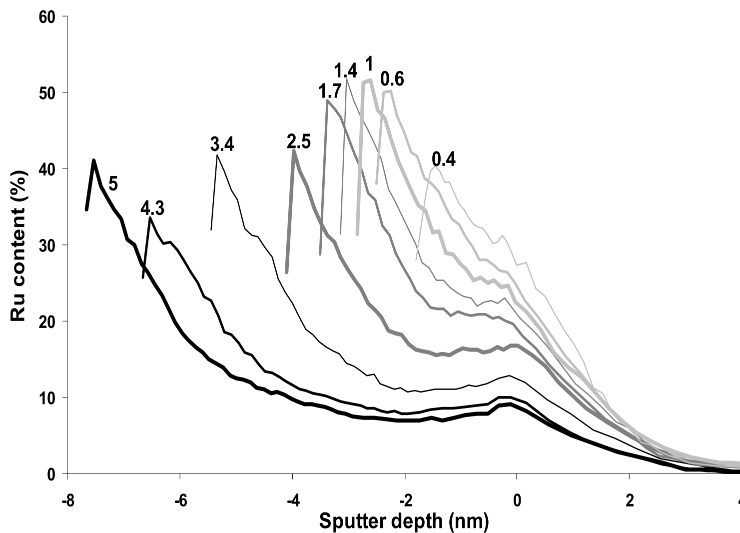

Figure 34: *In-depth Ru content in atomic percent for various B_4C barrier layer thicknesses (labeled in nm) as determined by XPS sputter depth profiling.*

The smearing out of Mo when thicker B_4C diffusion barriers are applied on top can be attributed to some loss of depth resolution. The Si appears to diffuse upward into the on top B_4C, due to its lower surface free energy[13,14,15]. We do not observe a shift of the Si2p electron binding energy (BE) from its elemental value of 99.3 eV. This suggests that recombination of atomically deposited B_4C occurs at the Si substrate layer and no kinetically unfavorable SiB_x and SiC_x are formed. To consider the in-depth Ru

distribution in more detail, it has been plotted separately for all investigated underneath B_4C diffusion barrier thicknesses in Fig. 34, with the abscissa similar to Fig. 33.

Observed from the Ru surface, all depth profiles in Fig. 34 show a similar exponential decay in Ru content over a depth of several nm, as would be expected for a layered structure. The Ru diffuses through both the B_4C and the Si, agglomerating at the Si-on-Mo interface as defined at 0 nm depth. Within the investigated range of B_4C barrier thicknesses, none of the B_4C diffusion barriers is observed to completely inhibit Ru diffusion. The increasing Ru residue below the B_4C layer for decreasing B_4C layer thickness has been confirmed using Auger electron spectroscopy depth profiling[7]. Ru, Rh, Y, Nb and Ir also diffuse through a Mo and Si layer to agglomerate at the Si-on-Mo interface, generalizing the observations for a range of d-metals[4]. To verify that the observations are not a result of lateral Ru on B_4C growth inhomogeneity, Fig. 35 shows an AFM image of a Ru/B4C capped multilayer surface when a 2.0 nm thick B_4C diffusion barrier is applied.

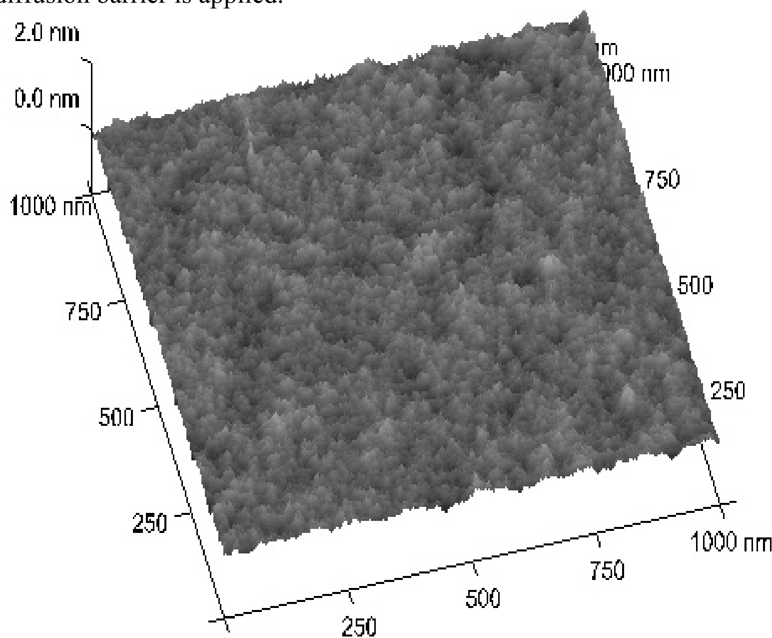

Figure 35: *AFM image of a Ru capped multilayer with a 2.0 nm thick B_4C diffusion barrier.*

The AFM image in Fig. 35 reveals a 0.1 nm RMS and 0.57 nm peak-to-valley roughness, indicating that Ru on B_4C growth and the observed diffusion do not increase roughness compared to Ru/Mo/Si/(Mo/Si) multilayers, for which Ru agglomeration at the Si-on-Mo interface front was also visible in 0.5 and 0.25 keV Ar^+ depth profiles[4]. The Ru agglomeration persisted or even increased after 48 hours anneal at 300° C, implying that the agglomeration is a thermodynamically preferred configuration.

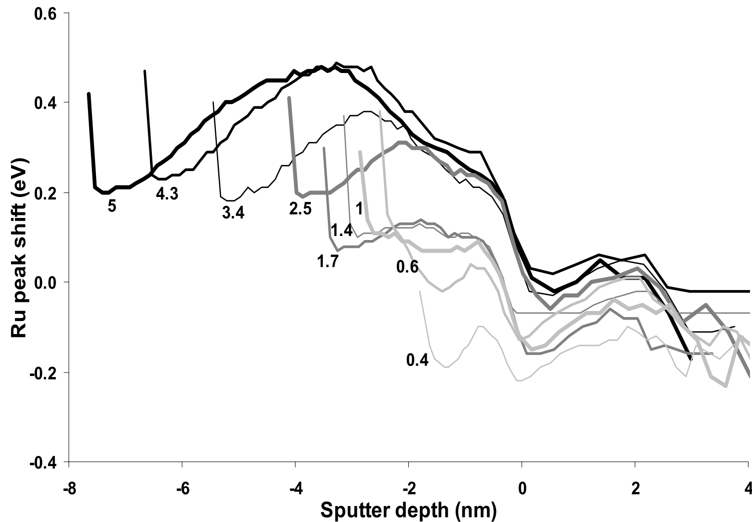

Figure 36: *$Ru3d_{5/2}$ peak deviation from it elemental value of 280.0 eV BE for various B_4C barrier layer thicknesses (labeled in nm) as established by in-depth XPS analysis.*

Figure 36 shows the $Ru3d_{5/2}$ in-depth peak shift from its elemental value in reference to the Fermi level, giving an indication of the chemical state and compound formation. The in-depth $Ru3d_{5/2}$ BE modulation up to 0.5 eV in the 4.3 and 5.0 nm thick B_4C layers cannot be attributed to oxidation as is the case at the surface, since no subsurface oxygen is observed in XPS. A coinciding B1s BE increase from 188.0 to 188.6 eV suggests RuB formation at the cost of B_4C decomposition. The C1s peak appears to shift from 282.0 eV to 282.8 eV, suggesting a transition from carbide (B_4C) in the direction of the elemental value of 284.5 eV. Towards the Si/Mo interface, the Si2p BE increase of 0.3 eV suggests silicide formation. The $Mo3d_{5/2}$ peak at 227.8 eV BE excludes neither elemental Mo nor a silicide. At the Si/Mo interface, the decrease of $Ru3d_{5/2}$ BE observed in Fig. 36 suggests Ru_2Si_3 formation. This means that the Ru agglomeration as observed in Fig. 34 coincides and likely is a result of Ru_2Si_3 formation at the Si/Mo interface, which would sustain Ru migration. Towards the Si/Mo interface, a change in the nearest neighbor distance and/or formation of Mo silicides could accommodate Ru_2Si_3 formation. With $E_{act} \approx 130$ kJ/mole, $MoSi_2$ could be an intermediate or precursor for Ru_2Si_3 formation, for which $E_{act} \approx 174$ kJ/mole[16]. Ronay and Schad observed similar precursor functionality of Cu_3Si, which was found to lower the formation temperature of $ReSi_2$[17]. Like Ru, B is observed to agglomerate at the Si/Mo interface, as can be seen in Fig. 37.

The B tail in Fig. 37 shows a similar slope for the various B_4C layer thicknesses systems. Small differences can be attributed to ion mixing which is more prominent when more B_4C is present in the system. The B agglomeration is accompanied by a significant B1s electron binding energy increase in the Mo layer, suggesting that B migration towards the Mo layer is accommodated by MoB_x formation, which stops further B diffusion. A similar mechanism occurs in the multilayer when B_4C diffusion barriers are applied[3,18,19,20]. Figure 38 shows a ~0.3 nm beam size EELS cross section of a multilayer with five periods of 3.5 nm thick Mo and Si layers on five periods of 3.0 nm thick Mo

and Si layers with a 1.0 nm thick B_4C barrier at each interface. The profiles are corrected for the total transmission of the TEM sample, which is much less in Mo than in Si.

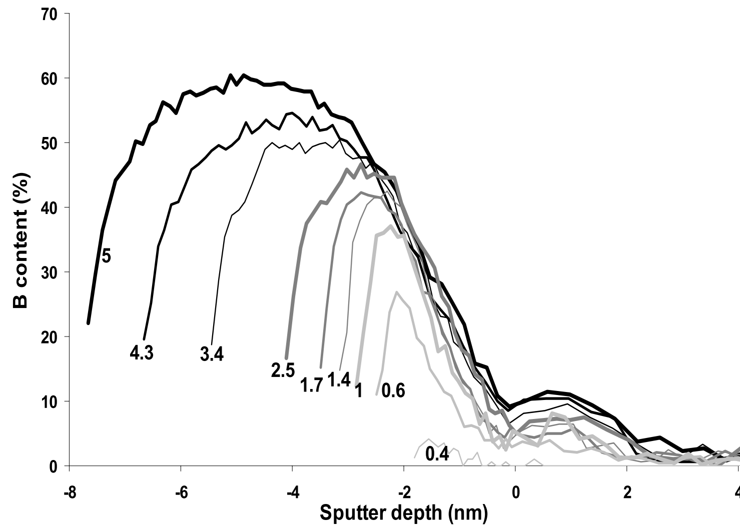

Figure 37: *In-depth B distribution for various B_4C barrier layer thicknesses (labeled in nm) as established by XPS sputter depth profiling.*

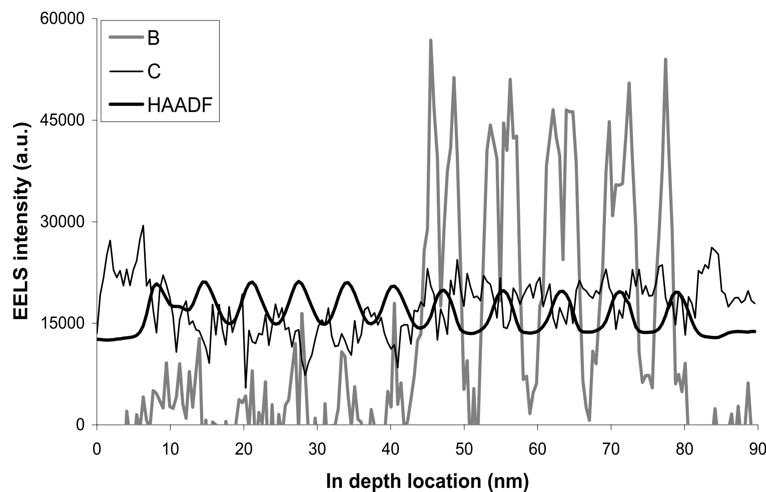

Figure 38: *Cross section EELS of a multilayer with five periods of 3.5 nm thick Mo and Si layers on five periods of 3.0 nm thick Mo and Si layers with a 1.0 nm thick B_4C barrier at each interface. Peaks in the HAADF intensity correspond to Mo layers, valleys to Si layers.*

The CS-EELS in Fig. 38 reveals highly localized B peaks that are predominantly located in the Mo layers. This means that the B diffuses from both the Mo/Si and Si/Mo interface into the Mo layer, where it can form MoB_x. The in-depth C distribution appears very diffusive with probably a large contribution from the sample preparation. The 16–84%

Mo-on-Si and Si-on-Mo interface widths are 1.08 and 1.24 nm respectively, compared to 1.75 and 1.50 nm without B_4C. The difference at the Si-on-Mo interface is within the finite resolution and the instrumental error, but the Mo-on-Si interface profits from reduced segregation by application of a B_4C diffusion barrier. HAADF-STEM analysis with a beam diameter <0.3 nm confirms the observations (Fig. 39), although the barrier layers are not individually identifiable.

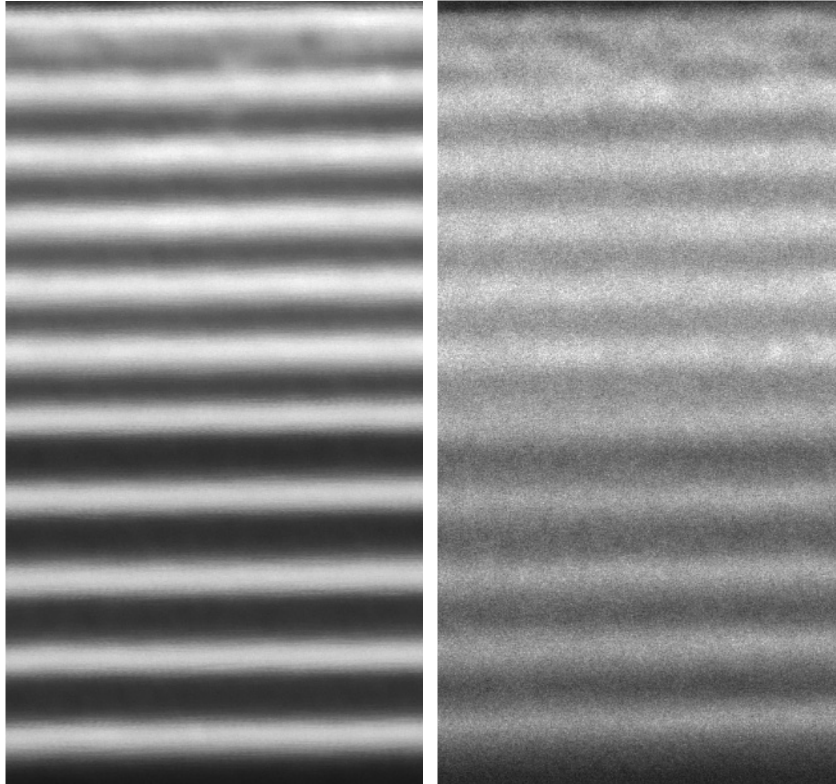

Figure 39: *Cross section HAADF-STEM image with a <1 nm (left) and <0.3 nm (right) footprint of a Ru capped 5x(Mo/Si) 5x(Mo/B_4C/Si/B_4C) multilayer.*

In Fig. 39, the B and C presence also appear to reduce layer inhomogeneity and interface diffuseness. In XPS depth profiling studies on Si/Mo multilayers with B_4C diffusion barriers, we observe a locally B-rich stoichiometry, while C is more diffused[3]. In the case of Si and B_4C, borides will not spontaneously form, due to unfavorable formation enthalpy. Only elemental C, that is in equilibrium with B_4C, can react with Si to form SiC, with ΔH^{for}_{SiC} = -65 kJ/mole, considering the chemical equilibrium (K) of compound formation

$$K = e^{\frac{-\Delta G^{for}}{RT}} = e^{\frac{\Delta S^{for}}{R}} \cdot e^{\frac{-\Delta H^{for}}{RT}}, \tag{8}$$

where the ΔS^{for} term covers differences in phase and crystal structure. Since these differences are small for solid-solid interactions occurring at the interface, we take $\Delta G^{for} \approx \Delta H^{for}$. B_4C deposition onto Si results in a chemically inactive interface with significant B_4C segregation towards the subsurface to maintain a surface monolayer of Si, of which both the surface free energy and the enthalpy for vacancy formation are lowest. When B_4C is atomically deposited onto Ru or Mo, the largest kinetic gain is obtained respectively by;

$$4\,\mathrm{Ru} + 4\,\mathrm{B} + \mathrm{C} \rightarrow 4\,\mathrm{RuB} + \mathrm{C}\text{, and} \quad (9)$$

$$6\,\mathrm{Mo} + 4\,\mathrm{B} + \mathrm{C} \rightarrow 4\,\mathrm{MoB} + \mathrm{Mo_2C}\text{,} \quad (10)$$

with ΔH^{for}_{RuB} = -35 kJ/mole, ΔH^{for}_{MoB} = -62 kJ/mole, ΔH^{for}_{Mo2C} = -46 kJ/mole[16] and negligable Ru and Mo lattice energy. This implies formation of RuB via equation (9), MoB and Mo_2C via equation (10) at the respective interfaces, and negligible B_4C recombination. Surface segregation is not energetically favorable, and the decreasing Ru and Mo atom supply to the surface upon boride formation can favor another stoichiometry. When surface Ru or Mo are finally depleted, B_4C recombination can occur.

The experimental results show reactive interfaces when B_4C is used in multilayer applications. Increased B concentration and B1s electron binding energy at the B_4C/Mo interface hint at MoB formation via equation (10). Transition metal boride and carbide formation at B_4C interfaces has also been observed by P. Mogilevsky et al.[21]. In the experiments, various metal borides and carbides appear to be favored over B_4C, in accordance with the earlier described thermodynamics. To identify the adsorbate/substrate dependency of thin layer growth mechanisms, Fig. 40 shows an XPS sputter depth profile of a four material multilayer with interfaces in all the possible orientations; Si/Ru/Mo/B_4C/Si/Mo/Ru/B_4C/Mo/Si/B_4C/Ru/Si. Ru and Mo layers are 4 nm thick, first and last Si layer 7 nm, B_4C and other two Si layers 15 nm.

From the depth profile, it is clear that the sputter rate for B_4C is significantly lower than for Si. Si segregation into B_4C is again visible for B_4C on Si, and to lesser extends for B_4C on Ru and B_4C on Mo, indicating a moderately high surface free energy of the deposited B_4C. Like Ru, diffusion of Mo into a B_4C substrate layer is significant. Clear Mo segregation into Si and relatively sharp B_4C/Mo and Si/Mo interfaces are also visible. For in-depth chemical analysis, Fig. 41 shows the B1s, C1s, Ru3d, Mo3d and Si2p peak shifts from bulk values, superimposed on the depth profile.

Segregation of Mo, similar to Ru, delays B_4C depletion and results in a broad MoB and Mo_2C interlayer. Si2p, Mo3d and Ru3d electrons all show a considerable upward binding energy shift when the corresponding materials are deposited onto B_4C, while the shift is much smaller when these materials form the substrate layer for B_4C growth. Significant B1s peak shifts are observed for B_4C interfaces with Mo and Ru. When Ru is replaced by Y, which has the lowest surface free energy per unit area of the d-metals, we observe quite similar diffusion and compound formation. It is remarkable that the binding energy shifts appear much more adsorbate/substrate than material dependent and that instead of B_4C dissociation, the supply of atoms via segregation is of main influence.

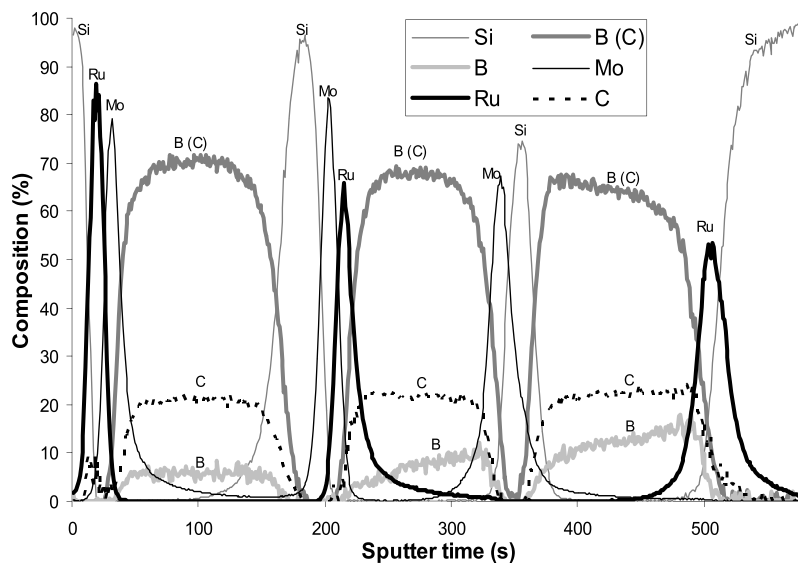

Figure 40: *XPS sputter depth profile of a four material multilayer system with all ad-/substrate layer combinations; B bonded to C is denoted B (C).*

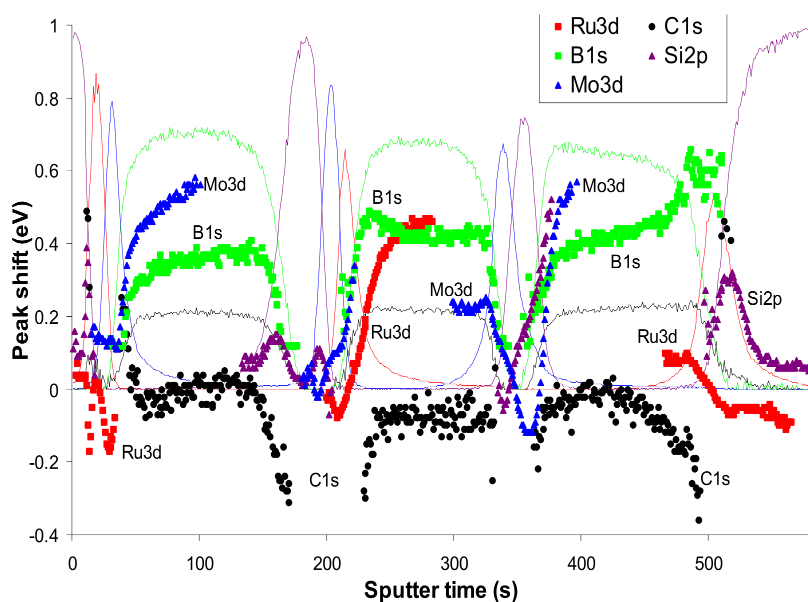

Figure 41: *Peak-shifts (dots, superimposed on the depth profile) for Ru3d, C1s, B1s, Si2p and Mo3d as determined by XPS sputter depth profiling. A 0.0 eV peak shift represents binding energies of 280.0, 283.0, 188.0, 99.3, and 227.8 eV for the respective materials.*

6.5 Conclusions

Diffusion and compound formation in Ru, Mo, Si and B_4C layers have been characterized with XPS, CS-EELS, HAADF-STEM and EDX. Minimization of the surface free energy causes significant B_4C surface segregation into the Si, driving Si towards the surface. The intermixture is not accompanied by chemical activity. The B1s, C1s and Si2p electron binding energies reveal no SiB and SiC, both species not being kinetically favored over B_4C.

Significant Ru surface segregation and further diffusion into the B_4C and Si layer occur for all B_4C diffusion barrier thicknesses up to 5.0 nm. Ru diffusion coincides with Ru3d, B1s and C1s electron binding energies that suggest Ru boride formation at the cost of B_4C, particularly for the thickest B_4C layers.

Ru and B diffuse through the Si layer towards the Si/Mo interface front, where agglomeration occurs. This is in accordance with earlier experimental results, which showed Ru agglomeration to also be persistent after annealing. Shifts of the Ru3d and B1s electron binding energies suggest the agglomeration is accompanied by Ru_2Si_3 and MoB formation. Our results confirm earlier conclusions that the Si/Mo interface front acts as a precursor for Ru silicide formation, accommodating Ru migration to minimize the energy. The observations for Ru can be generalized to other d-metals including Y, Nb, Rh and Ir. B agglomeration is found to be accommodated by MoB formation, which is strongly favored over the endothermic SiB formation process and to a lesser extend over formation of RuB.

6.6 Acknowledgements

This work is part of the FOM Industrial Partnership Programme I10 ('XMO') which is carried out under contract with Carl Zeiss SMT AG, Oberkochen and the 'Stichting voor Fundamenteel Onderzoek der Materie (FOM)', the latter being financially supported by the 'Nederlandse Organisatie voor Wetenschappelijk Onderzoek (NWO)'. The author wishes to thank Dr. J.G.M. van Berkum of Philips Research for the CS-EELS, HAADF-STEM and EDX measurements.

6.7 References

[1] T. Young, "An Essay on the Cohesion in Fluids", Philos. Trans. 95, 65 (1805).
[2] H. Roder, R. Schuster, and K. Kern, "Monolayer-confined mixing at the Ag-Pt(111) interface", Phys. Rev. Lett. 71, 13 (1993).
[3] I. Nedelcu, R. W. E. van de Kruijs, A. E. Yakshin, F. Bijkerk, "Microstructure of Mo/Si multilayers with B4C diffusion barrier layers", Appl. Opt. 48, 2, 155 (2009).
[4] T. Tsarfati, E. Zoethout, R. W. E. van de Kruijs, F. Bijkerk, "In-depth agglomeration of d-metals at Si-on-Mo interfaces", J. of Appl. Phys. 105, 064314 (2009).
[5] L. E. Klebanoff, M. E. Malinowski, P. A. Grunow, W. M. Clift, C. Steinhaus, A. H. Leung, and S. J. Haney, Proc. SPIE 4343 Emerging Lithographic Technologies V, Elizabeth A. Dobisz, 3422001 (2001).
[6] T. Tsarfati, E. Zoethout, R. W. E. van de Kruijs, F. Bijkerk, "Growth and sacrificial oxidation of transition metal nanolayers" Surf. Sci. 603, 7, 1041 (2009).

[7] S. Bâjt, J.B. Alameda, T.W. Barbee Jr, W.M. Clift, J.A. Folta, B. Kaufmann, E.A. Spiller, "Improved reflectance and stability of Mo-Si multilayers", Opt. Eng. 41(8) 1797 (2002).

[8] E. Louis, H.-J. Voorma, N.B. Koster, L. Shmaenok, F. Bijkerk, R. Schlatmann, J. Verhoeven, Yu. Ya. Platonov, G.E. van Dorssen and H.A. Padmore, "Enhancement of reflectivity of multilayer mirrors for soft x-ray projection lithography by temperature optimization and ion bombardment", Microelectron. Eng. 23**,** 215 (1994).

[9] A.E. Yakshin, E. Louis, P.C. Görts, E.L.G. Maas, F. Bijkerk, "Determination of the layered structure in Mo/Si multilayer by grazing incidence X-ray reflectometry", Physica B. D.K.G.d. Boer. Amsterdam, Elsevier, 283, 143 (2000).

[10] R. W. E. van de Kruijs, E. Louis, A. E. Yakshin, P. Suter, E. Zoethout, F. Bijkerk, S. Müllender, H. Enkisch, H. Trenkler, M. Wedowski, M. Weiss, B. Mertens, B. Wolschrijn, R. Jansen, A. Duisterwinkel, A. van de Runstraat, R. Klein, S. Plőger and F. Scholze, "Optimization of protective capping layers for EUVL optics" Proc. 2nd Int. EUV Lithography Symposium, Belgium (2003).

[11] J. F. Ziegler, and J. P. Biersack, Computer code SRIM 2008 program package, http://www.srim.org

[12] S. Tanuma, C. J. Powell, D.R. Penn, "Calculations of electron inelastic mean free paths. II. Data for 27 elements over the 50-2000 eV range", Surf. and Interface Anal. 17, 911 (1991).

[13] A-L. Barabási, "Surfactant-Mediated Growth of Nonequillibrium Interfaces", Phys. Rev. Lett. 70, 26 (1993).

[14] B. M. Clemens, W. D. Nix, and V. Ramaswamy, "Surface-energy-driven intermixing and its effect on the measurement of interface stress", J. Appl. Phys. 87, 6 (2000).

[15] T. Tsarfati, E. Zoethout, R. W. E. van de Kruijs, F. Bijkerk, "Near normal incidence reflective multilayer optics for short wavelength radiation sources and next generation Extreme UV lithography", submitted

[16] F. R. de Boer, R. Boom, W. C. M. Mattens, A. R. Miedema, and A. K. Niessen, "Cohesion in Metals: Transition metal alloys" (North-Holland, Amsterdam, 1988).

[17] M. Ronay, and R. G. Schad, "New insight into silicide formation: The creation of silicon self-interstitials", Phys. Rev. Lett. 64, 2042 (1990).

[18] A. Patelli, V. Rigato, G. Salmaso, N.J.M. Carvalho, J.Th.M. De Hosson, E. Bontempi, L.E. Depero, "Ion bombardment effects on nucleation of sputtered Mo nano-crystals in Mo/B4C/Si multilayers", Surface & Coatings Technology 201, 143 (2006).

[19] L.G. Jacobsohn, R.D. Averitt, M. Nastasi, "The role of trapped Ar atoms in the mechanical properties of boron carbide films deposited by dc-magnetron sputtering", J. Vac. Sci. Technol., A. Vac. Surf. Films 21, 5, 1639 (2003).

[20] T. Böttger, D.C. Meyer, P. Paufler, S. Braun, M. Moss, H. Mai, E. Beyer, "Thermal stability of Mo/Si multilayers with boron carbide interlayers", Thin Solid Films 444, 1, 165 (2003).

[21] P. Mogilevsky, E. Y. Gutmanas, I. Gotman, and R. Telle, "Reactive formation of coatings at boron carbide interface with Ti and Cr powders", Journal of the European Ceramic Society 15, 6, 527 (1995).

7 Reflective multilayer optics for 6.7 nm wavelength radiation sources and next generation lithography

7.1 Abstract

Reported is a computational and chemical analysis of near normal incidence reflective multilayer optics for 6.7 nm wavelength applications in e.g. the Free Electron Laser FLASH and next generations of EUV lithography. We model that combinations of B or B_4C with La offer a reflectivity of ~70%. The small reflection bandwidth poses problems in applications, but it can be significantly improved by replacing La with Th or U. Reflectometry, CS-TEM, and in-depth XPS analysis of B/La and B_4C/La multilayers reveal chemical reactivity at the interfaces. Significant LaB_x interlayer formation is observed in especially B/La multilayers, stressing the relevance of interface passivation. We propose nitridation of the interfaces, which mitigates interlayer formation and simultaneously increases optical contrast.

7.2 Introduction

We present a computational and experimental survey of multilayer optics to maximize reflection around the 6.7 nm range at near normal angle of incidence (AOI). New short wavelength radiation sources, e.g. soft x-ray free electron lasers (X-FELs) and next generation lithography call for high reflection optics, in most cases preferably at near normal AOI[1]. Fig. 1 shows some reported reflectivity values (R) in the 2 to 20 nm wavelength and AOI range[2].

7

7.3 Results and discussion

Figure 42 shows a positive correlation between wavelength and reflection, due to optical properties and the influence of e.g. layer diffuseness. We will here concentrate on optics for $\lambda = 6.7$ nm, the position of the boron K absorption edge, where B and B_4C can act as low absorbing spacer layers. Several studies have shown that, compared to B_4C/Mo, B_4C/La multilayers offer significantly better reflectivity at relatively grazing AOI[3,4,5], with applications in e.g. soft x-ray spectroscopy, fluorescence analysis and imaging.

Figure 43 shows the calculated reflection curve at 1.5° off normal AOI for the best candidate quarter-wave multilayers, assuming a 0.3 nm interface diffuseness which is conventional fur Mo/Si multilayer optics in EUV lithography[6]. Somewhat inferior candidates include B and B_4C combinations with e.g. CsI and LaF_3. The number of periods is 200, the effective maximum that contributes to reflection.

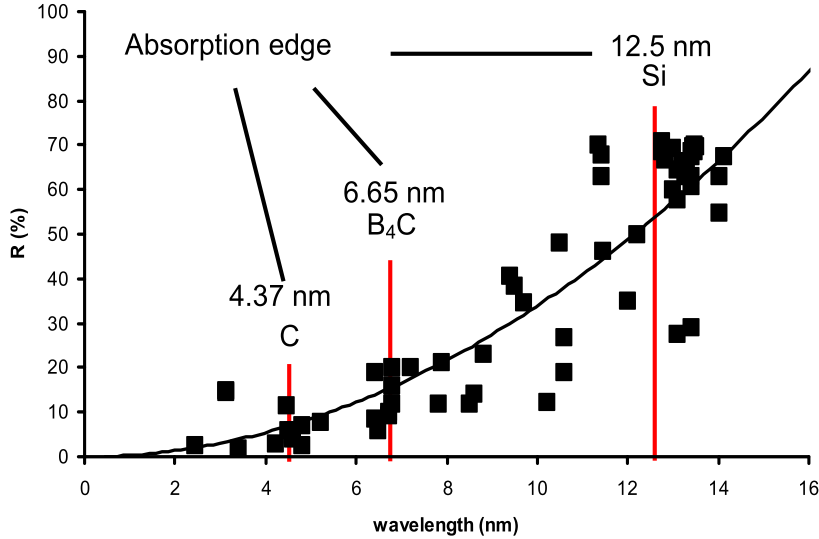

Figure 42: *Reported reflectivity values for < 5° off normal AOI. The C, B_4C and Si absorption edges are indicated.*

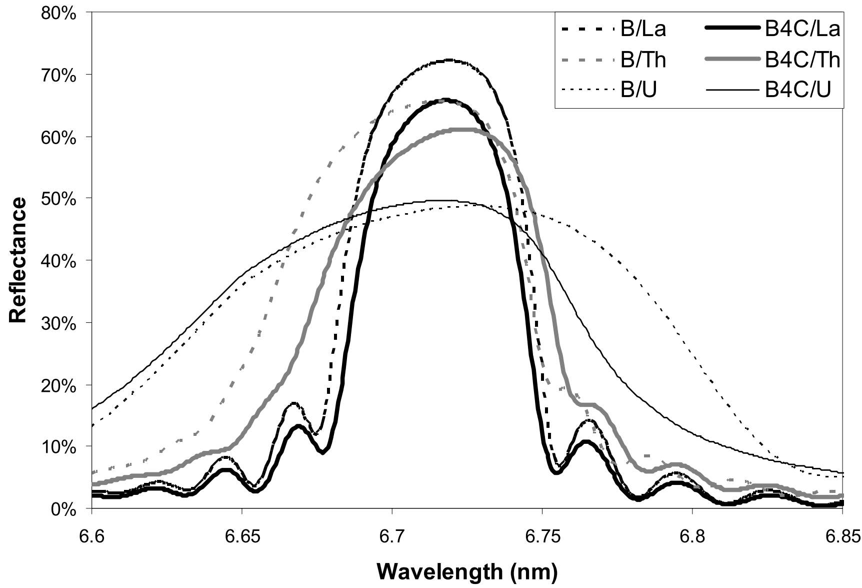

Figure 43: *Calculated reflectivity curves of the best performing 200 period multilayers at 1.5° off normal AOI, assuming 0.3 nm interface diffusiveness.*

IMD simulations[7] show that the reflection bandwidth is only ~0.06 nm for the B_4C/La multilayer, which is ~11% of the Si/Mo multilayer reflection bandwidth for 13.5 nm EUV reflection. When B or B_4C is combined with Th or U, simulations indicate significantly larger bandwidths of 0.09 and 0.17 nm resp., due to the higher optical contrast at the interfaces. AFM and TEM studies on Al/U and Si/U multilayers have

revealed that these systems yield an interface diffuseness of ~0.5 nm[8]. Radioactivity hazard of Th or U are calculated to be of no significance in mirror applications[9,10]. Most multilayer deposition setups do however not accommodate experimental research with these metals and we will therefore here consider only experimental B/La and B_4C/La multilayers.

Reflections of 53% at 65.5° with 50 periods[3] and 39.3% at 75.0° with 150 periods[11] have been reported at λ = 6.77 nm. We can model these results with a B_4C/La bilayer structure with interface diffuseness up to 0.75 nm, which might be attributed to polycrystallinities. We will show that the high chemical activity of La with B and C results in significant interlayer formation, explaining the experimental data.

The presence of nano-size crystallites[12] was investigated with x-ray diffraction (XRD) spectrum at λ = 0.154 nm (Cu-K_α) for two B/La and a B_4C/La multilayer that were produced with our multilayer deposition facilities[13], as shown in Fig. 44. The cross-section transmission electron microscopy (CS-TEM) image of the B_4C/La multilayer is also shown.

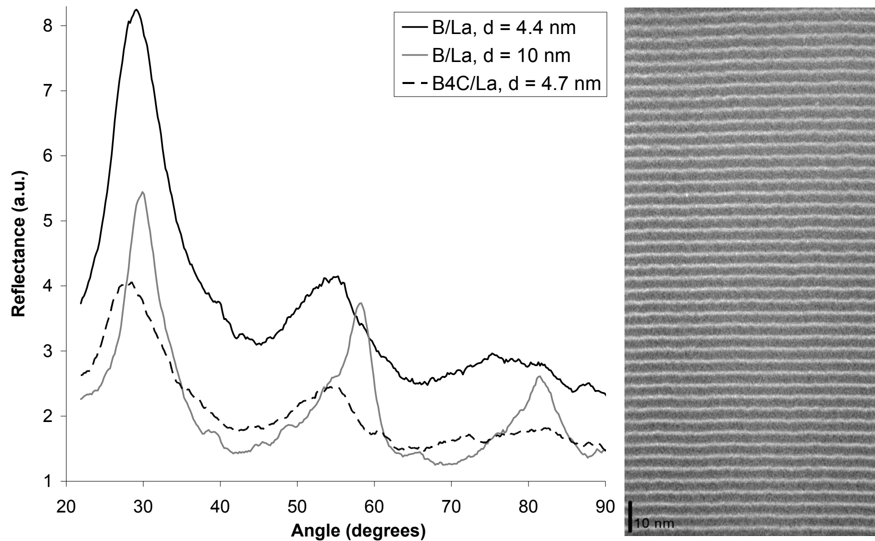

Figure 44: *XRD spectra at λ = 0.154 nm (Cu-K_α) of three multilayers (left) and the CS-TEM image of the B_4C/La multilayer (right).*

The XRD peaks at 27.3°, 56.3°, and 77.2° in Fig. 44 can originate from crystalline La <100>, La <200>, and La <210> planes respectively. The relative shifts of up to 5% would however indicate considerable lattice stress, and the absences of 2nd order peaks in the spectra suggest an amorphous structure for all three multilayers with a general nearest neighbor distance only. Also CS-TEM reveals no crystallinity in the multilayers, but we can observe an increasing lateral waviness of the layers from bottom to top. This is likely caused by relaxation of the lattice stress due to the significant lattice parameter differences[14]. We do observe La crystallization of 7 nm thick La layers in CS-TEM. The B_4C-on-La interfaces appear to be more diffuse than La-on-B_4C interfaces, attributable to the lower surface free energy of La, compared to B and B_4C[15,16,17].

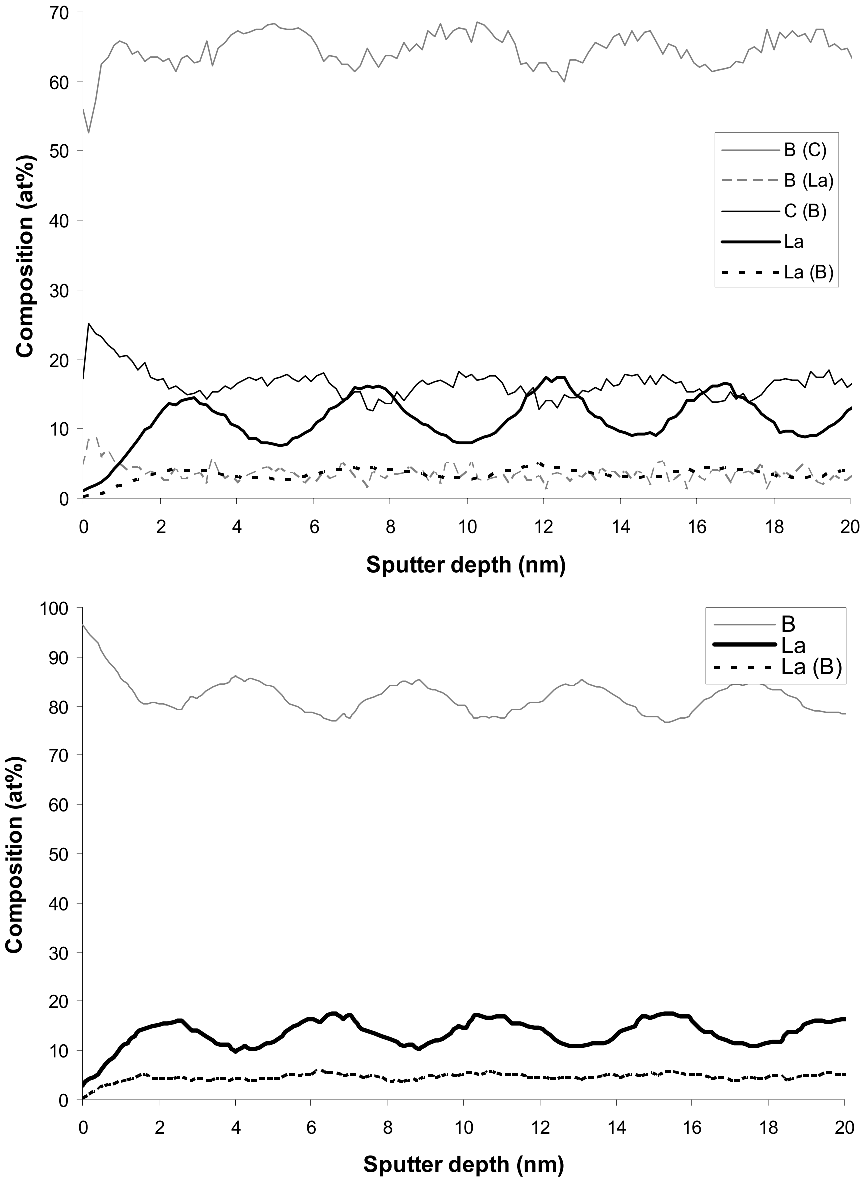

Figure 45: *In-depth XPS analysis of a B_4C /La (top) and B/La (bottom) multilayer, with 4.4 and 4.7 nm d-spacing respectively. In brackets the species to which they are likely bonded.*

Reflection measurements of the B_4C/La multilayer suggest a ~0.67 nm interface diffuseness[15,18,19] or up to 1.5 and 0.5 nm thick kinetically favorable LaB_6 and LaC_2 interlayers at the B_4C-on-La and La-on-B_4C interface resp. In-depth x-ray photoelectron spectroscopy (XPS) analysis of Mo/Si multilayers with B_4C diffusion barriers reveal a B-rich stoichiometry, while C appears to be more diffused and weakly bounded[20]. The experimental results show reactive interfaces when B_4C is used in multilayer applications, and stable metal borides and carbides appear indeed to be favored over B_4C.

Metal boride formation at the cost of B_4C has also been observed by P. Mogilevsky et al.[21].

With in-depth XPS analysis by 0.5 kV Ar^+ sputtering, we observe considerable intermixing of B and B_4C with La, as can be seen in Fig. 45 for the B/La and B_4C/La multilayer with a d-spacing of 4.4 and 4.7 nm respectively.

The multilayer profiles shown in Fig. 45 can be reconstructed using the atomic mixing and information depth component from the mixing-roughness-information depth (MRI) model[22] with a calculated atomic mixing (g_w) of 2 nm and an information depth (g_λ) of 3 nm in linear approximation. We model a bilayered structure with 1.2 nm thick B and La layers for the B/La, and 2.8 nm thick B_4C and 1.6 nm thick La layers for the B_4C/La multilayer. The reconstruction does not suggest significant interface gradients, although we observe a second La4d doublet at ~3.5 eV lower binding energy. Although XPS literature on La is very limited, this doublet might be attributed to LaB_6 and LaC_2 that are diffusely distributed throughout the multilayers. Taking also reflectometry, CS-TEM, angular resolved XPS measurements[23,24], formation enthalpy (ΔH^{for}) and optical constants as shown in Table III into account, we model an interface gradient that can be attributed to formation of LaB_6 and LaC_2, predominantly at the La layer front. This suggests atomic deposition of B and C[25], since incorporation of the dissociation of B_4C in the reaction via $7\,\mathrm{La} + 6\,\mathrm{B_4C} \rightarrow 4\,\mathrm{LaB_6} + 3\,\mathrm{LaC_2}$ practically cancels out any energy gain. La deposition onto an already recombined B_4C substrate layer thus yields limited interlayer formation at the La-on-B_4C interface. This could explain the better localization of La in a B_4C/La multilayer compared to a B/La multilayer. During photo exposure, energy supplied to the system can however shift this balance, yielding interlayer formation also at this interface. In Fig. 45 La (B) and for B_4C/La also B (La) incorporated in a LaB_x compound have been partially identified, but cannot account for up to 1.5 and 0.5 nm thick LaB_x interlayers, as modeled by reflection measurements. Table III shows the ΔH^{for}, the refractive index (n) and the absorption constant (β) at λ = 6.7 nm for La, B, B_4C, LaC_2, LaB_6, BN and LaN[26,27,28,29,30].

Compounds	La	B	B_4C	LaC_2	LaB_6	BN	LaN
ΔH^{for} (kJ/mol)	0	0	-71	-89	-130	-255	-303
n	0.984	1.001	0.999	0.986	0.992	0.995	0.981
β (10^{-3})	1.075	0.414	0.528	0.996	0.853	0.894	1.420

Table III. *Formation enthalpy and optical constants for compounds relevant to this work.*

The ΔH^{for} values in Table III reveal that LaB_6 and LaC_2 formation is kinetically favorable. To identify further possible presence of non-stoichiometric LaB_x, we consider the individual B1s, La3$d_{5/2}$ and La3$d_{5/2}$ (B) peak position, visible in Fig. 46.

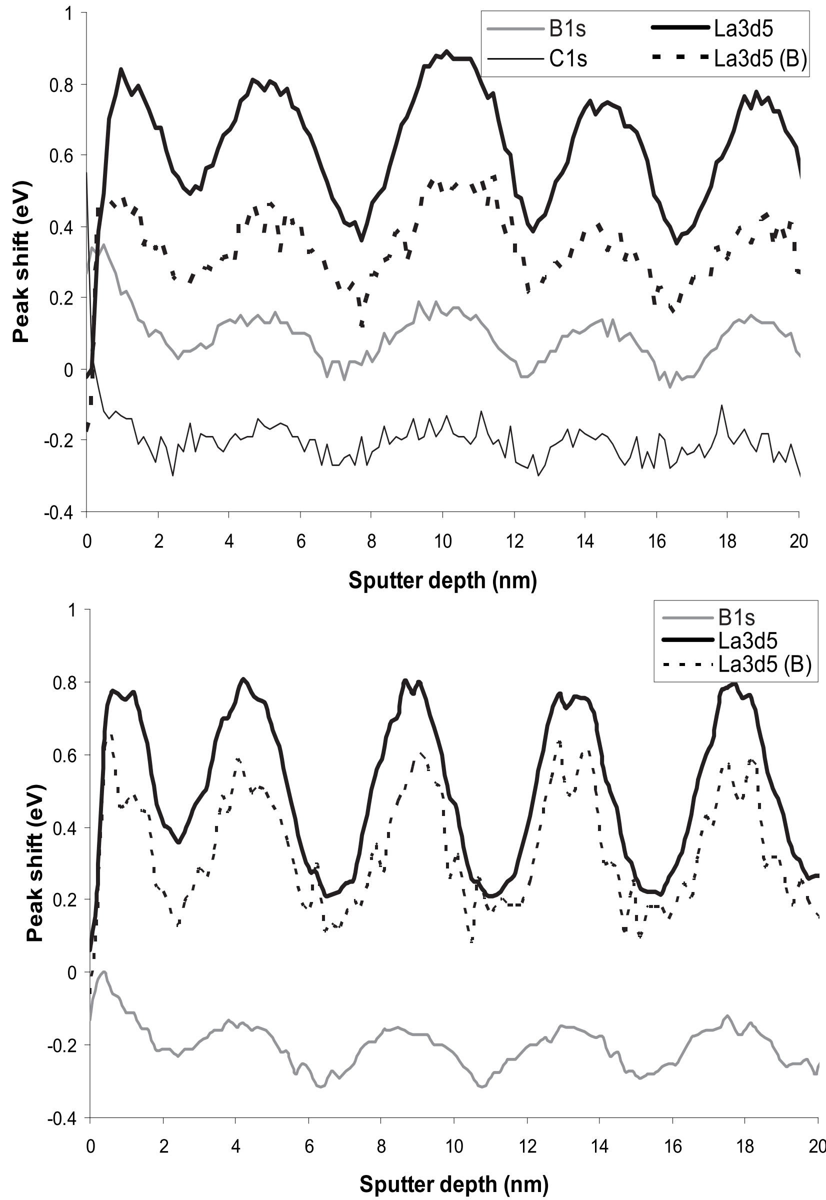

Figure 46: *Peak shifts for B1s, (C1s), La3d$_{5/2}$ and La3d$_{5/2}$ (B) in the B_4C/La (top) and B/La (bottom) multilayer in Fig 4. A 0.0 eV peak shift represents binding energies of 188.0, (283.0), 836.0 and 832.5 eV for the respective materials.*

The modulations in B1s peak position shown in Fig. 46 are very similar for the B/La and B_4C/La multilayers, while its absolute position is about 0.3 eV higher in the latter. The C1s peak at 282.8 eV is conventional for carbides and can be attributed to B_4C as well as LaC_2. Fig. 46 reveals a considerable modulation in the La3d peak position for both cases, especially the B/La multilayer. This suggests that considerable amounts of a LaB_x

compound are formed specifically in the B layers. Judging from the modulation in La3d peak position, B_4C appears somewhat more resistant to LaB_6 formation.

Considering the kinetic and optical properties as shown in Table III, we can passivate both interfaces by applying kinetically more stable compounds such as BN and LaN at the interfaces that simultaneously increase optical contrast[31]. An interface of B or B_4C with LaN should be entirely passivated against any interlayer formation. Nitridation of the interfaces is possible by bombardment with low energy N_2^+ to avoid ion induced layer intermixture[23]. With non-destructive angular resolved XPS analysis of bilayered systems, we observe surfactant-mediated growth by weakly bonded N_2 that diffuses from the substrate layer into the adlayer[23]. Multilayers with nitridated interfaces also show significantly improved layer contrast and reflectivity, as presented in the next chapter[23,24].

7.4 Conclusions

In conclusion, we presented a survey of multilayer reflective optics for use in the 6.7 nm wavelength range at near normal AOI and analyzed their chemical reactivity. We modeled that La, Th and U are the optimum contrast materials in B or B_4C spaced multilayers. With a suited experimental setup for Th and U deposition, the reflection bandwidth is calculated to improve by respectively ~50% to almost 300% in comparison to La, at the cost of 7% to 17% peak reflectance. B/La and B_4C/La combinations offer the highest theoretical reflection, but especially B/La multilayers are observed to yield chemical reactivity and interlayer formation at the interfaces. This has detrimental effects on optical contrast and reflection, stressing the importance of techniques to passivate the interfaces and improves layer contrast by e.g. nitridation. Applications are in e.g. X-FELs, next generations of Extreme UV photolithography, soft x-ray spectroscopy, fluorescence analysis and imaging.

7.5 Acknowledgements

This work is part of the FOM Industrial Partnership Programme I10 (‘XMO’) which is carried out under contract with Carl Zeiss SMT AG, Oberkochen and the ‘Stichting voor Fundamenteel Onderzoek der Materie (FOM)’, the latter being financially supported by the ‘Nederlandse Organisatie voor Wetenschappelijk Onderzoek (NWO)’. The author wishes to thank dr. N. Ghafoor of Linkoping University for the TEM measurements.

7.6 References

[1] E. Louis, A.R. Khorsand, R. Sobierajski, E.D. van Hattum, T. Tsarfati, M. Jurek, D. Klinger, J.B. Pelka, L. Juha, J. Chalupsky, J. Cihelka, V. Hajkova, U. Jastrow, S. Toleikis, H. Wabnitz, K.I. Tiedtke, J. Gaudin, F. Bijkerk, “Damage studies of multilayer optics for XUV FELs”, submitted

[2] www.CXRO.lbl.gov

[3] C. Michaelsen, J. Wiesmann, R. Bormann, C. Nowak, C. Dieker, S. Hollensteiner, and W. Jäger, Opt. Lett. 26, 11 (2001).

[4] P. Ricardo, J. Wiesmann, C. Nowak, C. Michaelsen, R. Bormann, Appl. Opt. 40, 16 (2001).
[5] J.-M. Andre, P. Jonnard, C. Michaelsen, J. Wiesmann, F. Bridou, M.-F. Ravet, A. Jérome, F. Delmotte, E. O. Filatova, 34 (2005).
[6] I. Nedelcu, R.W.E. van de Kruijs, A.E. Yakshin, F.D. Tichelaar, E. Zoethout, E. Louis, H. Enkisch, S. Müllender, F. Bijkerk, Thin Solid Films 515, 2, 434 (2006).
[7] D. Windt. IMD - Software for Modeling the Optical Properties of Multilayer Films. Computers in Physics. 12, 4, 360 (1998).
[8] J.E. Johnson, D.D. Allred, R.S. Turley, W.R. Evans, R.L. Sandberg, Materials Research Society (2005).
[9] D.D. Allred, M.B. Squires, R.S. Turley, W. Cash, A. Shipley, X-ray Mirrors, Crystals and Multilayers, A.K. Freund, A.T. Macrander, T. Ishikawa, J.T. Wood, Proc. SPIE 4782, 212 (2002).
[10] B.R. Sandel, A.L. Broadfoot, C.C. Curtis, R.A. King, T.C. Stone, R.H. Hill, J. Chen O.H.W. Siegmunt, R. Raffanti D.D. Allred, R. S. Turley and D.L. Gallagher, Space Sci. Rev. 91, 197 (2000).
[11] Y. Platonov, L. Gomez, D. Broadway, SPIE 12, 4782 (2002).
[12] R.W.E. van de Kruijs, E. Zoethout, A.E. Yakshin, I. Nedelcu, E. Louis, H. Enkisch, G. Sipos, S. Müllender, F. Bijkerk, Thin Solid Films 515, 2, 430 (2006).
[13] E. Louis, H.-J. Voorma, N.B. Koster, L. Shmaenok, F. Bijkerk, R. Schlatmann, J. Verhoeven, Yu.Ya. Platonov, G.E. van Dorssen, H.A. Padmore, Microelectron. Eng. 23, 215 (1994).
[14] R.W.E. van de Kruijs, E. Zoethout, A.E. Yakshin, I. Nedelcu, E. Louis, H. Enkisch, G. Sipos, S. Müllender, F. Bijkerk, Thin Solid Films 515 2, 430, (2006).
[15] F.R. de Boer, R. Boom, W.C.M. Mattens, A.R. Miedema, A.K. Niessen, Cohesion in Metals: Transition Metal Alloys (North-Holland, Amsterdam, 1988).
[16] T. Tsarfati, E. Zoethout, R.W.E. van de Kruijs, F. Bijkerk, Surf. Sci. 603, 7, 1041 (2009).
[17] T. Tsarfati, E. Zoethout, R.W.E. van de Kruijs, F. Bijkerk, J. Appl. Phys. 105, 064314 (2009).
[18] A. Patelli, V. Rigato, G. Salmaso, N.J.M. Carvalho, J.Th.M. De Hosson, E. Bontempi, L.E. Depero, Surface & Coatings Technology 201, 143-147 (2006).
[19] L.G. Jacobsohn, R.D. Averitt, M. Nastasi, J. Vac. Sci. Technol., A. Vac. Surf. Films 21, 1639 (2003).
[20] T. Tsarfati, E. Zoethout, R.W. E. van de Kruijs, F. Bijkerk, J. Appl. Phys. 105, 104305 (2009).
[21] P. Mogilevsky, E.Y. Gutmanas, I. Gotman, and R. Telle, Journal of the European Ceramic Society 15, 6, 527 (1995).
[22] S. Hofmann, Surf. Interface Anal. 27, 825 (1999).
[23] T. Tsarfati, E. Zoethout, E. Louis, R. W. E. van de Kruijs, F. Bijkerk, submitted
[24] T. Tsarfati, E. Zoethout, E. Louis, R. W. E. van de Kruijs, A. Yakshin, S. Müllender, and F. Bijkerk, Proc. SPIE Advanced Lithography 7271, 72713V (2009)
[25] I. Nedelcu, R.W.E. van de Kruijs, A.E. Yakshin, F. Bijkerk, Appl. Opt. 48, 2, 155 (2009).
[26] N. Ooi, V. Rajan, J. Gottlieb, Y. Catherine, J.B. Adams**,** Structural properties of hexagonal boron nitride, Modelling Simul. Mater. Sci. Eng. 14, 515 (2006).

[27] I. Narita, T. Oku, Synthesis of boron nitride nanotubes by using NbB_2, YB_6 and YB_6/Ni powders, Diamond and related materials 12, 1912 (2003).
[28] G. Vaitheeswaran, V. Kanchana, M. Rajagopalan, Solid State Communications 124, 97 (2002).
[29] G. Kalpana, B. Palanivel, M. Rajagopalan, Phys. Rev. B 50, 12318 (1994).
[30] G. Kalpana, B. Palanivel, M. Rajagopalan, , Phys. Rev. B 52, 4 (1995).
[31] T. Tsarfati, E. Zoethout, E. Louis, F. Bijkerk, "Method to Enhance layer contrast of a multilayer for reflection at the B absorption edge", US 61/079307 (US), DE102008040265 (Germany), priority date 16 September 2008.

8 Nitridation and contrast of B_4C/La interfaces and multilayers

8.1 Abstract

Chemical diffusion and interlayer formation in thin layers and at interfaces is of increasing influence in nanoscopic devices such as nano-electronics, magneto-optical storage and multilayer x-ray optics. We show that with the nitridation of reactive B_4C/La interfaces, both the chemical and optical contrast can be greatly enhanced. Although interaction and upward diffusion of N_2 from the substrate towards the adlayer does occur, this surfactant mediated growth contributes to chemical and optical interface properties that enable major reflectivity improvements of multilayer optics for $6.7 < \lambda < 7.0$ nm.

8.2 Introduction

Chemical reactivity and differences in lattice parameters and surface free energy are of significant influence on the morphology and kinetics in layer-on-layer growth[1,2]. Interfaces in e.g. B_4C/La multilayer optics for B-K_α reflection (λ = 6.65 nm)[3,4,5] suffer from surface segregation and exothermic interlayer formation via $7\,\mathrm{La} + 6\,\mathrm{B_4C} \rightarrow 4\,\mathrm{LaB_6} + 3\,\mathrm{LaC_2}$[6]. Vapor or sputter deposition of B_4C occurs in separate B and C atoms[7,8], making the B_4C-on-La interface even more reactive. Chemically inactive, high contrast interfaces are however essential for the optics. For reflection at near-normal angle of incidence (AOI), La/B_4C multilayers considered as highly reflective coatings operating at λ = 6.65 nm typically require 200 periods of 2.0 nm thick B_4C and 1.6 nm thick La layers. Considering the formation enthalpy (ΔH^{for}), refractive index (n) and absorption constant (β) at λ = 6.65 nm for LaN, BN, LaB_6, LaC_2, B_4C, and La as shown in Table III of chapter 7, we observe that passivation of the B_4C/La interface is possible by nitridation, which would simultaneously improve the optical contrast, i.e. the reflectivity. Nitridation could also suppress roughening by grain formation[9,10] and diffusion at elevated temperatures.

8

The ΔH^{for} values imply that B_4C/LaN and BN/LaN interfaces are chemically inactive and do not suffer from LaB_6 and LaC_2 interlayer formation. IMD calculations[11] indicate that a relative increase of 20% in peak reflection and bandwidth can be achieved in comparison to a 200 period B_4C/La multilayers when LaN monolayers are created at every interface in a B_4C/LaN/La/LaN multilayer.

8.3 Experimental details

To verify the calculations on kinetic and optical properties, we investigated the nitridation and chemical reactivity in La and B_4C layers. These were grown by magnetron sputter deposition onto natively oxidized super polished Si (100) substrates in a Leybold Optics A1105 UHV facility with a base pressure of $1\cdot10^{-6}$ Pa[12]. A Kaufmann source was used for N-ion beam treatment. To study the depth and diffusion range of the nitridation process, N-treatment was applied either during deposition (NIBAD), or after deposition of individual layers. The nitridation of La and B_4C single-, bi- and multilayers is investigated using, angular resolved photoelectron spectroscopy (ARPES), cross-section transmission electron microscopy (CS-TEM) and selected area electron diffraction (SAED). For in-vacuo ARPES layer analysis and quantification[13,14,15], we assume the

bulk densities of 6.73, 6.17, 2.25 and 2.37 g/cc for respectively LaN, La, BN and B_4C[16]. Optical analysis of seven multilayers with nitridation steps at various stages is done with grazing incidence x-ray reflectometry (GIXR) and at-wavelength reflection measurements.

8.4 Results and discussion

For a post N-treatment of the B_4C layer, we observe that the BN overlayer thickness is linearly dependant on the N_2^+ beam voltage (V_b) in the 15 V to 120 V range. Over this range, we form 0.45 to 2.7 nm thick BN overlayers of similar composition as the BN obtained by NIBAD. In the case of La, already for the lowest N_2^+ beam voltage applied, two additional La4d doublets can be identified at ~2 eV higher and lower than the elemental electron binding energy. We identify three N1s peaks at 395.8, 396.9 and 398.5 eV. The spectral peaks hint at partial recombination to N_2 that forms dinitrogen complexes and intermediates such as $La(N_2)$[17,18]. Above ~100 V_b, the doublet that represents elemental La decreases. The La3d doublet shows only a slight increase at the low binding energy side, similar as observed for La_2O_3. With ARPES, we model[19,20,21] that post N-treatment with V_b = 70 V for 60 s. yields a 1.5 nm thick BN film on a B_4C substrate layer, and a ~1.3 nm thick LaN film on a La substrate layer, i.e. slightly thinner than the 2.0 nm thick B_4C and 1.6 nm thick La layers that are required for the multilayer.

The chemical interaction in B_4C/La interfaces is now investigated in three La-on-B_4C and three B_4C-on-La bilayers; either with post N-treatment or NIBAD of the substrate layer, or without N-treatment. For both post N-treatment and NIBAD, V_b = 70 V was used.

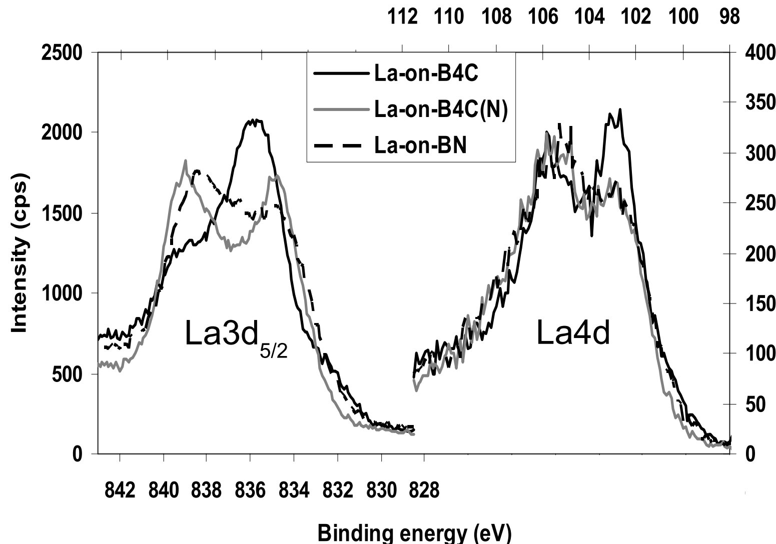

Figure 47: *The La3d$_{5/2}$ and La4d peaks of the three discussed bilayers. For the La-on-B_4C(N) interface, the B_4C substrate layer was post N-treated, for the La-on-BN interface, it was grown by NIBAD.*

Figure 47 shows the La3d$_{5/2}$ and La4d XPS peaks for the three La-on-B_4C bilayers. It reveals that upon nitridation of the B_4C substrate layer on which the La layer is grown,

the La3$d_{5/2}$ peak at 835.8 eV decreases while peaks at 835.0 and ~838.8 emerge. The La4$d_{5/2}$ peak at 102.8 eV also decreases while a second doublet emerges at ~2 eV higher binding energy. This suggests that N_2 diffuses from the B_4C substrate layer, up into the La layer to form a LaN or La(N_2) film that is approximately 0.3 nm thick. The observed nitridation of La is theoretically beneficial for the optical contrast, as earlier concluded from Table III. The La-on-BN interface, with NIBAD of the B_4C substrate layer, is observed to suffer least from diffuseness and yields superior chemical contrast.

For the case when a B_4C layer is deposited onto a La layer, the highest contrast B_4C-on-La interface is obtained with NIBAD of the La substrate layer. Only in that case we observe a clear second La4d doublet at ~2 eV lower binding energy from LaN in addition to the elemental La4d doublet. There is no indication of La(N_2) presence, possibly due to surface free energy driven upward diffusion[22] of N_2 into the B_4C adlayer. By occupying the surface, the diffusing N_2 could improve the B_4C-on-LaN growth. With ARPES we observe that the N_2 diffusion results in a BN film with a thickness of 0.6 nm for post- La deposition N-treatment, and of ~0.9 nm for NIBAD of the La. Due to the diffusion, the substrate layer retains only a 0.4 nm thick LaN film. From the bilayer experiments, we conclude that nitridation can enhance layer-by-layer growth both via chemical passivation and surfactant-mediated growth[17] of diffusing N_2 that is loosely bonded in dinitrogen complexes.

For optical analysis of the interfaces, we have grown seven multilayers with 51 B_4C/La periods; without nitridation (ML1), with NIBAD of both B_4C and La (ML2), NIBAD of only the B_4C (ML3), NIBAD of only the La (ML4), post N-treatment of both B_4C and La (ML5), post N-treatment of only B_4C (ML6), and post N-treatment of only La (ML7). In all cases, the same magnetron deposition times were used in order to investigate the effect of the N-treatment on layer thickness. We used XPS depth profiling with 0.5 keV Ar^+ to determine the in-depth material distribution and compound formation in these multilayers. Noting that the relocation range of the ions can occasionally exceed the calculated penetration depth, the low energy sputtering induces only moderate ion beam mixing compared to the XPS probing depth[23].

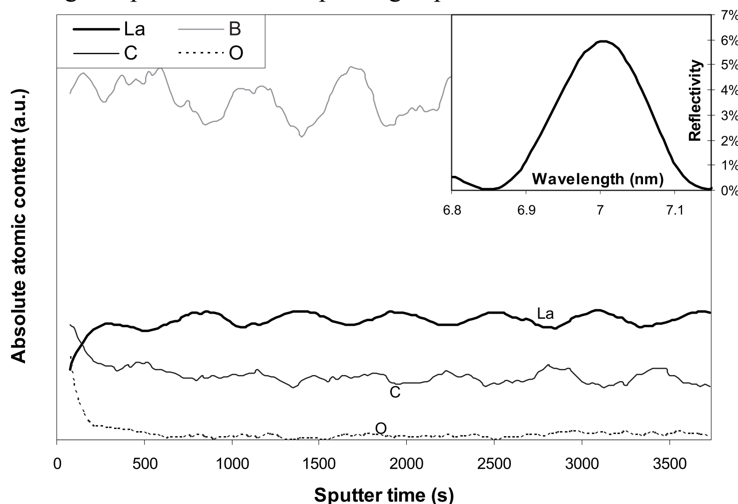

Figure 48: *XPS depth profile of a La/B_4C multilayer. The inset shows the reflectivity curve at 1.5° AOI.*

Figure 48 shows the XPS depth profile of the reference non-nitridated B_4C/La multilayer (ML1) with a period of 3.540 nm thick and a La-ratio (Γ) of 0.52, as established with GIXR at λ=0.154 nm. The approximate multilayer profile can be reconstructed with the mixing-roughness-information depth (MRI) model[24,25,26,27]. By using a calculated atomic mixing (g_w) of 2 nm and an information depth (g_λ) of 3 nm in linear approximation, we model a 0-100% interface gradient of 1 nm, leaving pure B_4C and La layers of ~0.6 and 0.8 nm thick respectively. These findings are supported by reflectometry, CS-TEM and XPS measurements and suggest that the interface gradient can partially be regarded as a LaB_6 and LaC_2 interlayer, which is thickest for the B_4C-on-La interface. For individual layer thicknesses of up to 5.0 nm, no crystallization is visible in XRD[6] and CS-TEM[28]. The reflection of 5.94% at λ = 7.00 nm, 1.5° AOI can be modeled[29] by 1.5 and 0.5 nm thick interlayers at the B_4C-on-La and La-on-B_4C interfaces respectively, with an interface diffuseness of 0.47 nm. The values are in good agreement with GIXR results of J.-M. André et al.[5]. An extrapolated 37% reflection at λ = 7.00 nm for a 200 period multilayer would also be in accordance with results obtained by other growth methods[30].

To investigate the effect of N-treatment on the chemical reactivity and optical performance of a B_4C/La multilayer, NIBAD of B_4C and La is now applied (ML2). A N1s peak around 397.4 eV, a B1s peak at 190.0 eV, and two C1s peaks at 282.7 and 286.0 eV indicate that all B and 40% of the C is bonded to N, possibly in a BN:C complex[31]. Judging from the C content, chemical etching via formation of volatile CN and C_2N_2 is limited, while sputtering or lower sticking of BN yields a more than 50% lower B content in the multilayer upon NIBAD. Modeling of the two doublets with $La4d_{5/2}$ at 102.2 and 104.5 eV suggests that the majority of the La is nitridated and possibly in equilibrium with a $La(N_2)$ dinitrogen complex. GIXR confirms the very poor layer contrast, although a net period thickness increase to 4.460 nm can still be determined, attributable to significant layer swelling upon BN formation. The peak reflectance is only 0.04% at λ = 8.80 nm, 1.5° AOI.

With NIBAD of only the B_4C layer (ML3), the peak positions and the nitride quantity are similar to when NIBAD is used for B_4C and La (ML2). The nitridation of La is only marginally decreased, confirming the significant N_2 diffusion that we observed in the La-on-BN bilayer. The XPS depth profile, CS-TEM, GIXR, and the peak reflection of 0.09% at λ = 10.88 nm, 1.5° AOI all reveal severe interdiffusion of the layers. The period thickness of 5.302 nm compared to 3.540 nm (ML2) confirms that NIBAD of B_4C results in significant layer expansion.

NIBAD of only the La layers (ML4) yields a multilayer period of 3.388 nm thick and $\Gamma <$ 0.3. We observe two La4d doublets with the $La4d_{5/2}$ peak at 101.6 and 103.9 eV in a 2:3 ratio. The combined peak area suggests a 25% lower La content compared to the non-nitridated multilayer (ML1). The peaks for B1s at 188.0 eV, C1s at 282.7 eV and N1s at 397.4 eV indicate that no nitridation of B_4C occurs and that the N resides in the midst of the La layer. In Cr/Sc multilayers that were grown in a N_2 rich background vacuum, N was also observed to reside in the midst of the layers[32,33]. MRI reconstruction of the asymmetric multilayer depth profiles and GIXR modeling suggest that the 0-100% interface gradients are less than 0.2 and 0.6 nm thick for respectively the La-on-B_4C and the B_4C-on-La interface. CS-TEM and the 11.52% reflectivity at λ = 6.74 nm, 1.5° AOI confirm the lower diffusion and better layer localization than without nitridation (ML1), or with NIBAD of B_4C (ML2, ML3). We model a reflectivity of 43% at λ = 6.72 nm for a

200 period multilayer. Nitridation of La thus appears the key step to obtain a major increase in reflectivity.

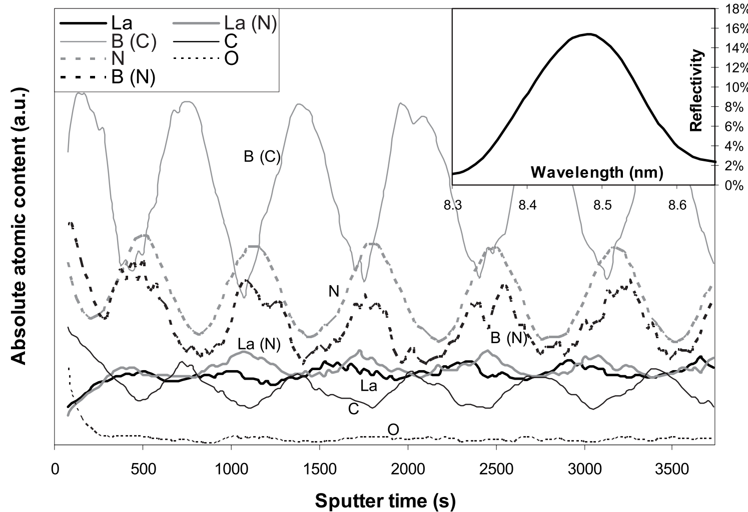

Figure 49: *XPS depth profile of a La/B_4C multilayer with 60 s. N-treatment after each layer. Brackets denote chemical bonds to other elements. The inset shows the reflectivity curve at 1.5° AOI.*

We now address the effects of N-treatment after deposition of the La and B_4C layers. A 60 s. N-treatment both after completion of B_4C and La (ML5) results in a period thickness increase to 4.34 nm and a decrease in Γ to 0.30, again attributed to layer expansion upon N-treatment of B_4C. The peak reflectance of 15.37% at 8.47 nm, 1.5° AOI suggests a high degree of periodicity and low interface diffuseness. The XPS depth profile of ML5 is shown in Fig. 49. Figure 49 reveals a high degree of localization for the B_4C and BN, with possibly surfactant-mediated growth by N or N_2. Based on MRI reconstruction and GIXR modeling, we estimate that the 0-100% interface gradients are less than 0.3 nm thick. The nitride content in the La layer shows a modest gradient from about 50% at the N-treated top to 60% at the bottom of the layer. This suggests that N_2^+ is implanted deeper into the La layer and that nitridation starts from there, similar as in Si[34]. A 200 period multilayer is modeled to yield 51% reflection at λ = 6.72 nm and 44% at λ = 7.00 nm.

With post N-treatment of only the B_4C layers (ML6), we observe a lower BN content at the La-on-B_4C than when also the La layer is post N-treated (ML5). This confirms surfactant-mediated growth of B_4C-on-LaN interfaces by N or N_2 and subsequent nitridation of B_4C. The prominent nitridation of the La implies a similar process at the other interface, with N_2 diffusion from the previously N-treated B_4C layer surface. The period is 4.190 nm thick, Γ is 0.44 and the peak reflectivity is 11.48% at λ = 8.22 nm. A 200 period multilayer is modeled to reflect 29% at λ = 6.72 nm and 23% at λ = 7.00 nm.

Finally, when only the La layers are post N-treated (ML7) we observe that about 60% of the La is nitridated, and in addition BN is observed at the La-on-B_4C interface. This suggests N implantation deep into the La layer and diffusion to the subsurface interface that possibly acts as precursor for nitridation[7,35]. The period is 4.000 nm thick and Γ is

0.46 for this multilayer. The increase in period thickness compared to 3.540 nm (ML1) appears solely attributable to the BN formation that was observed in the B_4C-on-La(N) bilayer and in Fig. 49. The peak reflectance is 15.53% at λ = 7.85 nm. A 200 period multilayer is modeled to yield 45% reflection at λ = 6.72 nm and 39% at λ = 7.00 nm. The dramatic reflectivity improvement that is obtained with post N-treatment of B_4C and/or La in comparison to NIBAD is partially explained by better localization of the nitrides at the interfaces. Especially BN has a higher optical absorption than B_4C (Table III).

8.5 Conclusions

In conclusion, the investigations on B_4C and La layer nitridation by N_2^+ bombardment have shown that the B_4C/La interface gradient can be substantially decreased by nitridation of the interface. The highest best results are achieved when the La and B_4C, or only the La layers are post N-treated. From the experimental results, extrapolated IMD modeling suggests peak reflectivities of up 51% at λ = 6.72 nm for a 200 period multilayer. Complete interdiffusion is observed upon NIBAD of B_4C. The N_2^+ bombardment of La appears to yield an equilibrium that involves dinitrogen complexes. The loosely bound N or N_2 in the B_4C or La substrate layers partially diffuses into the adlayer, resulting in surfactant mediated adlayer growth. Subsequent nitridation of the adlayer is observed, yielding nitridated interfaces that are chemically inactive to LaB_6 and LaC_2 interlayer formation. B_4C swells considerably upon nitridation, while the B content is significantly lower. Reflectometry and CS-TEM reveal that these processes occur without significantly affecting interface diffuseness in the case of post N_2^+ bombardment.

In effect, we substantially improved optical contrast, reflectivity maximum and bandwidth in La/B_4C multilayers by applying N-treatment after individual layer growth. This makes application in reflective optics highly advantageous for e.g. free electron lasers such as FLASH, next generation photolithography, soft x-ray spectroscopy, fluorescence analysis and imaging.

8.6 Acknowledgements

This work is part of the FOM Industrial Partnership Programme I10 ('XMO') which is carried out under contract with Carl Zeiss SMT AG, Oberkochen and the 'Stichting voor Fundamenteel Onderzoek der Materie (FOM)', the latter being financially supported by the 'Nederlandse Organisatie voor Wetenschappelijk Onderzoek (NWO)'. The author wishes to thank Prof. Dr. J. Birch and Dr. N. Ghafoor at the Thin Film Physics department of Linköping University in Sweden for the TEM and SAED sample preparation and measurements.

8.7 References

[1] T. Young, An Essay on the Cohesion in Fluids, Philos. Trans. 95, 65 (1805).
[2] H. Roder, R. Schuster, and K. Kern, Monolayer-confined mixing at the Ag-Pt(111) interface Phys. Rev. Lett. 71, 13 (1993).

[3] C. Michaelsen, J. Wiesmann, R. Bormann, C. Nowak, C. Dieker, S. Hollensteiner, W. Jäger, Multilayer mirror for x-rays below 190 eV, Opt. Lett. 26, 11 (2001).
[4] P. Ricardo, J. Wiesmann, C. Nowak, C. Michaelsen, R. Bormann, Improved analyzer multilayers for aluminium and boron detection with x-ray fluorescence, Apl. Opt. 40, 16 (2001).
[5] J.-M. André, P. Jonnard, C. Michaelsen, J. Wiesmann, F. Bridou, M.-F. Ravet, A. Jérome, F. Delmotte, E. O. Filatova, La/B_4C small period multilayer interferential mirror for the analysis of boron, X-Ray Spectrom. 34, 203 (2005).
[6] T. Tsarfati, E. Zoethout, R. W. E. van de Kruijs, F. Bijkerk, submitted
[7] T. Tsarfati, E. Zoethout, R. W. E. van de Kruijs, F. Bijkerk, J. Appl. Phys. 105, 104305 (2009).
[8] I. Nedelcu, R. W. E. van de Kruijs, A. E. Yakshin, F. Bijkerk, Microstructure of Mo/Si multilayers with B_4C diffusion barrier layers, Appl. Opt. 48, 2, 155 (2009).
[9] H. L. Bai, E. Y. Jiang, C. D. Wang, R. Y. Tian, Improvement of the thermal stability of Co/C soft x-ray multilayers through doping with nitrogen, J. Phys.: Condens. Matter 9, L205 (1997).
[10] H. L. Bai, E. Y. Jiang, C. D. Wang, Interdiffusion in CoN/CN soft X-ray multilayer mirrors, Thin Solid Films 304, 287 (1997).
[11] D. Windt. IMD - Software for Modeling the Optical Properties of Multilayer Films. Computers in Physics. 12, 4, 360 (1998).
[12] E. Louis, H.-J. Voorma, N.B. Koster, L. Shmaenok, F. Bijkerk, R. Schlatmann, J. Verhoeven, Yu. Ya. Platonov, G.E. van Dorssen and H.A. Padmore, Microelectron. Eng. 23, p. 215 (1994).
[13] T. Tsarfati, E. Zoethout, R. W. E. van de Kruijs, F. Bijkerk, In-depth agglomeration of d-metals at Si-on-Mo interfaces, J. of Appl. Phys. 105, 064314 (2009).
[14] M. H. Upton, T. Miller, T.-C. Chiang, Absolute determination of film thickness from photoemission: Application to atomically uniform films of Pb on Si, Appl. Phys. Lett. 85, 7 (2004).
[15] A. Brevet, L. Imhoff, M.C. Marco de Lucas, B. Domenichini, S. Bourgeois, Angle resolved X-ray photoemission spectroscopy double layer model for in situ characterization of metal organic chemical vapour deposition nanometric films, Thin Solid Films 515, 6407 (2007).
[16] D. L. Perry, S. L. Phillips, Handbook of Inorganic Compounds, Electronic Database.
[17] A. -L. Barabási, Surfactant-Mediated Growth of Nonequillibrium Interfaces, Phys. Rev. Lett. 70, 26 (1993).
[18] G. V. Chertihin, W. D. Bare, L. Andrews, J. Phys. Chem. A 102, 3697 (1998).
[19] P.J. Cumpson, J. Elec. Spec. Rel. Phen. 73, 25 (1995).
[20] P.C. Zalm, Surf. Interface Anal. 26, 352 (1998).
[21] T. Tsarfati, E. Zoethout, R. W. E. van de Kruijs, F. Bijkerk, Growth and oxidation of transition metal nanolayers, Surf. Sci. 603, 7, 1041 (2009).
[22] B. M. Clemens, W. D. Nix, and V. Ramaswamy, Surface-energy-driven Intermixing and its Effect on the Measurement of Interface Stress, J. Appl. Phys. 87, 6 (2000).
[23] S. Tanuma, C. J. Powell, D.R. Penn, Calculations of electron inelastic mean free paths. Part II. Data for 27 elements over the 50-2000 eV range, Surf. Interface Anal. 17, 911 (1991).
[24] S. Hofmann, J. Vac. Soc. Jpn. 33, 721 (1990).
[25] S. Hofmann, Ultimate Depth Resolution and Profile Reconstruction in Sputter Profiling

with AES and SIMS, J. Vac. Sci. Technol. A 9, 1466 (1991).
[26] S. Hofmann, Surf. Interface Anal. 21, 673 (1994).
[27] S. Hofmann, Surf. Interface Anal. 27, 825 (1999).
[28] C. Michaelsen, J. Wiesmann, R. Bormann, C. Nowak, C. Dieker, S. Hollensteiner, and W. Jäger, Multilayer mirror for x rays below 190 eV, Optics. Lett. 26, 11 (2001).
[29] IMD, version 4.1.1, written by David L. Windt (2000).
[30] Y. Platonov, L. Gomez, D. Broadway, Proc. SPIE 4782, 152 (2002).
[31] M. P. Johansson, dissertation, Linköping (1998).
[32] N. Ghafoor, F. Eriksson, E. M. Gullikson, L. Hultman, J. Birch, Incorporation of nitrogen in Cr/Sc multilayers giving improved soft x-ray reflectivity, Appl. Phys. Lett. 92, 091913 (2008).
[33] J. Birch, T. Joelsson, F. Eriksson, N. Ghafoor, L.Hultman. Single crystal CrN/ScN superlattice soft X-ray mirrors: Epitaxial growth, structure and properties. Thin Solid Films 514, 10 (2006).
[34] I. Kusunoki, T. Takaoka, Y. Igari, K. Ohtsuka, J. Chem. Phys. 101, 9 (1994).
[35] T. Tsarfati, E. Zoethout, R. W. E. van de Kruijs, F. Bijkerk, J. of Appl. Phys. 105, 104305 (2009).

9 Valorisation and Outlook

9.1 Photolithography for Society

Photolithography has since the invention of the transistor in 1947 been the key and most critical step in manufacturing semiconductor devices in the 207 billion dollar[1] chip industry. The highly competitive and innovative technique has enabled the miniaturization process of integrated circuits (ICs) by imaging the electrical circuitry patterns from a mask onto semiconductor wafers coated with photo resist. ASML alone, the market leader in optical lithography and contractor for this research, employs 6,750 people at 60 locations in 16 countries and booked a record turnover of 3.8 billion euro in 2007, with an average selling price of approximately 16 million euro per commercial lithography tool. Although the international semiconductor community has clearly been affected by the economical crisis that started in 2008, industry agrees that funding for R&D remains necessary to meet the future market demands.

This research project is the first to be fully carried out as part of the FOM Industrial Partnership Program I10 ('XMO'), under contract with Carl Zeiss SMT AG. The motivation and broader context of the research has been described in sections 1.1 and 1.2. During the course of this research, several results proved to be of exceptional interest to the application of multilayer optics in EUVL. The awareness of valorisation and patenting possibilities during this project go hand in hand with the recent policy notes and review reports of STW and FOM on "physics for society". The patents and other valorisation opportunities that followed from this research project could generally be filed in parallel to the scientific publications with minor delay. This chapter describes the valorisation and outlook on potential spin-offs of the research presented in this thesis.

9

9.2 Improving the Optics Lifetime

One of the most strenuous and ambitious goals in the XMO program during the course of this PhD research project was to further increase the effective optics lifetime from 300 to 30.000 hours, with less than 2% reflectivity loss per multilayer being allowed during operational lifetime. The lifetime is for a large part limited by oxidation processes that occur already in ambient environment and further accelerate during the intense illumination under lithography tool vacuum background conditions. The oxidation is generally considered to be irreversible and could hinder the economic applicability of EUVL. The results presented in Fig. 17 and 18 of chapter 3 show that 0.3 nm thick surface layers of Ni and Co sacrificially prevent oxidation of the underneath Mo in ambient environment. For other surface layers, thicknesses of 1.5 nm or more are typically required to prevent underlying Mo oxidation. If the results are similar under EUV illumination, application in multilayer optics increases their active lifetime without a significant loss of initial multilayer peak reflectance due to absorption in the surface layer. In the field of nano-devices, Ni or Co could prevent the oxidation of e.g. essential electronic parts that need to remain entirely metallic. The results received great interest of Carl Zeiss in the search for capping layers that enable the requirements on the lifetime of optics. During oral conference presentations, scientific interest has initiated a broader

collaboration with the Thin Film Physics department of Linköping University in Sweden on e.g. the research that is presented in chapter 8.

In ambient environment, and in lithography tool vacuum under the enormous radiation fluxes of the EUV source, hydrocarbons absorb and dissociate at the surface[2,3,4,5]. This results in condensed carbonaceous and oxide contaminants at the nanolayer surface[6,7,8]. Several methods to reduce this have been explored in the EUVL community, including a more oxidative tool vacuum, and off-line cleaning with thermally dissociated atomic H. The first method has the inherent risk of irreversible damage to the multilayer optics, although the results as presented in chapter 3 might resolve this problem. The loss of effective imaging time for off-line cleaning with thermally dissociated atomic H was found to be economically unacceptable. Cleaning of the surface should instead be performed on-line during EUV illumination, without loss of imaging time. Together with the filament for dissociation, this exposes the multilayer optics to heat loads that cannot be effectively cooled and lead to irreversible degradation by diffusion. In extension of the research of chapter 3, the non-destructive cleaning of caps by catalytically dissociated H has been investigated in chapter 4. Catalytic dissociation yields atoms with very low kinetic energy and reduces the risk of multilayer surface erosion, of which we found no indication. The heat load on the multilayer remains well below the load during EUV illumination, and the technique is applicable for on-line use. It is currently being considered for implementation in next lithography tools.

The chemical characterization of surfaces that were exposed to atomic H exposure has revealed that next to partial removal of the carbonaceous contaminants, also the oxidized capping layers can be completely reduced to metallic state. This enables a more effective way for faster cleaning of carbonaceous contamination by atomic O. Dissociation of O_2 was not possible by the conventional hot wire method, but can be readily achieved by the catalytic dissociation method that was employed in chapter 4. Cleaning with atomic O removes the carbonaceous contamination more effectively and leaves a clean metal oxide surface without erosion of the multilayer via volatile metal oxides. Full metallic state of the surface is recovered by atomic H treatment, offering an attractive technique of non-destructive surface cleaning of the optical elements in lithography. The findings could readily be applied in the rapidly growing field of nano-devices to control oxidation that would render electronics useless. The research is also connected to the more or less reversed process of photo dissociation of water to oxygen and hydrogen for production of clean fuels. This is currently studied at Rijnhuizen in the new research theme ‘physics for energy’.

Another limiting factor in the lifetime of optics is chemical reactivity and diffusion in the multilayer. Interlayer formation and the loss of interface contrast reduce coherent interference and thus reflectivity. In chapters 5 and 6, the in-depth distribution and chemical state of the elements in the surface region of multilayers is investigated. The use of B_4C to reduce diffusion yields dissociation and diffusion of B to this interface. Silicides and borides, notably $RuSi_x$ and MoB_x, are formed at the Si-on-Mo interface front rather than in the midst of the Si layer. The MoB is a stable compound that does appear to reduce diffusion and has optically favorable properties for EUV. During the

course of this research, the invention of MoB_x interface diffusion barriers has been patented by Carl Zeiss for application in multilayer optics[9].

9.3 Beyond EUVL

In chapter 7 of this thesis, we have already initiated research on the physical challenges for optics that are required for e.g. X-ray Free Electron Lasers and lithography beyond the wavelength of 13.5 nm. In line with ASML and Carl Zeiss, we anticipate on further development of lithography at $6.65 < \lambda < 7.00$ nm. The computational survey on suitable reflective multilayer optics in chapter 7 includes combinations of B or B_4C with metals such as La, Th and U. The reflection bandwidth of a standard B_4C/La multilayer is typically only 0.06 nm. Together with the significant chemical activity that we observed in B/La and B_4C multilayers, this poses a major concern for wavelength matching of the optics to the source in lithography applications. We calculate that at the cost of several to tens of percents peak reflectivity, the reflection bandwidth can theoretically be increased by a factor three with Th or U instead of La, opening the door to broadband reflective optics for $6.65 < \lambda < 7.00$ nm.

Considering that Th or U can generally not be used in experimental setups, and that peak reflectivity is the major issue, improvements of B_4C/La multilayers have been investigated in chapter 8. Approaching this challenge from a kinetic and optical perspective, we modeled that nitridation of the interfaces significantly increases their chemical and optical contrast. This can increase both the reflection maximum and the bandwidth. Our investigation of the diffusion and surfactant-mediated growth of nitridated B_4C/La interfaces have shown that the performance is indeed much improved. The results obtained and their relevance to innovations in photolithography were immediately recognized and patented by Carl Zeiss[10]. For further valorisation, we are currently performing pilot experiments at the FLASH free electron laser to study and improve the optics lifetime upon illumination. The research as a whole is scheduled to be continued through a recently funded STW project with the Technical University of Twente, in close collaboration with the potential end users, e.g. ASML and Carl Zeiss.

With the aim to fully exploit physics for society, our ValoRIGHT proposal has recently been granted to open a “Valorisation officer” position at the Rijnhuizen Institute for Plasma Physics. This officer is to create awareness, make an inventory and explore further possibilities for valorisation of the research performed in this institute. The interaction with interested parties and patent lawyers will also be facilitated.

9.4 References

[1] Worldwide turnover in 2007, Photonik international, 2008

[2] B. Mertens, M. Weiss, H. Meiling, R. Klein, E. Louis, R. Kurt, M. Wedowski, H. Trenkler, B. Wolschrijn, R. Jansen, A. van de Runstraat, R. Moors, K. Spee, S. Plöger, R. van de Kruijs, Microelectronic Engineering 73–74 (2004)

[3] H. Oizumi, A. Izumi, K. Motai, I. Nishiyama, A. Namiki, Jpn. J. of Appl. Phys. 46, 25 (2007)

[4] S. Bajt, H. N. Chapman, N. Nguyen, J. Alameda, J. C. Robinson, M. Malinowski, E. Gullikson, A. Aquila, C. Tarrio, S. Grantham, Appl. Opt. 42, 28, 5750 (2003)

[5] J. Chen, C. J. Lee, E. Louis, F. Bijkerk, R. Kunze, H. Schmidt, D. Schneider, R. Moors, Diamond & Related Materials (2008), doi:10.1016/j.diamond.2008.11.030

[6] S. Graham, C. E. Steinhaus, M. Clift, L. E. Klebanoff, and S. Bajt, “Atomic hydrogen cleaning of EUV multilayer optics,” in Emerging Lithographic Technologies VII, R. L. Engelstad, ed., Proc. SPIE 5037, 460–469 (2003)

[7] H. Oizumi, H. Yamanashi, I. Nishiyama, K. Hashimoto, S. Ohsono, A. Masuda, A. Izumi, H. Matsumura, Emerging Lithographic Technologies IX. Edited by Mackay, R. Scott, Proc. SPIE 5751, 1147 (2005)

[8] M. E. Malinowski, P. Grunow, C. Steinhaus, W. M. Clift, L. E. Klebanoff, Proc. SPIE 4343, 347 (2001)

[9] R. W. E. van de Kruijs, S. Bruijn, T. Tsarfati, A.E. Yakshin, F. Bijkerk, E. Louis, “Reduction of diffusion at Mo/Si interfaces by boride barriers and boron passivation”, P17091PUSPRO, priority date 7 May 2008

[10] T. Tsarfati, E. Zoethout, E. Louis, F. Bijkerk, “Method to Enhance layer contrast of a multilayer for reflection at the B absorption edge”, US 61/079307 (US), DE102008040265 (Germany), priority date 16 September 2008

10 Summary

In the broad scientific field of thin films, applications have rapidly expanded since the second half of the 20th century, as has been described in the valorization chapter. This thesis describes research at the interface between surface chemistry and physics. The characterization of d-metal surface nanolayer caps in chapter 3 has revealed that they can actually promote oxidation of the Mo layer on which they are deposited. Vise versa, Ni and Co caps themselves oxidize, but in monolayer quantities already prevent Mo oxidation. We attribute these observations to sacrificial e^- donation, and in the case of Au and Cu, also to roughening of the surface. Chapter 4 shows that all cap oxide and part of the MoO_3 can be reduced by atomic H exposure, which also removes part of the carbonaceous contaminants that absorb on the surface both in ambient air and during use in lithography tools. The carbonaceous contaminants are hydrogenated to volatile hydrocarbons that desorp from the surface. Atomic O exposure removes remaining C and leaves a clean metal oxide surface without erosion via volatile metal oxides. With subsequent atomic H treatment, this offers an attractive technique for non-destructive surface cleaning of the optical elements in lithography.

The in-depth chemical and vacancy mediated diffusion have further been investigated in chapter 5 and 6 with XPS, AES, CS-EELS, HAADF-STEM and EDX. Several capping layers and boron are observed to diffuse into and through the underlying Mo, B_4C and Si layers without significant chemical interaction, towards the subsurface Si-on-Mo interface, where d-metal silicide formation and agglomeration occurs. Rather than in the mid-Si layer, kinetically favorable silicides and borides are formed at the Si-on-Mo interface front, notably $RuSi_x$ and MoB_x. The MoB_x appeared to be an attractive barrier material and has been patented. Reversed "substrate-on-adlayer" interfaces can yield entirely suppressed reactivity and diffusion, stressing the influence of surface free energy and the supply of atoms to the interface via segregation on thin layer growth.

Chemical diffusion and LaB_6 and LaC_2 interlayer formation in La/B_4C multilayers for reflection of wavelengths just above 6.65 nm have been studied in chapter 7 and 8. The research in chapter 8 reveals surfactant mediated growth and chemical stabilization of the La/B_4C interface by nitridation. We have shown in chapter 8 that B_4C is more readily nitridated by N_2^+ bombardment during or after growth than La, which apparently yields an equilibrium that involves dinitrogen complexes. The loosely bound N or N_2 in the La/B_4C interface substrate partially diffuses into the adlayer, resulting in surfactant mediated growth. Subsequent nitridation of the adlayer is observed, yielding nitridated interfaces that are chemically inactive to LaB_6 and LaC_2 interlayer formation. These processes occur without significantly affecting interface diffuseness when N_2^+ bombardment is applied after individual layer growth, yielding local BN and more diffuse LaN formation. Complete interdiffusion is observed when N_2^+ bombardment is applied during B_4C growth. Nitridation of the interfaces has greatly improved the reflective properties of La/B_4C multilayers. This makes application in reflective optics highly advantageous for short-wavelength light sources, e.g. the FLASH free electron laser, next generation photolithography beyond EUVL, soft x-ray spectroscopy, Rontgen fluorescence analysis and imaging.

11 Samenvatting

Op het brede wetenschappelijke gebied van dunne films hebben de toepassingen zich sinds de tweede helft van de 20^e eeuw snel uitgebreid, zoals in het valorisatiehoofdstuk is beschreven. Deze dissertatie beschrijft onderzoek op het grensvlak van oppervlaktechemie en fysica. De karakterisering van beschermende d-metaal oppervlakte nanolagen (*caps*) in hoofdstuk 3 heeft aangetoond dat ze de oxidatie van de Mo laag waarop ze worden aangegroeid kunnen bevorderen. Omgekeerd blijken Ni en Co *caps* zelf wel sterk te oxideren maar voorkomen ze al in monolaag-hoeveelheden de oxidatie van Mo. We schrijven deze observaties toe aan e^- donatie, en in het geval van Au en Cu ook aan verruwing van het oppervlak. Hoofdstuk 4 toont dat al het *cap* oxide en een deel van het MoO_3 door blootstelling aan atomair waterstof kan worden verminderd, een methode die ook een deel van de koolstofhoudende contaminatie verwijderd. De koolstofhoudende contaminatie adsorbeert zowel in atmosfeer als tijdens gebruik in lithografieapparaten aan het oppervlak. Het wordt gehydrogeneerd tot vluchtige koolwaterstoffen die desorberen van het oppervlak. De blootstelling aan atomair zuurstof verwijdert het resterende C en resulteert in een schoon metaaloxideoppervlak zonder erosie via vluchtige metaaloxides. Blootstelling aan katalytisch gedissocieerd zuurstof en waterstof biedt zo een aantrekkelijke en niet-destructieve techniek voor het reinigen van het oppervlak van de optische elementen in lithografie.

De chemische en vrije roosterruimte geïnduceerde diffusie in de diepte zijn verder onderzocht in hoofdstukken 5 en 6 met XPS, AES, CS-TEM, HAADF-STEM en EDX. Verscheidene *caps* en ook boor blijken zonder significante chemische interactie in en door de onderliggende Mo, B_4C and Si lagen heen naar de Si-op-Mo grenslaag te diffunderen, waar het d-metaal een silicide vormt en agglomereert. In plaats van midden in de Si laag vormen kinetisch geprefereerde silicides en borides zich aan de Si-op-Mo grenslaag, in het bijzonder $RuSi_x$ en MoB_x. MoB_x bleek ook een aantrekkelijk barrière materiaal te zijn en is gepatenteerd. Omgekeerde, “substraat-op-adsorbaat” grenslagen kunnen in volledig onderdrukte reactiviteit en diffusie resulteren, wat bij dunne laaggroei de invloed benadrukt van oppervlakte vrije energie en de aanvoer van atomen naar de grenslaag via segregatie.

Chemische diffusie en LaB_6 en LaC_2 tussenlaagvorming in La/B_4C multilagen voor reflectie van een golflengte net boven de 6.65 nm zijn in hoofdstuk 7 en 8 bestudeerd. Het onderzoek in hoofdstuk 8 toont aan dat bij nitridatie het stikstof deels diffundeert naar het oppervlak en door *surfactant mediated* groei zo de La/B_4C grenslaag kan stabiliseren. We hebben in hoofdstuk 8 aangetoond dat B_4C makkelijker genitrideerd wordt door N_2^+ bombardement tijdens of na de groei dan La, waarbij een evenwicht met distikstofcomplexen ontstaat. Zwak gebonden N of N_2 in de onderliggende laag bij de La/B_4C grenslaag diffundeert gedeeltelijk naar de bovenliggende laag, wat resulteert in *surfactant mediated* groei. Verdere nitridatie van die laag resulteert in genitrideerde grenslagen die chemisch inactief zijn voor LaB_6 en LaC_2 tussenlaagvorming. Deze processen vinden plaats zonder de ruwheid van de grenslaag significant te beïnvloeden wanneer het N_2^+ bombardement na de individuele laaggroei wordt toegepast, resulterend in lokale BN en meer diffuse LaN vorming. Volledige interdiffusie vindt plaats wanneer het N_2^+ bombardement tijdens groei van de B_4C wordt toegepast. Nitridatie van de grenslagen heeft de reflectie-eigenschappen van La/B_4C multilagen sterk verbeterd. Dit maakt de techniek zeer aantrekkelijk bij toepassing in reflecterende optica voor

lichtbronnen van korte golflengten, bv. de FLASH vrije elektronenlaser, de volgende generatie fotolithografie na EUVL, *soft x-ray* spectroscopie, en röntgenfluorescentie-analyse en afbeelding.

12 Analytical recommendations

During the course of this research, several analytical techniques have been considered to investigate the processes that occur at the multilayer surface. For chapters 3 and 4, the use of Reflection Absorption Infra-Red Spectroscopy (RAIRS) has been explored to identify the hydrocarbon species. Next to ellipsometry and the analysis of surface acoustic waves, RAIRS is in consideration for in-situ characterization of the multilayer photochemistry. The multilayered structure has so far proved to be unsuited for analysis of the surface. The spectrum was dominated by vibrations that originated from the crystalline Si substrate wafer or multilayer stack. The options to grow single layers on more suitable substrates, e.g. gold, will be further explored to obtain high surface sensitivity and unique insight in the nature of the adsorbents on multilayer surfaces.

In chapter 4, the surface monolayer of several multilayers was studied with Low Energy Ion Scattering (LEIS). The effect of oxygen plasma exposure supported our findings on atomic oxygen exposure to clean multilayer surfaces. It is also exploited in a novel way to study the diffusion of Mo and Si through B_4C barrier layers, which has overlap with the research as described in chapter 6, and the patent on MoB diffusion barriers. The related technique of scanning helium ion microscopy is currently further being developed in context of the new CP^3E industrial partnership program to accommodate the main research topics of multilayer surface contamination and cleaning. In-vacuo, LEIS has the best potential to obtain information on the surface monolayer.

For the investigation of surface morphology, atomic force microscopy (AFM) was used. It provided supporting evidence that Au and Cu capping layers on Mo grow in islands and yield significant roughening of the surface, promoting the oxidation of Mo. The deposition, chemical treatment, and analysis facility has recently been expanded with in-vacuo scanning tunneling microscopy (STM), which will be exploited in addition to AFM to further investigate the morphology of the surface upon illumination and cleaning.

For the chapters handling chemical diffusion, the use of Extended X-ray Absorption Fine Structure is considered to enable characterization of nearest neighbors in unit cells. A proposal for such research has been granted. Beside the Transmission Electron Spectroscopy (TEM) with Energy Dispersive X-ray analysis (EDX) and Electron Energy Loss Spectroscopy (EELS) that were used and can be further exploited for cross section characterization, also Electron Recoil Detection (ERD) is planned in collaboration with the Linköping University.

13 Acknowledgements

When I was still studying Physics and Chemistry at Utrecht University, I hadn’t really considered PhD research as a part of my career plan. When Fred and Eric offered me a position as PhD-student, I had some good night sleep and discussion with family and friends about my occupation for statistically the next five years. The collaboration with industrial companies, a healthy mix of researchers and technicians in the groups of Andrey, Fred, and Eric, and hybrid atmosphere of Rijnhuizen as led by Aart, also my mentor, did in the end convince me. After four years, I’m thankful that they managed to maintain this biosphere and offered me the guidance that made my research possible.

At the start, I was part of the relatively small group by the name of LPX. Along the course of my project, the group has swollen to no less than the nSI department, with many new PhD fellows. Working, talking and at times conference visiting with Ileana, Hirokazu, college friend Toine, Véronique, Saskia, Juequan, Jeroen, and Alexey was great.

Authors of a thesis often mention the distinct solitude or instead the team nature in which they carried out their PhD project. Neither of these apparently contradictory classifications adequately describes my period at Rijnhuizen. Considering the clear industrial motivation, I experienced great individual freedom in choosing and developing research topics and entering scientific side streets, albeit sometimes with dead ends. I enjoyed exploring these unpaved lanes together with Erwin, my most direct colleague in daily research. The visits of prof. dr. Peer Zalm from Philips Research were very helpful (and sociable) to keep an eye on some actual destination. He pointed out some topics that formed part of the fundament for chapter 5 and 6. Robbert, my direct supervisor and also project leader by now, always had very elaborate and precise remarks when the results should finally be put on paper. With the useful comments and guidance of my promoter Fred, we then went on to get the articles through the industrial clearance process by Carl Zeiss. The process was at times a headache, but working together with the people there has been a pleasure.

The technicians helped me a lot with the experimental buildup, made sure these positively tipped the balance of functionality, all in shiny RAL 735 grey and not taped together in “University style”. Next to these people, the soccer team and many colleagues in other departments were good confreres that made my time at Rijnhuizen very bearable indeed. Outside Rijnhuizen, my family, friends and others around me were an essential support and distraction.

Hidden behind first insight, lies the confusion.

Tim Tsarfati

14 Curriculum Vitæ

Tim Tsarfati was born in Utrecht on January 7, 1982. He finished his pre-university education (VWO) at the Niels Stensen College in Utrecht, 2000. He then studied Experimental Physics and Astronomy, and Chemistry at Utrecht University. The one year graduate research project for Experimental Physics and Astronomy was performed on the length definition of astronomical Gamma Ray Bursts, under the supervision of prof. dr. A. Achterberg and dr. N.J.A.M. van Eijndhoven. For Chemistry, the one year graduate research project was performed on the anisotropy in the surface chemistry of silicon in alkaline solution, under supervision of prof. dr. J.J. Kelly and dr. H.H.G. Philipsen. A nine months internship was carried out at the FOM Institute for Plasma Physics Rijnhuizen in Nieuwegein on the topic of protective surfaces for multilayer reflective x-ray optics, under supervision of prof. dr. F. Bijkerk and dr. ir. R.W.E. van de Kruijs. In March 2005, Tim obtained his masters degree for Experimental Physics, and four months later for Chemistry, both with the distinction "*met genoegen*" ("with pleasure"). He accepted a PhD research position at the FOM institute for Plasma Physics Rijnhuizen in Nieuwegein on the topic of the diffusion and chemistry at multilayer surfaces and interfaces under the supervision prof. dr. F. Bijkerk. The research resulted in several articles, patents, conference presentations, and this thesis.